Universität Potsdam
Institut für Erd- und Umweltwissenschaften

Water flow and heat transport modelling at the interface between river and aquifer

Kumulative Dissertation

**zur Erlangung des Doktorgrades der Naturwissenschaften (Dr. rer. nat.)
in der Wissenschaftsdisziplin Geoökologie**

**eingereicht an der
Mathematisch-Naturwissenschaftlichen Fakultät
der Universität Potsdam**

**von
Dipl. Geoökol. Matthias Munz**

Potsdam, April 2017

Published online at the
Institutional Repository of the University of Potsdam:
URN urn:nbn:de:kobv:517-opus4-404319
http://nbn-resolving.de/urn:nbn:de:kobv:517-opus4-404319

Abstract

The functioning of the surface water-groundwater interface as buffer, filter and reactive zone is important for water quality, ecological health and resilience of streams and riparian ecosystems. Solute and heat exchange across this interface is driven by the advection of water. Characterizing the flow conditions in the streambed is challenging as flow patterns are often complex and multidimensional, driven by surface hydraulic gradients and groundwater discharge. This thesis presents the results of an integrated approach of studies, ranging from the acquisition of field data, the development of analytical and numerical approaches to analyse vertical temperature profiles to the detailed, fully-integrated 3D numerical modelling of water and heat flux at the reach scale. All techniques were applied in order to characterize exchange flux between stream and groundwater, hyporheic flow paths and temperature patterns.

The study was conducted at a reach-scale section of the lowland Selke River, characterized by distinctive pool riffle sequences and fluvial islands and gravel bars. Continuous time series of hydraulic heads and temperatures were measured at different depths in the river bank, the hyporheic zone and within the river. The analyses of the measured diurnal temperature variation in riverbed sediments provided detailed information about the exchange flux between river and groundwater. Beyond the one-dimensional vertical water flow in the riverbed sediment, hyporheic and parafluvial flow patterns were identified. Subsurface flow direction and magnitude around fluvial islands and gravel bars at the study site strongly depended on the position around the geomorphological structures and on the river stage. Horizontal water flux in the streambed substantially impacted temperature patterns in the streambed. At locations with substantial horizontal fluxes the penetration depths of daily temperature fluctuations was reduced in comparison to purely vertical exchange conditions.

The calibrated and validated 3D fully-integrated model of reach-scale water and heat fluxes across the river-groundwater interface was able to accurately represent the real system. The magnitude and variations of the simulated temperatures matched the observed ones, with an average mean absolute error of 0.7 °C and an average Nash Sutcliffe Efficiency of 0.87. The simulation results showed that the water and heat exchange at the surface water-groundwater interface is highly variable in space and time with zones of daily temperature oscillations penetrating deep into the sediment and spots of daily constant temperature following the average groundwater temperature. The average hyporheic flow path temperature was found to strongly correlate with the flow path residence time (flow path length) and the temperature gradient between river

and groundwater. Despite the complexity of these processes, the simulation results allowed the derivation of a general empirical relationship between the hyporheic residence times and temperature patterns. The presented results improve our understanding of the complex spatial and temporal dynamics of water flux and thermal processes within the shallow streambed. Understanding these links provides a general basis from which to assess hyporheic temperature conditions in river reaches.

Zusammenfassung

Die Interaktion zwischen Oberflächenwasser und Grundwasser hat einen entscheidenden Einfluss auf die Wasserqualität und die ökologische Beschaffenheit von Seen, Flüssen und aquatischen Ökosystemen. Der Austausch von Wärme und gelösten Substanzen zwischen diesen beiden Kompartimenten ist maßgeblich durch die Austauschraten und die Strömungsrichtung des Wassers beeinflusst. Somit ist die Charakterisierung dieser beiden Größen in dem Übergangsbereich zwischen Oberflächenwasser und Grundwasser von besonderer Bedeutung. Diese Arbeit präsentiert die Entwicklung und Anwendung von Methoden zur Untersuchung der zeitlichen und räumlichen Dynamik des Wasser- und Wärmeflusses an der Schnittstelle zwischen Oberflächenwasser und Grundwasser.

Die Arbeit besteht im Wesentlichen aus zwei Schwerpunkten. Der erste Schwerpunkt beinhaltet die Entwicklung und Bewertung von analytischen und numerischen Methoden zur Bestimmung der horizontalen Strömungsrichtung und Austauschraten unter Verwendung von kontinuierlich gemessenen Temperaturzeitreihen entlang vertikaler Profile im gesättigten Sediment. Flussbetttemperaturen können relativ einfach und kostengünstig entlang eines Flussabschnittes in verschiedenen Tiefen und unterschiedlichsten Flussbettsedimenten (organisch, sandig bis grob kiesig) gemessen werden. Die Hauptverwendung solcher Temperaturprofile ist bisher auf die analytische Quantifizierung vertikaler Austauschraten limitiert. Im Rahmen dieser Arbeit wurde ein Ansatz entwickelt, der eine punktuelle Ermittlung der horizontalen Strömungs-komponente, basierend auf der Veränderung der täglichen Temperaturamplitude mit zunehmender Tiefe, ermöglicht. Weiterhin wurde ein inverser, numerischer Ansatz entwickelt, der die ein-dimensionale Wärmetransportgleichung numerisch löst und mittels inverser Optimierungsalgorithmen die simulierten Temperaturen bestmöglich an die gemessenen Flussbetttemperaturen anpasst. Diese Methode ermöglicht die automatische, zeitlich variable Quantifizierung vertikaler Austauschraten an der Schnittstelle zwischen Oberflächenwasser und Grundwasser sowie eine einfache Unsicherheitsbetrachtung aufgrund der zugrunde liegenden Parameterunsicherheiten.

Der zweite Schwerpunkt der Arbeit liegt auf der Anwendung der entwickelten Methoden und der Erstellung eines dreidimensionalen Simulationsmodelles entlang eines Flussabschnittes der Selke. Numerische Strömungs- und Stofftransportmodelle ermöglichen die gekoppelte Simulation von Fließprozessen im offenen Gerinne und im darunter liegenden porösen Medium. Die Parametrisierung des Modells erfolgte anhand empirischer Daten die im Untersuchungsgebiet detailliert erhoben wurden. Die Simula-

tionsergebnisse zeigten zum einen gebietsspezifische Gegebenheiten auf, ermöglichten darüber hinaus jedoch auch die Beschreibung allgemeiner Muster und Zusammenhänge welche die Wasserfluss- und Wärmetransportprozesse an der Schnittstelle zwischen Oberflächenwasser und Grundwasser beeinflussen. So zeigten die Ergebnisse dieser Arbeit, dass maßgeblich die natürlich vorhandenen Flussbettstrukturen die Austauschraten und die Strömungsrichtung zwischen Oberflächenwasser und Grundwasser beeinflussen und somit den hyporheischen Austausch bestimmen. Wichtige Einflussfaktoren auf die untersuchten Austauschprozesse waren die Lage im Gerinne relativ zur Flussbettstruktur und der vorherrschende Wasserstand (Abfluss). Bedingt durch den Wasser- und Wärmeaustausch prägten sich im Untersuchungsgebiet Bereiche aus in denen die täglichen Temperaturschwingungen tief in das Sediment eindringen (Anstrombereich der Flussbettstrukturen), als auch Bereiche in denen relativ konstante Temperaturen, nahe der Grundwassertemperatur, vorherrschten. Die durchschnittliche Temperatur in der hyporheischen Zone wurde durch die saisonalen Temperaturschwankungen im Oberflächenwasser dominiert, wobei die Temperaturen entlang einzelner Fließpfade stark von der Verweilzeit des Oberflächen- oder Grundwassers im gesättigten Sediment und dem Temperaturgradienten zwischen Fluss und Grundwasser abhängig waren. Trotz der Komplexität dieser Zusammenhänge, ermöglichten die Simulationsergebnisse die Ableitung einer allgemeinen empirischen Beziehung zwischen den hyporheischen Verweilzeiten und Temperaturmustern. Sowohl die Verweilzeiten als auch die Temperatur im gesättigten Sediment haben einen entscheiden Einfluss auf biogeochemische Prozesse in dem Übergangsbereich zwischen Oberflächenwasser und Grundwasser und sind somit von besonderer Bedeutung für die Wasserqualität von Seen, Flüssen und aquatischen Ökosystemen.

Contents

List of figures

List of tables

1 General introduction

1.1 Background and motivation

The limited resource water is vital for all of us. We depend on its availability and quality for drinking water and use it in many industrial processes and for irrigation in food production. Water is also crucial for sustaining the Earth's ecosystems. Sufficient water supply at the appropriate quality is a key factor for the health and well-being of humans and ecosystems, as well as social and economic development (United Nations).

Population growth, climate change and increasing environmental pollution seriously harm the global water resources. Some typical threats to water quantity include over-exploitation of groundwater and rivers and the resulting drawdown often lead to salt-water intrusion or upconing into aquifers (Reilly and Goodman, 1987; Barlow and Reichard, 2009). Specific sources for the degradation of water quality can be caused by diffuse pollution from fertilizers and pesticides used in agriculture and landscaping, and point sources such as waste-water discharged from treatment facilities or even without treatment. The nutrient enrichment in rivers may cause algal blooms, eutrophication and potentially lead to ecosystem stress, loss of biodiversity and reduces ecosystem function (Brunke and Gonser, 1997; Duff and Triska, 2000; Battin et al., 2016).

Managing and developing water resources in a way that balances social and economic needs, and that ensures the protection of ecosystems for future generations requires an integrated water resource management. Such management strategies are based on the knowledge that surface water and groundwater are hydraulically connected (Winter, 1998) (Fig. 1.1). Additionally, the interaction between surface water and groundwater must be recognized for their impact on both the quality and quantity of water resources (Krause et al., 2011; Boano et al., 2014). For instance, in the mixing zone between streams and groundwater, biofilms adsorb, retain, amplify and transform organic substances and nutrients in the matrix, thereby accumulating substances that are otherwise highly diluted in the stream water, such as dissolved organic carbon or contaminants (Battin et al., 2016). The boundary between groundwater and surface water forms an important interface that requires observation and quantification of fluxes. How much water is exchanged across the river-groundwater interface? Which flow paths and directions are dominant? How does surface water-groundwater exchange influence the thermal regime and solute processing in the interaction zone? Precisely these questions are the focus of current research into hydrological processes and will be addressed also in this thesis.

1.2 Interactions of surface water and groundwater

Flow and transport processes at the interface between surface water and groundwater are mainly controlled by the distribution and magnitude of hydraulic conductivities of the saturated sediments and the relation of surface water level and groundwater level evoking hydraulic head gradients. Surface water interacts with groundwater in three basic ways: water flows either (1) from groundwater to surface water (gaining condition, Fig. 1.2A), (2) from surface water to groundwater (loosing condition, Fig. 1.2B), or (3) no interaction occurs when water level of surface water and groundwater are equal (neutral condition) or there just is no hydraulic connection (Winter et al., 1998; Woessner et al., 2000). Exchange processes at the interface between surface water and groundwater are characterized by high spatial and temporal variability. This variability is associated with heterogeneities in hydraulic streambed properties from scales of single, local structures up to the scale of entire surface water bodies, with abrupt changes in streambed slope and with changes in hydraulic boundary conditions at time scales of days via months to years (e.g. Thibodeaux and Boyle, 1987; Elliot and Brooks, 1997; Storey et al. 2003; Salehin et al., 2004; Cardenas and Wilson, 2007; Boano et al., 2009; Sawyer and Cardenas, 2009, Stonedahl et al., 2010). For example gaining stream reaches are usually located at the upstream end of in-stream geomorphological structures such as pool riffle sequences and fluvial islands, or upstream of channel bends in meandering streams (Fig. 1.1). Typical temporal variations in stream-groundwater interaction occur due to rapid rise in stream stage caused by floods due to heavy rains or rapid snowmelt.

The subsurface zone below and alongside a stream, where stream water infiltrates into the subsurface, flows through the streambed sediments and exfiltrates back to the stream, is referred to as the hyporheic zone (e.g. Harvey and Bencala, 1993; Winter, 1998; Wondzell and Gooseff, 2013). Hyporheic flow paths commonly range in length from meters to kilometres (Poole et al., 2008). Small scale hyporheic exchange is driven by stream bed morphology from grain scale roughness to ripples and dunes, while large scale exchanges depend on larger geomorphological features like pool riffle sequences, partly submerged bars and fluvial islands or meander bends (Tonina and Buffington, 2009; Stonedahl et al., 2010; Boano et al., 2014). The hyporheic zone can be seen as the mixing zone of stream water and groundwater (Triska et al., 1989; Winter et al., 1998) and is characterized by enhanced biogeochemical activity as a result of high inputs of oxygen, organic matter and nutrients into the subsurface environment, where bacteria and biofilm-forming microorganisms are abundant (Stanford and Ward, 1988; Brunke and Gonser, 1997; Boulton et al., 1998).

Solute processing in the hyporheic zone has been shown to depend on residence times (Boano et al., 2010; Zarnetske et al., 2011; Marzadri et al., 2012). For instance, long residence times promote denitrification, because usually oxygen must first be sufficiently depleted before denitrification occurs. In particular, denitrification is of great importance because it enables a permanent removal of nitrogen from the aquatic system (Harvey and Bencala, 1993; Zarnetske et al., 2011; 2012). In general, hyporheic exchange flows have a crucial impact on the health of our riparian ecosystems by increasing solute residence times and thus solute exposure to microbial communities, which in turn fosters biogeochemical cycling of nutrients and contaminants (Triska et al., 1989; Mulholland et al., 2008; Battin et al. 2016). Beside subsurface residence times also temperature has been shown to control microbial processes in hyporheic sediments (Thamdrup and Fleischer, 1998; Acuna et al., 2008; Boulton et al., 2008), but the temperature sensitivity varies between different sites (Gillooly et al., 2001; Enquist et al.,2003; Yvon-Durocher et al., 2012). Solute transformation rates in gravel bed rivers have been observed to vary by a factor of 10 for temperature differences of 10 °C (Vieweg et al., 2016). The functioning of the surface water-groundwater interface as buffer, filter and reactive zone is therefore critically important for the water quality, the ecological health and the resilience of streams and riparian ecosystems.

Highest exchange rates between surface water and groundwater are hypothesized to occur in tributaries and aggrading reaches, while channelized reaches are believed to be disconnected (Dahm et al., 1998). One of the key factors for the understanding of bio-

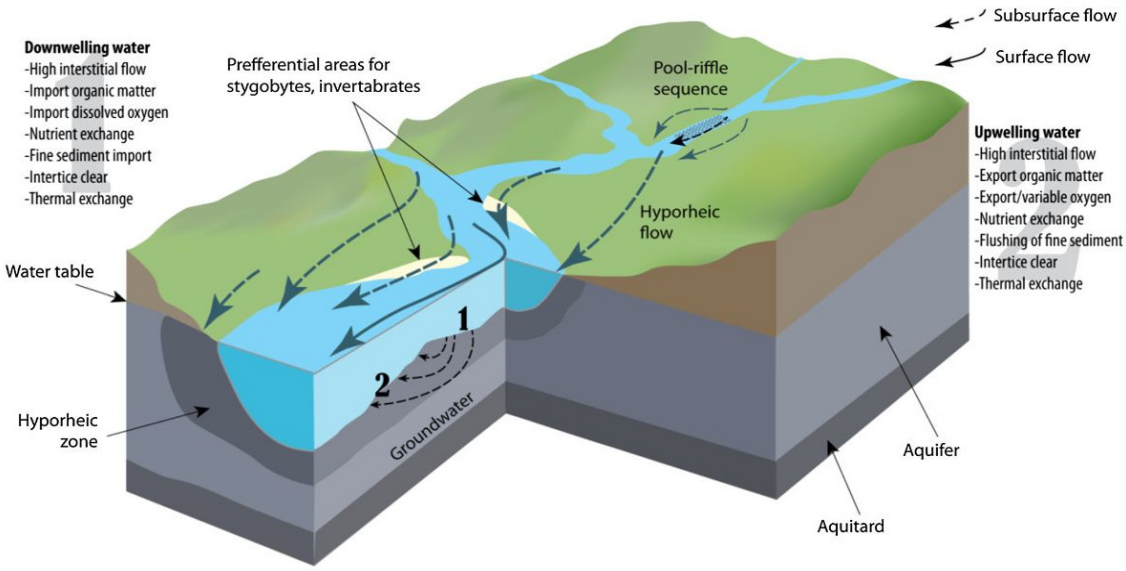

Figure 1.1: Conceptual scheme of flow and transport processes at the interface between surface water and groundwater with spatial scales ranging from centimetres to hundreds of meters and temporal scales ranging from seconds to years. The hyporheic zone is located beneath the streambed. Surface water is typically well mixed, oxygenated, and illuminated when entering hyporheic flow paths (from Bertrand et al., 2014).

chemical processes in the hyporheic zone is tied to an understanding of the surface water-groundwater exchange, hyporheic residence times and temperature dynamics. Understanding the interplay of hyporheic zone processes requires the coupling of multi-scale sampling and monitoring strategies, spatio-temporal data analysis, interpretations and interpolations, as well as sophisticated modelling techniques (Mouhri et al., 2013).

1.3 Basic principles of heat transport – heat as a tracer

Heat carried between surface water and groundwater substantially influences the temperature regime within the shallow saturated sediments and can be used as a tracer for shallow groundwater movement and to identify surface water-ground water interaction (Anderson, 2005; Constantz, 2008; Rau et al., 2014). Heat transport is driven by advection (the transport of heat by flowing water) and conduction (diffusive molecular transfer of heat). Heat conduction is a function of the temperature gradient and the properties of the medium through which the heat is transferred. In saturated porous media heat is conducted through both the fluid and liquid phase. The ability of the porous medium to conduct heat is described by the bulk volumetric heat capacity and thermal conductivity of the saturated sediment. Within the porous media, at the interface between surface water and groundwater, heat advection and conduction create dynamic spatial and temporal streambed temperature patterns (Conant, 2004; Hannah et al., 2009; Krause et al., 2011). The daily and annual surface water temperature oscillations, as regular cyclical patterns, are typically represented by sine functions that are fully described by their mean, amplitude, phase and period. Temperature oscillations are attenuated (damped in amplitude) and delayed (shifted in phase) with depth in the streambed sediments (Arrigoni et al., 2008; Constantz, 2008). The amplitude damping and phase shift are sensitive to the magnitude and direction (gaining or losing) of surface water groundwater exchange flux. The period, however, mainly determines how deep the temperature oscillations penetrate into the sediments. For the purely conductive case daily fluctuations affect the groundwater only to a distance of approximately 0.14 m while the seasonal fluctuations reach approximately 2.83 m into the aquifer (damping depth). Fig 1.2 summarizes the qualitative relationship between water and sediment temperatures for gaining and loosing stream conditions (Constantz, 2008).

Nowadays, measurements of vertical temperature profiles in the saturated sediment can be used to quantify heat flow, and thus to determine surface water-groundwater exchange fluxes indirectly. Analytical solutions based on the one-dimensional conductive-advective heat transport equation with a constant temperature boundary (Bredehoeft and Papadopulos, 1965; Schmidt et al., 2007) or with a sinusoidal temperature boundary (Suzuki, 1960; Stallman, 1965) have been developed to quantify water flow in near sur-

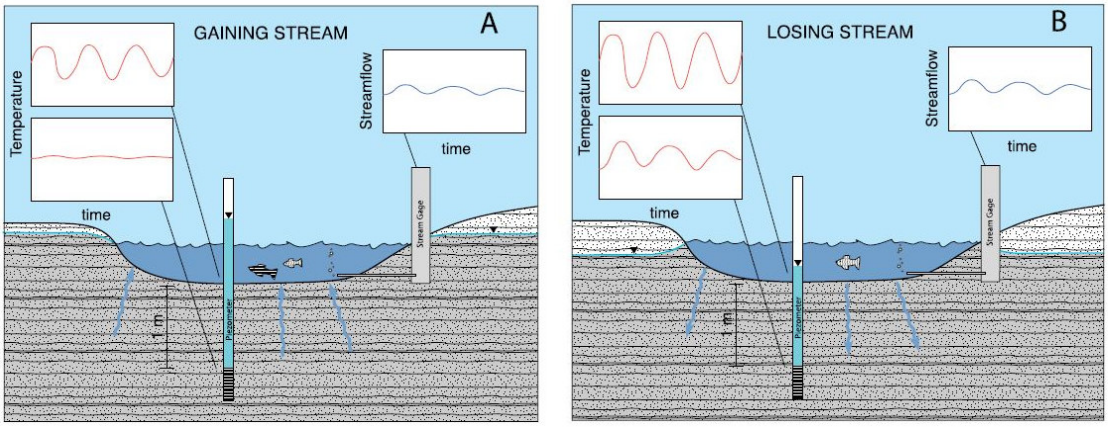

Figure 1.2: Thermal and hydrological conditions in streambeds for (A) gaining (groundwater upwelling) and (B) loosing (stream water downwelling) settings (from Constantz et al., 2008).

face sediments. Hatch et al. (2006) and Keery et al. (2007), for example, developed analytical methods to calculate vertical exchange fluxes from either the amplitude damping or phase shift between two temperature time series. These analytical solutions have been implemented in relatively comprehensive codes such as Ex-Stream (Swanson and Cardenas, 2011), and also in the code VFLUX (Gordon et al., 2012; Irvine et al., 2015) to automatically process measured temperature time series. Recently developed analytical solutions of the one-dimensional conductive-advective heat transport equation allow the inclusion of the entire temperature frequency spectrum into the estimation procedure (Wörman et al., 2012; Vandersteen et al., 2015). These methods overcome the problem that input temperature deviates from the assumption of sinusoidal temperature boundary but require temperature measurements over several days. For example Schneidewind et al. (2016) incorporated temperature measurements of 10-days to estimate vertical exchange flux.

Numerical codes iteratively solving the one-dimensional conductive-advective heat transport equation were specifically developed for simulating and inverting vertical temperature profiles with irregular temperature boundaries that cannot be approximated by a sine curve (Lapham, 1989; Voytek et al., 2013, Koch et al., 2015). However, the functionality of these numerical solutions is still limited to estimating the averaged exchange fluxes of the entire temperature time series provided as upper model boundary.

At the current stage using natural heat as a tracer has become a standard quantitative method to determine vertical water fluxes in near-surface sediments. Recent applications show spatially variable and non-uniform fluxes in the sediments (e.g. Fanelli and Lautz, 2008; Swanson and Cardenas, 2010; Jensen and Engesgaard, 2011) as well as temporally varying velocity results (e.g. Keery et al., 2007; Rau et al., 2010; Jensen and Engesgaard, 2011). The existing methods using heat as a natural tracer require well defined model boundary conditions such as a stationary one dimensional flow field or a

sinusoidal upper temperature boundary. In this thesis, I address these limitations to further advance the use of heat as a natural tracer to investigate water flow at the surface water-groundwater interface. We have developed methods to identify the geometry of the subsurface flow field (2D) and to automatically process long temperature time series with irregular temperature variation in a quasi-transient approach (1D; determination of one value per day). These developments are a further step towards the overarching goal of accurate flux estimations from temperature measurements including comprehensive error and uncertainty analysis.

1.4 Numerical modelling of coupled water flow and heat transport

The use of heat as a natural tracer allows the quantification of water fluxes even without any knowledge of the hydraulic conditions by using analytical or numerical solutions of the one-dimensional conductive-advective heat transport equation. A three-dimensional numerical approach potentially offers more insight into the coupled water flow and heat transport processes occurring at the surface water-groundwater interface, but at the same time requires more data as well as higher computational effort. To date a variety of numerical software packages have been developed to solve coupled groundwater flow and heat transport in 2D, e.g. VS2DH (Healy and Ronan, 1996), and in 3D, e.g. FEFLOW (Diersch, 2005), HydroGeoSphere (Therrien, 1992; Therrien and Sudicky, 1996), Hydrus 2D/3D (Šimůnek et al., 2006), Min3P (Mayer et al., 2002), OpenGeoSys (Kolditz et al. 2012), SEAWAT (Langevin et al., 2008), and SUTRA (Voss, 1990).

Most of these simulation platforms are limited to simulate thermal energy transport in the subsurface domain without taking into account a wide range of pertinent hydrological and meteorological processes known to influence the exchange processes that occur at the surface water-groundwater interface (e.g. fully integrated modelling of surface-subsurface water flow and heat transport; atmospherically driven energy balance). To address these requirements, HydroGeoSphere (Therrien, 1992; Therrien and Sudicky, 1996), a fully-integrated surface/subsurface flow and transport model was enhanced to include fully integrated thermal energy transport (Brookfield et al. 2009; Graf et al., 2010). HydroGeoSphere (HGS) is a three-dimensional finite element code which is designed to simulate the entire terrestrial portion of the hydrologic cycle. It uses a globally-implicit approach to simultaneously solve the 2D diffusive-wave equation and the 3D form of Richards' equation. HGS also integrates conductive-advective heat transport over the 2D land surface and in the 3D subsurface under variably saturated conditions. Similar simulation capabilities are available from the WASY groundwater software

FEFLOW coupled with the DHI surface water software MIKE11 yet the coupling is not iterative. After each time step, surface water-groundwater exchange fluxes calculated by FEFLOW at the coupled boundary points are exported to MIKE11 as an additional boundary condition. Mike 11 calculates the actual water levels for the next time step which are exported back to FEFLOW (Monninkhoff et al., 2014).

Multi-dimensional coupled water flow and heat transport models have been used to study patterns and dynamics of river–aquifer exchange (e.g. Brookfiled et al., 2009, Karan et al. 2014, Nützmann et al., 2014) and to define subsurface flow paths, flow velocities and residence time (e.g. Kulongoski and Izbicki, 2008; Birkinshaw and Webb, 2010; Naranjo et al., 2013). Temperature data were used in combination with hydraulic heads or measured fluxes to constrain coupled water flow and heat transport models (e.g. Doussan et al., 1994; Bravo et al., 2002; Naranjo et al. 2012,). Numerical models have furthermore been used to investigate the flow of water and its influence on the thermal signature in natural and antropized environments (e.g. Duque et al. 2010; Hester et al., 2009; Sawyer et al. 2012). However, numerical simulations at the reach scale, incorporating flexible and complex flux and temperature boundary condition, to study reach scale water and heat fluxes across the river groundwater interface, hyporheic residence times and temperature dynamics in three dimensions do not exist to the best of the author's knowledge. In order to evaluate the impacts of varying river discharge, transient temperature condition and complex streambed morphologies on water and heat fluxes across the river-groundwater interface it is critical to appropriately account for the hydrology and thermal interactions between the atmosphere, stream and groundwater in a fully-integrated manner. Hence, creating a robust model that can be used to evaluate the hydrological and thermal processes at the river groundwater interface, even to quantify hyporheic residence times and temperature dynamics which are known to have a significant impact on hyporheic solute turnover, is part of the objectives of this thesis.

1.5 Hyporheic research at multiple scales

Detailed process-based numerical models were developed at the scale of single geomorphological structures (1 – 10 m) (e.g. Cardenas and Wilson, 2007) up to the scale of the river reach (100 m – 1 km) (e.g. Stonedahl et al., 2010; as well as Munz et al., 2017), also coupled with heat and solute transport (with multiple reacting and interacting species) (e.g. Trauth et al., 2016; Zheng et al. 2016) and allow for a holistic investigation of exchange and transformation processes in the hyporheic zone. However, many essential questions remain unanswered about the mechanisms of hyporheic exchange and how surface-groundwater interactions influence heat and solute transport, microbial activity,

and biogeochemical transformations at the catchment scale (Boano et al., 2014). At this scale, the increased variability in geology, topography and in-stream geomorphological structures become more influential, particularly with regard to hyporheic exchange processes.

Current research lacks a formal approach for upscaling hyporheic exchange processes (Barthel and Banzhaf, 2015). Magliozzi et al. (2017) and Flipo et al. (2014) systematically review the scale dependent-factors controlling hyporheic exchange. They conclude that hyporheic exchange results from nested processes occurring at many different spatial and temporal scales (Fig. 1.3). Based on an analysis of hyporheic field studies, Ward (2016) elaborated that most research was conducted in second and third order streams. The spatial extent of these investigations was most common at local scales of 1 - 10 m (53 % of all reports) followed by 10 - 100 m scales (27 % of all reports). These studies commonly considered time scales of storm events to seasons (Ward, 2016). Overall, there is a lack of research in larger streams and at spatial scales larger than 1000 m up to the catchment scale.

At the catchment scale, Pryet et al. (2015) used an integrated surface water groundwater model to investigate water flux at the interface between surface water and groundwater. The geomorphological properties were estimated with a digital elevation model with a resolution of approximately 1 × 1 km². However, given the coarse model resolution it is difficult to represent the detailed morphological structure of the river network. Dimensional errors on river morphological features substantially impact the simulation of exchange processes at the interface between surface water and groundwater (Baratelli et al., 2016). In addition, the role of hyporheic processes in large streams and catchments is underestimated if small scale bedforms were not included (Kiel and Cardenas, 2014). Nonetheless, such an integrated model provided at the appropriate catchment scale is an essential tool for the implementation of an integrated water resource management (Pryet et al., 2015).

To handle the complexity of nested hyporheic exchange at the scale of entire catchments the development of efficient and parsimonious mathematical models is an important research focus. Stonedahl et al. (2010; 2012; 2013) present a quasi-three-dimensional model that can predict hyporheic exchange at the bedform to reach scale using readily measurable system characteristics. The primary model input parameters are stream velocity and slope, sediment permeability and porosity, and detailed measurements of the stream channel topography. The model simulations indicate that all scales of geomorphological structures between ripples and meanders have a significant effect on pore water flow fields and residence time distributions.

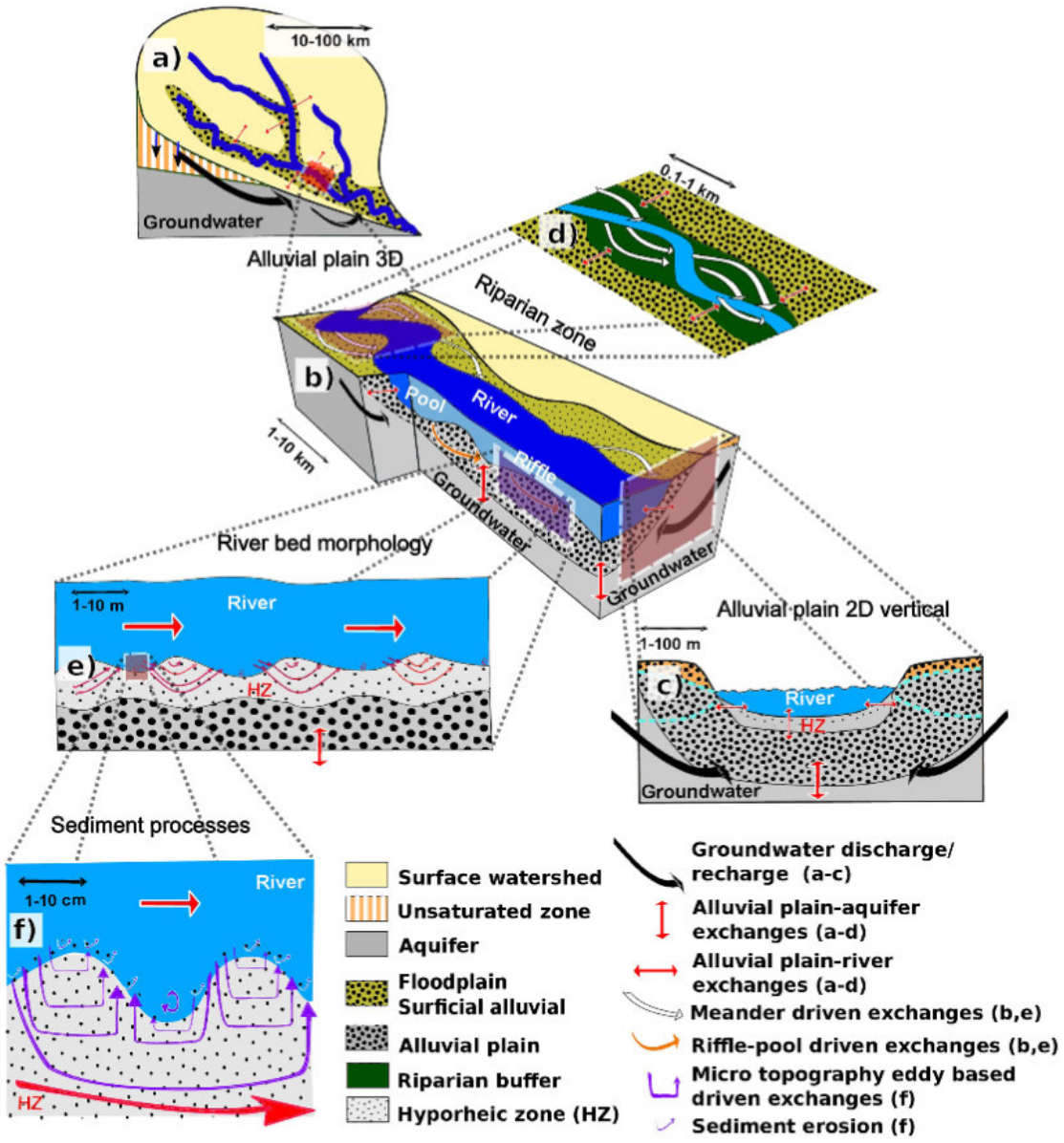

Figure 1.3: Nested stream aquifer interfaces: scales and features that influence hyporheic exchange (a) regional/catchment scale, (b-d) reach scale in an alluvial plane and (e, f) local scale of riverbed morphology (from Flipo et al., 2014).

Kiel and Cardenas (2014) and Gomez-Velez and Harvey (2014) developed parsimonious physically based models of hyporheic flow with potential for application in large catchments up to national scales. However, the model developed by Kiel and Cardenas (2014) only accounts for lateral exchange through meanders without considering vertical fluxes through the riverbed. Whereas Gomez-Velez and Harvey (2014) explicitly considered the multiple scales of geomorphic features and associated hyporheic exchange. Their Networks with EXchange and Subsurface Storage (NEXSS) model classifies hyporheic exchange including vertical exchange beneath submerged geomorphic features in the wetted channels and lateral exchange through much larger emergent alternate bars and meanders. These recent developments in parsimonious physically based

models will profit from the increased availability of high resolution airborne lidar and satellite data.

A major remaining challenge is the linkage between the small-scale physical drivers with their larger-scale fluvial and geomorphic context and ecological consequences (Harvey and Gooseff, 2015). Boano et al. (2014) inspire the use of predictive models of hyporheic flow and biogeochemistry to encourage innovative solutions to practical problems such as managing diffuse nutrient pollution and restoring ecological functions of river corridors at spatial scales from river reaches to the catchment scale.

1.6 Objectives and structure of the thesis

In this thesis I developed and applied analytical as well as numerical approaches to characterize stream-groundwater exchange, subsurface flow paths and temperature from the point scale to the scale of a river reach. Heat as a natural tracer is the key issue in all studies. At the point scale I continued to explore the use of heat as a natural tracer and expand the toolbox available to infer the geometry of the subsurface flow path and to quantify river-groundwater exchange fluxes allowing variable temperature time series as the boundary condition. These methods rely on measured temperature time series in vertical profiles and are used to continuously identify the direction and magnitude of local surface water-groundwater interactions in a losing reach of a gravel bed river (River Selke). At the reach scale I used three-dimensional coupled water flow and heat transport simulations to quantify the temporal and spatial variations in hyporheic exchange flux, hyporheic residence times and hyporheic temperatures and I have also identified their controlling factors. Furthermore, I used an empirical temperature relationship between the effective temperature and respiration rate to quantify the influence of hyporheic flow path residence time and temperature on hyporheic oxygen consumption.

The spatial and temporal variability of surface water-groundwater exchange, hyporheic exchange flows and heat exchange (thermal regime) are considered in relation to both experimental measurements and modelling of these phenomena. The experimental work at the Selke focussed on the implementation of a temperature sampling system. The study site is characterized by naturally occurring pool-riffle structures and an in-stream gravel bar, which are part of an intensive test site of the Helmholtz Centre for Environmental Research – UFZ within the TERENO initiative (http://teodoor.icg.kfa-juelich.de/observatories/HCGL_Observatory/hydrological- observatory-1/intensive-test-site-selke).

Each subsequent chapter within this thesis is based on an individual manuscript for journal publication, with each chapter having its own Abstract, Introduction, Methodology, Results, Discussion and Conclusions sections. The references, however, are cumulated and presented at the end jointly.

In chapter 2 (*Analysis of riverbed temperatures to determine the geometry of subsurface water flow around in-stream geomorphological structures*), I present an analytical method to identify the geometry of the subsurface flow field based on vertical temperature profiles. I apply this method using multiple time series collected at a losing reach of a gravel bed river. I systematically categorize the predominant subsurface flow field into purely vertical and non-vertical components (hyporheic, para fluvial) and investigate the spatial dependency of subsurface flow fields on the location in relation to characteristic geomorphological structures and on river levels.

In chapter 3 (*Estimation of vertical water fluxes from temperature time series by the inverse numerical computer program FLUX-BOT*) I present a numerical software developed to estimate water fluxes based on measured temperature profiles (FLUX-BOT), using variable temperature time series as the boundary condition. I show applications of FLUX-BOT to synthetic and to measured temperature data to demonstrate its performance.

In chapter 4 (*Coupled long-term simulation of reach scale water and heat fluxes across the river-groundwater interface, hyporheic residence times and temperature dynamics*), I used three-dimensional coupled water flow and heat transport simulations applying the HydroGeoSphere code in combination with high frequency observations of hydraulic heads and temperatures for quantifying reach scale water and heat flux across the river-groundwater interface and hyporheic temperature dynamics of a lowland gravel-bed river (River Selke). By means of particle tracking we evaluate hyporheic flow path length, hyporheic residence times and hyporheic flow path temperatures. I analyse the relationship between hyporheic flow path residence times and flow path temperature and assess their effects on hyporheic oxygen consumption.

In the closing chapter 5 general conclusions are drawn. The theoretical and methodological achievements are discussed with regard to possible scientific and practical applications. Additionally, further research directions are outlined.

2 Analysis of riverbed temperatures to determine the geometry of subsurface water flow around in-stream geomorphological structures

An article with equivalent content has been published as: Munz, M., S.E. Oswald, C. Schmidt (2016), Analysis of riverbed temperatures to determine the geometry of subsurface water flow around in-stream geomorphological structures, Journal of Hydrology, 539, 74–87, doi:10.1016/j.jhydrol.2016.05.012.

Abstract

The analytical evaluation of diurnal temperature variation in riverbed sediments provides detailed information on exchange fluxes between rivers and groundwater. The underlying assumption of the stationary, one-dimensional vertical flow field is frequently violated in natural systems where subsurface water flow often has a significant horizontal component. In this paper, we present a new methodology for identifying the geometry of the subsurface flow field using vertical temperature profiles. The statistical analyses are based on model optimization and selection and are used to evaluate the shape of vertical amplitude ratio profiles. The method was applied to multiple profiles measured around in-stream geomorphological structures in a losing reach of a gravel bed river. The predominant subsurface flow field was systematically categorized in purely vertical and horizontal (hyporheic, parafluvial) components. The results highlight that river groundwater exchange flux at the head, crest and tail of geomorphological structures significantly deviated from the one-dimensional vertical flow, due to a significant horizontal component. The geometry of the subsurface water flow depended on the position around the geomorphological structures and on the river level. The methodology presented in this paper features great potential for characterizing the spatial patterns and temporal dynamics of complex subsurface flow geometries by using measured temperature time series in vertical profiles.

Keywords: Temperature time series, Amplitude ratio, River-groundwater exchange, Hyporheic zone, In-stream geomorphological structures, River restoration

2.1 Introduction

The exchange of water, solutes and heat between rivers and groundwater control ecohydrological and biogeochemical conditions in the hyporheic zone (Boulton et al., 1998; Findlay, 1995; Krause et al., 2011a). Heat exchange moderates water column (Arrigoni et al., 2008; Burkholder et al., 2008; Webb et al., 2008) and hyporheic temperatures (Krause et al., 2011b; Schmidt et al., 2006). Heterogeneous temperature patterns, induced by variations in atmospheric energy input and complex subsurface flow patterns, provide thermal refugia for benthic fauna (Stubbington et al., 2009; Wood et al., 2010) and control biogeochemical reaction kinetics (Boano et al., 2010; Zarnetske et al., 2012). The combination of streambed temperatures and water flow in the streambed controls the energy fluxes across the sediment water interface (Caissie et al., 2014; Kurylyk et al., 2016).

Complex subsurface flow patterns are caused by heterogeneity in riverbed hydraulic conductivity (Salehin et al., 2004; Sawyer and Cardenas, 2009; Irvine et al., 2015), large geomorphological structures like pool-riffle sequences, point bars, in-stream gravel bars and meanders (Flipo et al., 2014; Stonedahl et al., 2010; Wondzell and Gooseff, 2013) and changes in ambient groundwater flow (Boano et al., 2009; Cardenas and Wilson, 2007; Fox et al., 2014). Such complex subsurface flow pattern are characterised by horizontal advective water and associated heat flux.

Continuous estimation of the direction and magnitude of river groundwater exchange in the field is limited to the availability of suitable measurement techniques and evaluation methods. Well-established quantification methods use local head differences (e.g. Käser et al., 2009; Mouhri et al., 2013), natural fluctuations of electrical conductivity (Schmidt et al., 2012; Vogt et al., 2010) and temperature (e.g. Constantz 2008; Rau et al., 2014). Analytical solutions to the one-dimensional heat transport equation (e.g. Goto et al., 2005; Hatch et al., 2006; Vandersteen et al., 2015) are accurate and reliable methods to calculate rates of river groundwater exchange based on the attenuation of a periodic temperature signal originating at the upstream boundary of the system (Lautz, 2012; Munz et al., 2011a; Rau et al., 2012). However, the application of such simple 1D methods can lead to significant errors in estimates of exchange flux where the model assumptions are violated in natural systems. The greatest source of error is due to non-vertical flow in the riverbed (Cuthbert and Mackay, 2013; Lautz, 2010; Roshan et al., 2012) and transient exchange fluxes (Rau et al 2015). Cuthbert and Mackay (2013) concluded that prior knowledge about the geometry of the flow field under consideration is needed to avoid misinterpretation of riverbed temperatures using 1D models.

The continuous, field-based quantification of the geometry of the subsurface flow field around non-submerged structures is of great importance in estimating the extent of surface water infiltration and of hyporheic exchange flows. The extent of hyporheic exchange flow and the related subsurface residence times strongly control biogeochemical reactions within the riverbed sediments, which, in turn, affect water quality and ecosystem functioning (Krause et al., 2013; Trauth et al., 2015; Zarnetske et al., 2012).

The purpose of this study is to develop and verify an analytical method to identify the geometry of the subsurface flow field based on vertical temperature profiles. We applied the method developed to multiple time series collected over two years at a losing reach of a gravel bed river in order to a) systematically categorize the predominant subsurface flow field into purely vertical and non-vertical components (hyporheic, para fluvial), b) investigate the spatial dependence of subsurface flow field on the location around characteristic geomorphological structures and c) investigate the temporal dependence of the subsurface flow field on river levels.

2.2 Study site and experimental setup

2.2.1 Study site

The study site is located at the catchment of the third-order Selke River, a 458 km² tributary of the Bode River, in the northern foreland of the Harz Mountains in central Germany (51°43'39.9"N 11°18'53.2"E). The aquifer beneath the river consists of up to 8 m thick fluvial sediments, with grain sizes ranging from medium sands to coarse gravels underlain by less permeable clay and silt deposits which confine the bottom of the alluvial aquifer. The top layer of the riverbed is covered by an armor layer of cobbles (D_{16}: 21mm, D_{50}: 42mm, D_{84}:100mm, sorting index: 4.76), which restricts considerable bed mobilization for river discharges occurring within the observation period. Average horizontal hydraulic conductivity of the riverbed is 1.4×10^{-3} m s^{-1} ranging from 1.1×10^{-4} m s^{-1} to 9.2×10^{-3} m s^{-1}. The hydraulic conductivity was determined by about 70 falling head tests distributed across the river reach. Individual slug tests were conducted at four different depth intervals below the streambed surface (0 - 0.2 m, >0.2 m - 0.4 m, >0.4 m – 0.6 m and >0.6 m – 0.8 m) at the same location using 1.6 m long piezometer pipes with a screened section of 0.05 m. For a detailed description of the slug test method, see Schmidt et al. (2006). No significant differences in the hydraulic conductivity were found with increasing depth, e.g. hydraulic conductivity is homogeneous in the z direction ($p\text{-value}_{ANOVA} > 0.05$; testing the effect of z on the mean of the hydraulic conductivity).

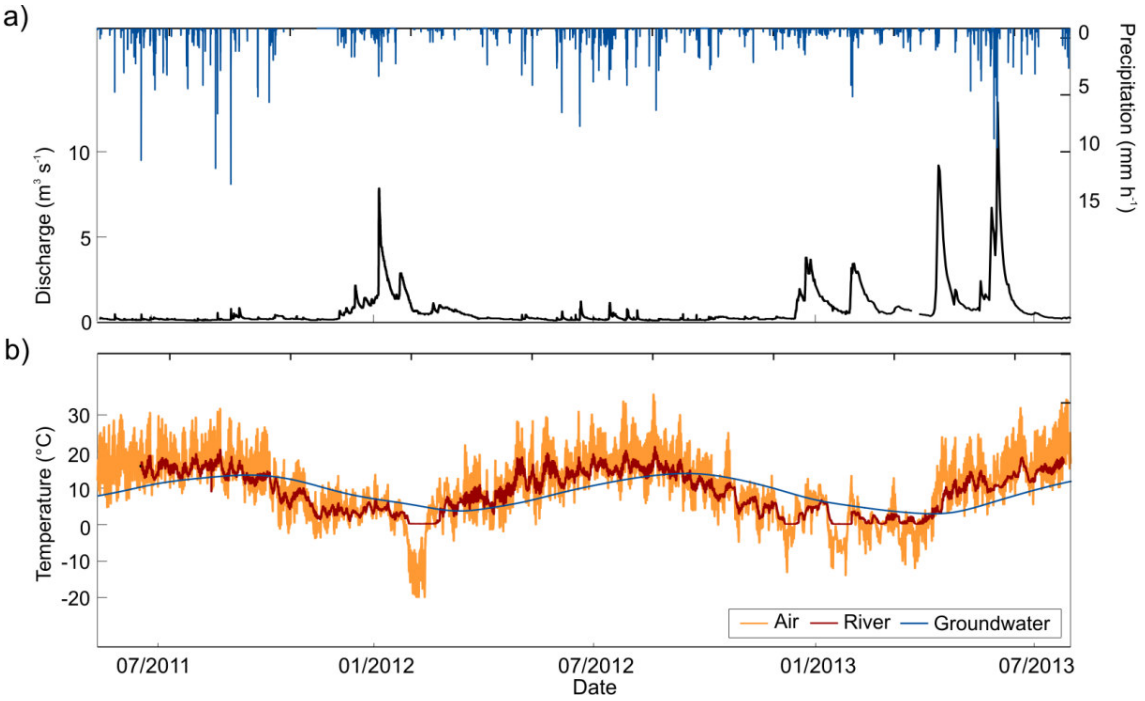

Figure 2.1: (a) Precipitation (DWD climate station Aschersleben) and stream discharge (gauging station Meisdorf) and (b) air, river (*1) and groundwater (*2, at 157.9 m a.s.l.) temperatures at the study site for the period from 01 July 2011 to 31 July 2013. Note that measurement locations of the temperature time series are indicated in Fig. 2.2a.

Mean river discharge at gauging station Meisdorf (4 km upstream of the study site) is 1.5 m^3 s^{-1}. Summer baseflow conditions usually occur from May to December, with minimum discharges of 0.11 m^3 s^{-1}. Snowmelt-induced flood peaks occur in spring with discharges up to 7.7 m^3 s^{-1} whereas rainfall-induced flood peaks occur in early summer with discharges up to 12.9 m^3 s^{-1} (Fig.2.1a). Mean annual air temperature is 9.67 °C. Air temperature varies seasonally from -22 °C in January to 34 °C in August (Fig. 2.1b).

The investigated river reach is 250 m long and includes a variety of natural fluvial morphological structures like meanders, pools and riffles, point bars and in-stream gravel bars (Fig. 2.2a), creating spatially varying river levels with the potential to drive hyporheic exchange flow (Tonina and Buffington, 2007; Wondzell and Gooseff, 2013). The two geomorphological structures studied, which are typical for the Selke and other third-order gravel bed rivers, were formed during strong flood events in 2010 and persisted without major sediment redistributions until June 2013. Visual inspection of the temperature sensors during regular data read out did not indicate scour or erosion in proximity to the sensor. The geomorphological structures are specified as follows:

A point bar, 27 m long and 3.5 m wide, overtopps the river level in the main channel over its full length during baseflow conditions of 0.25 m^3 s^{-1} (Fig. 2.2b, top). The pronounced back channel is abandoned from the main channel at the upstream end and connected back to the river at the downstream end of the point bar (upstream plugged,

abandoned channel, Wondzell and Gooseff (2013)). Major differences in river levels develop between the main channel and the back channel. With increasing discharge, the area of the point bar that is not submerged decreases until it is completely inundated at discharges higher than 3.6 m^3 s^{-1}, thus diminishing the water level differences between the main and back channels (Fig. 2.2b, top).

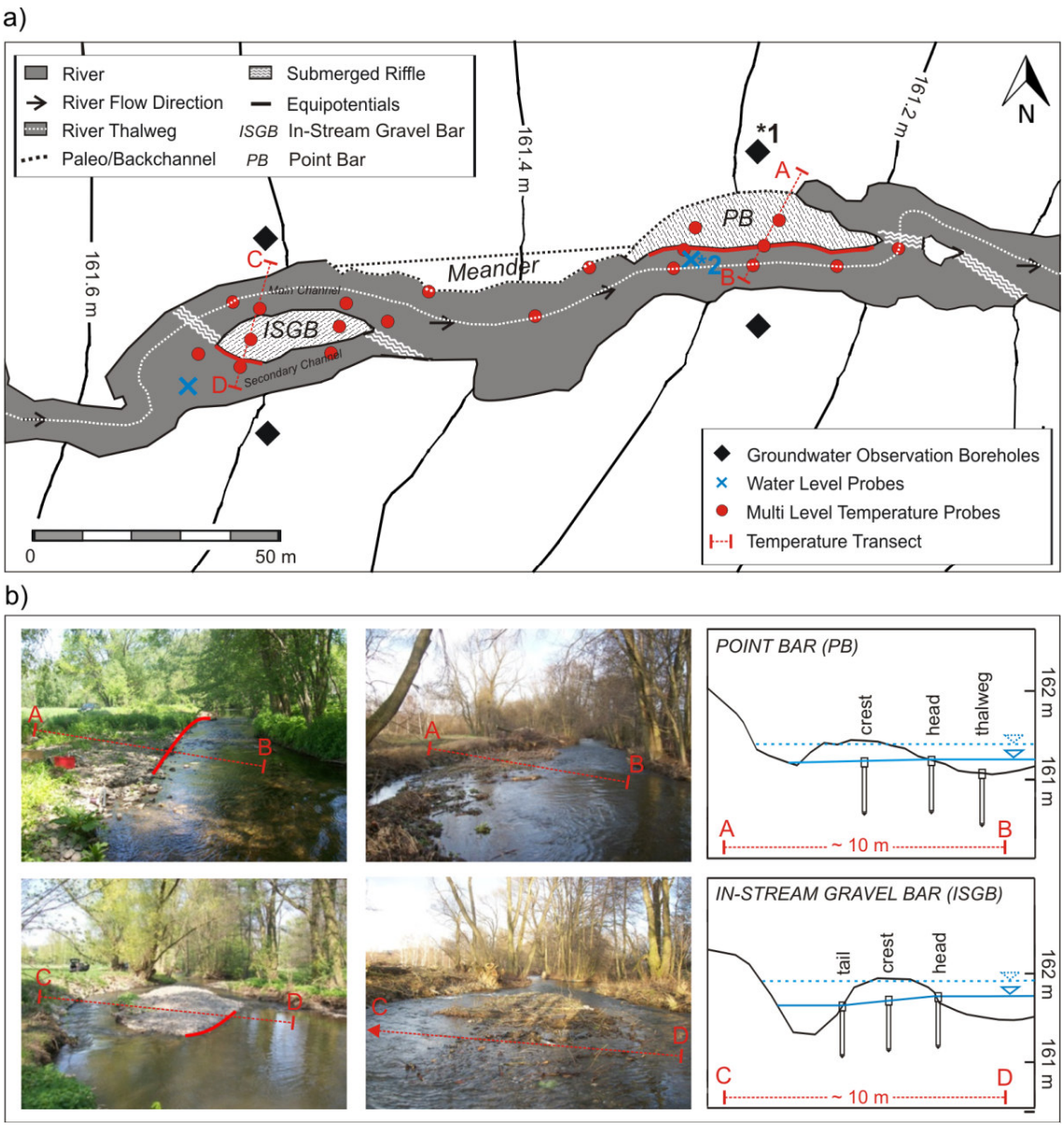

Figure 2.2: (a) Schematic showing experimental infrastructure around the in-stream gravel bar (left) and the point bar (right); riverbed temperatures were measured at 20 locations for seven depths at each location. River shape (shaded grey) and groundwater equipotentials for river discharge of 0.25 m^3 s^{-1}. Red line indicates the head site of the structures. Note that detailed temperature time series at *1 and *2 are shown in Fig. 2.1.

(b) Photographs and schematic cross section of the point bar (top) and the in-stream gravel bar (bottom) during low (q = 0.25 m^3 s^{-1}, left) and high (q = 3.60 m^3 s^{-1}, middle) river discharges. Red line indicates the head site of the structures (equal to Figure 2.2a). The cross sectional view shows the position of Multi Level Temperature Probes across the gravel bar (transect A-B) and island (transect C-D) for low (blue line) and high (dashed blue line) river discharges. Note the reduction in water level differences between main and side channels for high discharges.

An in-stream gravel bar, 20 m long and 6 m wide, exists between the main and a secondary river channel during baseflow conditions of 0.25 m^3 s^{-1} (Fig. 2.2b, bottom). The secondary channel (right side of the gravel bar) becomes dry for discharges smaller than 0.15 m^3 s^{-1}. Small riffles are located near the head of the gravel bar within the main channel and near the tail of the gravel bar within the secondary channel (diagonal opposed riffles, Wondzell and Gooseff (2013)), creating strong lateral hydraulic gradients across the in-stream gravel bar. For discharges higher than 3.6 m^3 s^{-1} the entire gravel bar is inundated, thus diminishing the water level differences between the main and secondary channels (Fig. 2.2b, bottom).

2.2.2 Experimental setup and data collection

Field data were collected over a two-year period between June 2011 and June 2013. Measurements include river and groundwater (GW) levels and air, river, riverbed and GW temperatures.

Water levels and temperatures were measured at the direct interface between river and riverbed and at four points in the alluvial aquifer at depths of 4.70 m below the surface at ten minute intervals using a data logger (Levellogger Solinst Canada Ltd., Canada, head/temperature accuracy: 0.05 % FS/± 0.1 °C). Monitored water levels were corrected for barometric pressure fluctuations using an atmospheric pressure sensor. All surface sensor positions were surveyed by a differential GPS (Trimble GPS R8).

Riverbed temperatures were measured at 20 locations for seven depths at each location using Multilevel Temperature Sensors (MLTS), Umwelt und Ingenieurtechnik GmbH, Germany (accuracy: ± 0.1 °C). Vertical probe placement was nominally at 0.00 m (river-GW interface), 0.05 m, 0.15 m, 0.20 m, 0.22 m, 0.25 m, 0.35 m and 0.55 m (below the river-GW interface). Real vertical sensor position in respect to the river-GW interface could vary by up to 0.05 m and were determined with an accuracy of ± 0.005 m. All temperatures were measured simultaneously at 10 min intervals. The applied MLTS setup has been proven to be a valuable and appropriate tool for providing representative riverbed temperatures for the accurate quantification of river-GW exchange fluxes (Munz et al., 2011a; Vandersteen et al., 2015).

Vertical temperature profiles were measured along the thalweg (the line of lowest elevation along the entire length of the riverbed) as well as at the head, crest and tail of representative geomorphological structures (Fig. 2.2a). The uppermost temperature measurements of all MLTS were located in the saturated sediment over the whole observation period, as well as for minimum river discharges. The MLTS at the head, crest and tail follow the highest lateral hydraulic gradient across the geomorphological structure

(Fig. 2.2, e.g. Temperature Transect A-B and C-D). The MLTS around the geomorphological structures and at the riverbank were installed where the riverbed slope from the thalweg towards the geomorphological structure or the riverbank was highest, most likely matching locations of intense lateral exchange flux (Munz et al., 2011b; Shanafield et al., 2010; Trauth et al., 2015). These locations were almost identical with the water table for minimum discharges during the observation period (Fig. 2.2b). The logger units of the MLTS were installed at the riverbanks to allow optimal protection and accessibility during high discharge events. Main data loss of the MLTS was caused by damages to the cable connecting the MLTS and the logger unit, damages to the logger unit through water intrusion during major floods or through vandalism and by disruption of the battery power supply. Details of the operation time of each sensor are presented in Appendix 2.A.

2.3 Methodology and data analysis

Spatial patterns and temporal dynamics of amplitude ratios (AR) were evaluated (see 2.3.1). The shape of $ln(AR)$ was analysed using simple conceptual models and linked to the geometry of the subsurface water flow (see 2.3.2). Characteristics in the subsurface flow direction were analysed for temporal dependence on hydraulic settings and spatial similarity (cluster analysis).

2.3.1 Amplitude ratio

The amplitude ratio for each day and depth is calculated as:

$$AR_z(t) = \frac{A_z}{A_0} \tag{2.1}$$

where A_0 is the amplitude of the daily temperature oscillation at the river-GW interface and A_z is the amplitude of the corresponding temperature oscillation at depth z. Temperature amplitudes were calculated as (T_{max} - T_{min})/2 where $T_{max/min}$ is the corresponding maxima and minima of the band-pass filtered temperature time series (Hatch et al., 2006; Munz et al., 2011a). At each MLTS location, riverbed temperatures were measured at seven depths, providing a fine vertical resolution of $AR_z(t)$. Under the assumption of stationary vertical flow, these amplitude ratios are functions of the magnitude of the river-GW exchange flux (Keery et al., 2007; Munz et al., 2011a).

The amplitude ratios are sensitive to the magnitude and direction (gaining or losing) of water flow. In order to assess the amplitude ratios at different locations and different

times we use the dampening depth as a flow-independent reference. For the purely conductive case, the dampening depth (D_e) is defined as the depth at which $\frac{1}{exp}$ of the daily temperature amplitude at z = 0 remains, i.e. where $AR_z(t) = 0.37$ (Stonestrom and Blasch, 2003):

$$D_e = \left(\frac{P \times \lambda}{\pi}\right)^{-1/2} \tag{2.2}$$

where P is the period of river temperature oscillation (1 d), and λ is the thermal diffusivity. A thermal diffusivity of 8 × 10^{-7} m² s^{-1} ± 4 × 10^{-7} m² s^{-1} was used to calculate D (Munz et al., 2011a; Stonestrom and Blasch, 2003). A pronounced river-GW exchange flux significantly alters the apparent $D(t)$ for each day. For exchange flux from the river to the groundwater (losing) the remaining temperature amplitude at a certain depth is higher than the amplitude of the purely conductive case; i.e. the apparent dampening depth will be higher than the purely conductive dampening depth ($D(t) > D_e$). To test the strength of the relationship between river level/hydraulic gradient and subsurface water flux (quantified by AR_{D_e}), we used the Pearson Correlation Coefficients (PCC). All presented correlation coefficients were significant concerning the null-hypothesis that there is no relationship between the observed phenomena ($p < 0.05$).

2.3.2 Evaluation of ln(Amplitude Ratio) using low order polynomials

One-dimensional heat transport in the subsurface can be quantitatively described by the decrease of A_0 with depth below the riverbed as (Keery et al., 2007):

$$\begin{gathered} A_z(t) = A_0(t) \times e^{-a_1 z}\ ; \\ \rightarrow ln\big(AR_z(t)\big) = -a_1 z; \quad a_1 = f(\vec{q}, \lambda, P);\ a_1 > 0 \end{gathered} \tag{2.3}$$

where a_1 is a function parameter depending on λ, P and also on the direction of vertical flow and its magnitude $\left(\overrightarrow{q(t)}\right)$, which is time-dependent. Eq. 2.3 describes a linear decrease of $ln\big(AR_z(t)\big)$ with respect to depth. This linear relationship, with no higher order terms, is valid for stationary one-dimensional vertical and uniform water flow. In case the vertical flow vanishes ($\overrightarrow{q(t)} = 0$), a_1 has a constant value set by the dampening properties only.

For non-vertical riverbed flux (e.g. hyporheic, parafluvial) or non-stationary flux, $ln(AR_z(t))$ will not decrease linearly with depth. This non-linear decrease of amplitude ratios can be described by higher order polynomial functions (model set) fitted to the z vs. $ln(AR_z(t))$ data:

$$p(z) = ln(AR_z(t)) = a_0 - a_1 z + a_2 z^2 + a_3 z^3 + \ldots + a_n z^n \quad (2.4)$$

$$\text{With } 1 \leq n < number\ of\ temperature\ sensors$$

where a_0 equals zero for all in-stream locations, as the uppermost temperature sensor is located directly at the river-GW interface at $z = 0$. If the uppermost temperature sensor is located at z < 0 (e.g. after sediment deposition around the temperature probe) a_0 would be negative. In the following, the polynomials are named "1st order" if $a_{2\ldots n} = 0$ (linear decrease in $ln(AR_z(t))$, cf. Eq. 2.3, vertical flow), "2nd order" if $a_2 \neq 0$ and $a_{3\ldots n} = 0$ and so on. Thereby, 1st order is always vertical flow and 2nd and 3rd order models indicate hyporheic and parafluvial subsurface flow fields, but these cannot be unambiguously assigned to the respective cases. The higher order models indicate transient water flux. Polynomial parameters ($a_{0\ldots n}$) were derived by fitting the model set to the $ln(AR_z(t))$ profiles. The best fit was achieved by minimizing the root mean square error of the model residuals. The method developed focus on amplitude variations as these are known to be most sensitive at low flow rates in the range of ± 2 m d^{-1} (regarding the temperature spacing used). In contrast the phase shift method has a lack of sensitivity at low flow rates (Hatch et al., 2006). Furthermore the phase shift method is prone to errors caused by filtering which can produce spurious phase shifts (Hatch et al., 2006).

The relation between polynomial coefficient a_2 and subsurface flow direction and magnitude was verified by numerical model simulation via HydroGeoSphere (Brookfield et al., 2009, Therrien et al., 2010). Two numerical models were created to simulate hyporheic exchange (Fig. 2.3a) and purely horizontal flux (Fig. 2.3b) through saturated porous medium following the model setup presented in Cranswick et al. (2014). Details of the numerical model are presented in Appendix 2.B.

2.3.2.1 Second order model (n=2)

If the 2nd order parameter a_2 is positive ($a_3 = 0$), then the shape of the model is concave (Fig 2.3c). The $ln(AR_z(t))$ is characterised by a rapid decrease in the upper segments of the profile followed by a comparatively low decrease in the deeper segments of the profile. With increasing depth, the slope of the fitted polynomial converges to zero (Fig. 2.3c). The deep temperature sensors of the profile receive almost the same temperature amplitude resulting from comparable travel times along the specific flow paths. The corresponding flow processes are typical for hyporheic exchange flux at locations where the horizontal flow component dominates (Fig. 2.3a) if subsurface sediment is homogeneous.

If the 2nd order parameter a_2 is negative ($a_3 = 0$), then the shape of the model is convex (Fig. 2.3c). The $ln(AR_z(t))$ is characterised by a slower decrease in the upper segments of the profile followed by a comparatively high decrease in the deeper segments of the profile. The signal reduction in the upper segment of the profile is lower than in the deep segment of the profile. Corresponding flow processes are characterised by strong horizontal advective fluxes through the riverbed with a significant groundwater contribution (Fig. 2.3b) if subsurface sediment is homogeneous.

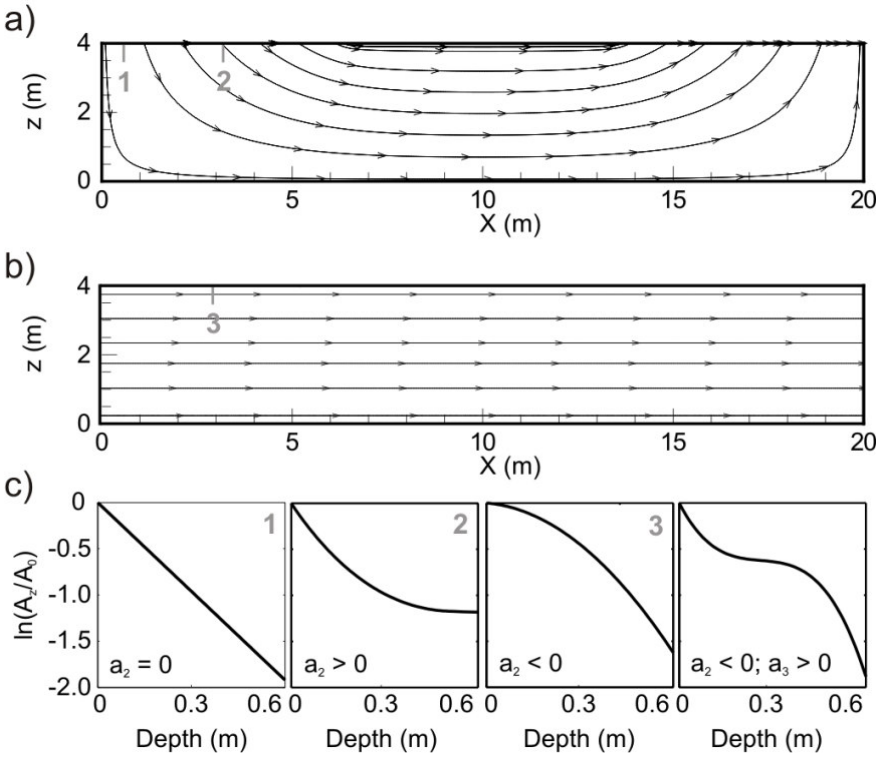

Figure 2.3: (a) Simulated flow vectors showing hyporheic exchange. Exchange flux range from vertically (v_z) dominated subsurface flow at the left hand side to horizontally (v_x) dominated subsurface flow at the centre of the domain; e.g. the horizontal flow component increases from the left to the centre of the domain. (b) Simulated flow vectors showing horizontal flow from left to right parallel to the surface. (c) Simulated amplitude ratio profiles for specified flow fields and positions in (a) and (b).

2.3.2.2 Higher order models (n≥3)

The third order model describes preferential horizontal flux through a limited section of the profile induced by a high permeable layer in the profile. The $ln(AR_z(t))$ is characterised by a rapid decrease in the shallow and deep segments of the profile intersected by a comparatively slow decrease in the mid segment of the profile (Fig. 2.3c). The fitted polynomial has a point of inflection at the depth where $p''(z) = 0$, that is for $z = {}^{a_2}/_{3a_3}$; the slope becomes zero in the midsection of the profile, where the horizontal water flux is highest.

All higher order models describe complex variations of the $ln(AR_z(t))$ profiles. Such complexity can be introduced by transient exchange flux and associated temperature signal non-stationarity (Appendix 2.C). For step changes in exchange velocities >= -0.5 m d^{-1} only the 4^{th} – 6^{th} order polynomials were identified as the best supported model, providing a reliable fit to the complex $ln(AR_z(t))$ profile.

In contrast, the second and third order models represent cases where the subsurface flow geometry deviates from the one-dimensional vertical flow direction (a_2 unequal to zero). Both show the dominance of horizontally dominated subsurface flux. If the occurrence of such a vertical flow component, e.g. the deviation from the vertical direction, should be quantified, it is sufficient to consider the magnitude of a_2.

2.3.2.3 Model performance

A stepwise selection using the Akaike Information Criterion with correction for finite sample size (AICc) and the Likelihood Ratio Test (LRT) was used to identify the best supported model (Akaike, 1973; Lewis et al., 2011). The procedure included the sequential comparison of the model set for each day of the observation period. Days where the 1^{st}, 2^{nd} or 3^{rd} order model was identified as the best supported model were analysed for their relative frequency.

The relative quality of the model is quantified by the AICc (*Akaike*, 1973):

$$AICc = 2\,k - 2\,ln(L) + \frac{2k\,(k+1)}{m-k-1} \tag{2.5}$$

where $ln(L)$ is the value of the logarithmic likelihood of the optimised model, k is the number of model parameters and m is the sample size. Besides the goodness of fit ($ln(L)$) the AICc includes a penalty term dependent on the number of fitted parameters. For the applied model set, the preferred model is the one with the minimum AICc value.

The LRT is a standard statistical test for comparing the performance of nested models, checking whether the log likelihood of the residuals is significantly reduced by constraining the model. The LRT statistic is defined as (Lewis et al., 2011):

$$LRT = 2(\log(L_{n\ order}) - \log(L_{n-1\ order})) \tag{2.6}$$

where $\log(L_{n\ order})$ /$\log(L_{n-1\ order})$ is the log likelihood for the residuals of the complex/restricted model. An LRT p-value < 0.05 provides evidence for the complex model against the reduced model, e.g. that the more complex model fits the data significantly better.

2.3.3 Spatial patterns of river-GW flow deviation

To identify the spatial pattern in the subsurface flow geometry around the geomorphological structures, we applied a hierarchical time series clustering to the time series of a_2. The polynomial parameter a_2 is defined as a measurement quantifying the deviation from the one-dimensional vertical flow even if the third order polynomial was identified as the best supported model (cf. 3.2.2.). The R package stats (R Development Core Team, 2011) was used to perform the cluster analyses. Locations with less than 250 calculated a_2 were excluded from the cluster analyses to guarantee sufficient temporal overlap between all remaining time series. The cluster algorithm partitions time series into groups based on a similarity measure (Euclidean distance). Thereby, time series within the same cluster are assumed to be similar, whereas time series in different clusters are not alike. The Euclidean distance L between two time series of $a_2(t)$ at location (x_1, y_1) and (x_2, y_2) is:

$$L = \sqrt{\sum_{t=1}^{n} \left(a_2(t, x_1, y_1) - a_2(t, x_1, y_1)\right)^2} \tag{2.7}$$

For hierarchical clustering of the time series, the complete linkage method is used. The clusters are generated by a stepwise aggregation of two time series separated by the shortest distance (Reimann et al., 2008), i.e. similar clusters are identified without prior assumption about their structure (number of clusters to extract).

2.3.4 Temporal dynamics of river-GW flow deviation

Temporal variations in the river level yields to temporal changes in the lateral hydraulic gradients across the geomorphological structures and to temporal changes in hydraulic

gradient between river and GW and in turn affects local river-GW exchange fluxes (Boano et al., 2009; Cardenas and Wilson, 2007; Stonedahl et al., 2010). In order to analyse the functional dependence of river level and hydraulic gradient on subsurface flow direction, we used scatter plots (a_2 vs. river level/hydraulic gradient) and regression analyses. For this, measured river and groundwater levels were filtered with a 1h moving average window to remove short-term noise in the time series (e.g. waves). The water levels were averaged to daily values (from 00:00 to 23:50), the same time resolution as given by calculated AR. Daily hydraulic gradients (Δh in m m^{-1}) were calculated using the averaged water levels of the river and the groundwater (distance between both measurement locations is 5 m). The hydraulic gradients are defined as positive when the hydraulic head in the river is higher than the hydraulic head in the groundwater.

2.4 Results and discussion

2.4.1 Hydrothermal conditions

The river level varied between 0.06 m and 1.3 m (Fig. 2.4a). The river level was predominantly higher than the groundwater level (positive hydraulic gradient, losing condition) throughout the observation period, with very few exceptions. The hydraulic gradients were highest during summer when groundwater level was low. Hydraulic gradients were also high during flood events when the river level was high (Fig. 2.4a). Multiple differential gauging measurements supported the assumption of predominantly losing conditions at the river reach studied.

The river temperatures warmed and cooled according to the atmospheric energy input, creating strong seasonal and daily temperature cycles. The average river temperature over the observation period from June 2011 until June 2013 was 8.62 °C. The river temperature varied seasonally from 1 °C in January to 21 °C in August (Fig. 2.1b). The average standard deviation between all river temperatures (16 locations distributed along the reach) at any time was 0.1 °C or less. Temperature refugia caused by shading effects from adjacent trees or local differences in river-GW exchange fluxes (Malcolm et al., 2004; Webb et al., 2008) were not observed at the study site. The river temperature was spatially homogeneous due to dominant turbulent river flux causing well mixed temperature conditions.

The average groundwater temperature at a depth of 4.6 m (8.66 °C) was similar to the average river temperature. The seasonal groundwater temperature amplitude was buffered (~ 50 %) and lagged (~ 39 days) relative to the river temperature (Fig. 2.1b). In spring/summer the groundwater temperature was generally lower (negative temperature

gradient), whereas in autumn/winter the groundwater temperature was generally higher (positive temperature gradient) than the river temperature. The summer temperature difference between river and groundwater rose to a maximum of 8.5 °C (Fig. 2.1b).

The daily temperature amplitudes in the river also exhibited a clear seasonal behaviour. The highest daily amplitudes of up to 4 °C were observed during summer (June/July 2011 and 2012). During high discharges in summer 2013, the river water was heated less and daily amplitudes were significantly lower than in 2011/12 (average difference in A was 0.7 °C, $\text{p-value}_{\text{Kruskal-Wallis}} = 7 \times 10^{-22}$). In winter (January/February 2012/2013), the daily temperature amplitude diminished completely when the air temperature fell below zero and parts of the river water started to freeze (Fig. 2.4b). For these periods, no calculation of AR was possible. Further data gaps (Fig. 2.4c-e) were caused by damage to the measurement devices.

2.4.2 Amplitude ratio

Figures 2.4c-e show the linearly interpolated amplitude ratios at the thalweg, head and crest of the point bar for all days of the observation period (cf. Fig. 2.2a, Temperature Transect A-B). The dampening depth for the purely conductive case at the thalweg and head of the point bar was 0.14 m (-0.04 +0.03 m, considering the range of λ, Eq. 2). However, amplitude ratios at 0.14 m were significantly higher than 0.37 throughout the observation period, indicating river water infiltration. In the following results we use the $AR_{0.15}$ to investigate the river groundwater exchange because the AR at that position for the purely conductive case is expected to be 0.37 and thus could be used as reference value indicating no exchange flux.

At the river thalweg, the AR exhibited clear seasonal behaviour (Fig 2.4c). During summer when the hydraulic gradient was high, the $AR_{0.15}$ was up to 0.75, pointing to strong river water infiltration into the riverbed. During winter when the hydraulic gradient was weak, the $AR_{0.15m}$ declined below 0.5. In December 2012 and February 2013, the $AR_{0.15}$ was at 0.37, indicating no river water infiltration into the riverbed. In general, we observed a weak negative correlation between river levels and $AR_{0.15}$ ($PCC_{\text{River-AR}} = -0.22$) and a positive correlation between hydraulic gradients and $AR_{0.15}$ ($PCC_{\Delta h\text{-AR}} = 0.46$) at the thalweg. Consistent with our results, Shanafield et al. (2010) showed by means of synthetic water flow and heat transport simulations that the hydraulic gradient had the strongest influence on total river groundwater exchange flux at the centre of the river channel.

In contrast to the thalweg, no distinct seasonal dynamics of $AR_{0.15}$ were observed at the head and crest of the point bar. In fact, the $AR_{0.15}$ at these locations depended on the river level. The lateral hydraulic gradient across the point bar increased with increasing river levels. The $PCC_{River\text{-}AR}$ increased compared to the thalweg (-0.22) up to 0.56/0.75 at the head/crest of the point bar. At the same time, dependency on the hydraulic gradient decreased compared to the thalweg (0.46) to $PCC_{\Delta h\text{-}AR}$ = 0.42/0.29, respectively. That implies that the river level determined the lateral hydraulic head gradients across the point bar, driving the river-GW exchange flow around the in-stream geomorphological structures independently of the vertical hydraulic gradient (losing condition).

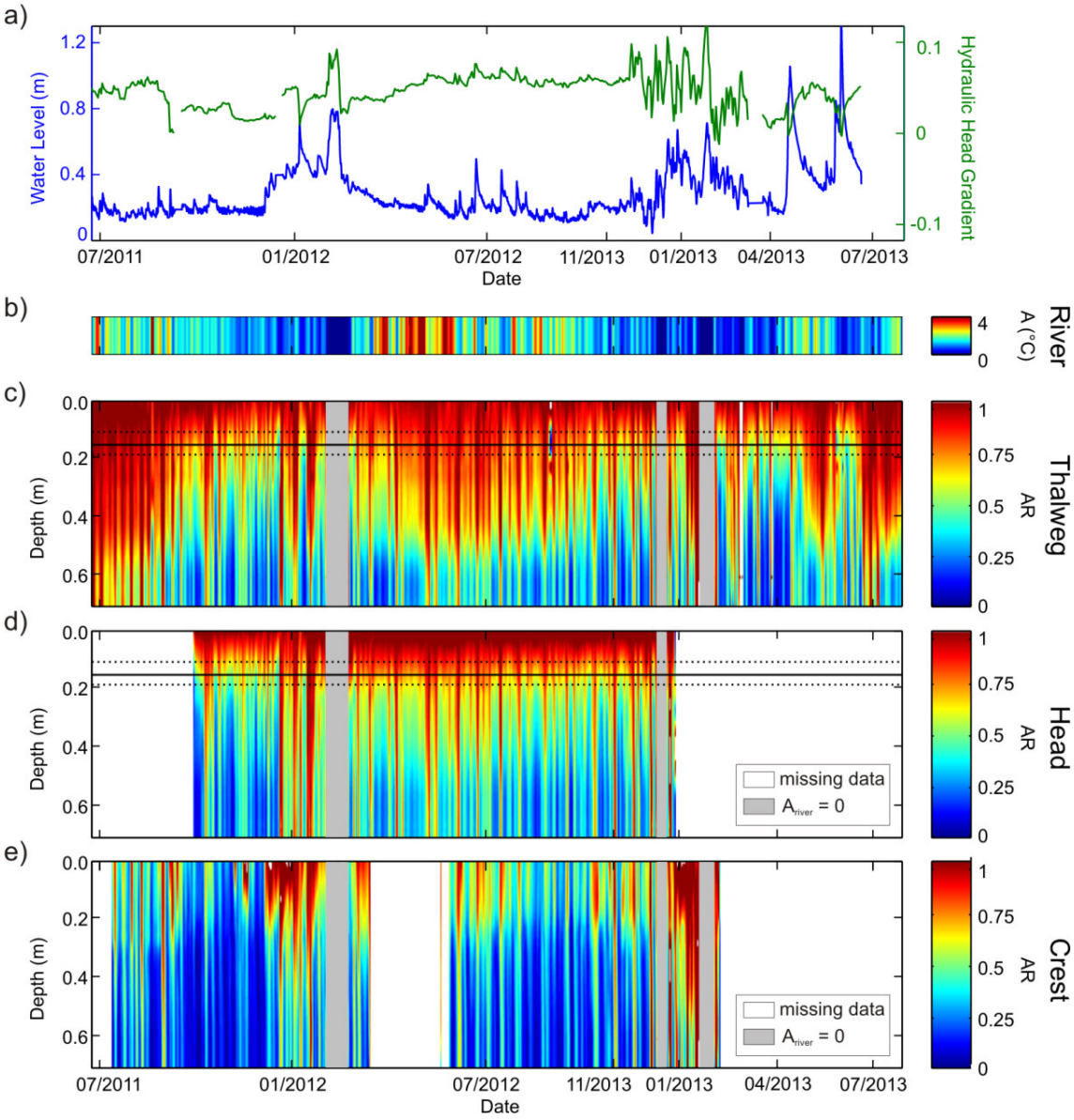

Figure 2.4: (a) River water level and hydraulic gradient between river and groundwater, (b) average daily temperature amplitudes of river water. Then the amplitude ratio depth profiles at river thalweg (c), head (d) and crest (e) of the point bar for the observation period from 01 July 2011 to 31 July 2013. Lines in (c) and (d) indicate the dampening depth according to Eq. 2.2 for thermal diffusivity of 0.8×10^{-6} m² s^{-1} (solid) ± 0.4×10^{-6} m² s^{-1} (dashed).

At the head and crest of the point bar, the ARs in the uppermost 0.17 m of the profile ranged between 0.6 and 1 throughout the observation period (Fig. 2.4d, e). Below 0.17 m, the amplitude ratios experienced a transition to values smaller than 0.37. This clear transition from high to low AR suggests that river water infiltrated into the main channel at the head of the point bar, forming a hyporheic flow cell with a characteristic penetration depth of about 0.17 m below the water table (high amplitudes in this section of the point bar, significant convection). Parts of the point bar below that penetration depth of about 0.17 m below the water table were characterized by vertical fluxes from the groundwater or static water (amplitudes close to zero, insignificant convection). The occurrence and shape of this hyporheic flow cell was supported by several subsurface salt tracer experiments during baseflow conditions. The highest signal of the introduced salt concentration was observed at a depth of 0.15 m following a subsurface flow path perpendicular to the river channel. Estimated flow velocities in the riverbed ranged between 0.76 m d^{-1} and 1.74 m d^{-1}, depending on the hydrological conditions at the time of the tracer test.

With increasing river levels, the AR at depths higher than 0.17 m below the water table increased substantially. This was caused by the increasing lateral hydraulic gradient across the point bar, leading to a deeper penetration depth of the hyporheic flow cell. When river levels rose above 0.58 m (discharge approx. 3.6 m^3 s^{-1}), the AR was higher than 0.6 over the entire profile (Fig. 2.4d, e). From that point onwards, the point bar was submerged (cf. Fig. 2.2), the lateral hydraulic head gradient across the point bar was diminished and water infiltration was in vertical direction from the river to the groundwater (losing condition). The river levels control lateral hydraulic gradients across the point bar and thus are the main driver of the formation and penetration depth of hyporheic flow cells across this geomorphological structure.

2.4.3 Evaluation of ln(Amplitude Ratio) using low order polynomials

2.4.3.1 Method verification and validation

The numerical simulations highlight the ability to use the polynomial parameter a_2 to determine the geometry of subsurface water flow direction around in-stream geomorphological structures. For hyporheic exchange (Fig. 2.3a), the magnitude of the polynomial parameter a_2 depend on the normalized difference between horizontal and vertical flux; independent of the magnitude of the exchange flux (Fig. 2.5a). The polynomial coefficient a_2 is close to zero at the sides of the domain where the vertical flow dominates, and increases to its maximum (up to 10) at the centre of the domain where the horizontal flow dominates (Fig. 2.5a).

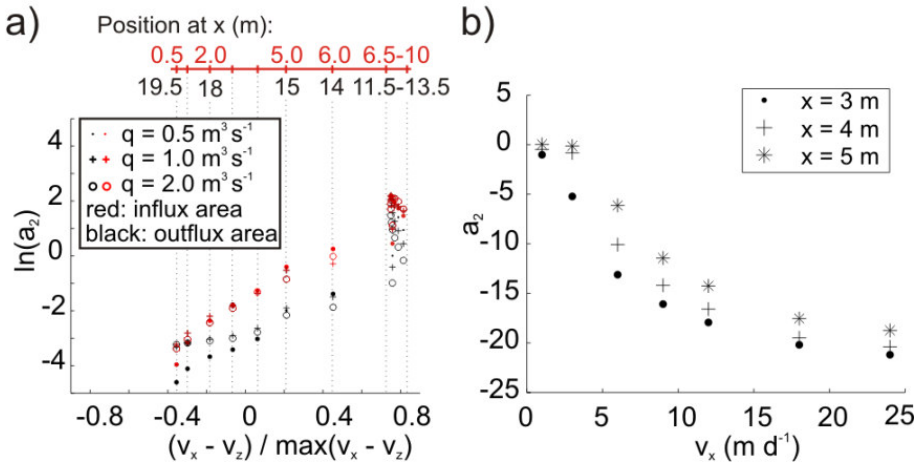

Figure 2.5: (a) Relation between dominant flow direction and polynomial coefficient a_2 for simulated amplitude ratio profiles for exchange fluxes of 0.5 m^3 d^{-1}, 1. m^3 d^{-1} and 2 m^3 d^{-1}. Corresponding subsurface flow pattern is shown in Fig. 2.3a. The position at x corresponds to the x axis in Fig. 2.3a.

(b) Relation between horizontal flow magnitude and polynomial coefficient a_2 for simulated amplitude ratio profiles for exchange fluxes of 1 m^3 d^{-1} to 24 m^3 d^{-1}. Corresponding subsurface flow pattern is shown in Fig. 2.3b. The position at x corresponds to the x axis in Fig. 2.3b.

For purely horizontal advective fluxes through the riverbed (Fig. 2.3b), the polynomial parameter a_2 was found to be proportional to the horizontal flow magnitude (Fig. 2.5b). For horizontal flow magnitudes <= 3 m d^{-1}, a_2 is around 0 with a linear decrease of $ln(A_z/A_0)$. For these exchange conditions, the system is dominated by heat conduction. With increasing exchange fluxes (up to 24 m d^{-1}) the magnitude of a_2 decreases to -20 (Fig.2.5b).

Figure 2.6a shows four examples of calculated amplitude ratio profiles at the head of the point bar and the optimised model set, demonstrating the good fit of the theoretical models to the observations. For each day, one of the 1st to 3rd order models was clearly identified as the best supported model concerning model residuals and model complexity (lowest AICc and LRT p-value < 0.05 cf. Fig. 2.6a). Both criteria provided consistent information. Thus the models of different complexity can be clearly ranked, allowing full consideration of the best supported model in terms of model residuals and model complexity. Minimizing the AICc for model selection is easy to assess and interpret. The LRT approach used in this investigation provides a formal test to use alternative models in the evaluation of amplitude ratio profiles. The model selection provides the shape of $ln(AR_z(t))$ and the optimised shape parameter (a_2), which in turn characterises the geometry of subsurface water flow direction.

2.4.3.2 Method application

We applied the method developed to multiple temperature time series collected over two years at a losing reach of a gravel bed river in order to categorize the predominant

subsurface flow field. Therefor the polynomial model set was fitted to the amplitude ratio profiles of each day and the best supported model was identified based on a step-wise selection using the Akaike Information Criterion with correction for finite sample size (AICc) and the Likelihood Ratio Test (LRT)**.**

The relative frequency of days where the 1st to 3rd order models were identified as best supported model averaged over all observation points is 0.95 (min = 0.88; max = 0.99); i.e. the presented models, up to 3rd order, are sufficient to fit the clear majority of daily $\ln(ARp)$ depth profiles for all locations (Fig. 2.6b). For the observation points at the thalweg, the 1st order model was the most frequent model, with a relative frequency between 0.49 and 0.71, i.e. subsurface water flow was purely vertical. For these cases, standard 1D analytical models (Hatch at al., 2006; Keery et al., 2007) and common thermal properties of the riverbed (Stonestrom and Blasch, 2003) could be used to accurately quantify the river groundwater exchange flux. At the thalweg close to the gravel bar (corresponding amplitude ratios are presented in Fig. 2.4c), the average exchange flux was 1.21 m d^{-1} with a minimum of 0.20 m d^{-1} in December 2012 and a maximum of 1.89 m d^{-1} and 8.64 m d^{-1} in July 2012 and January 2013, respectively. For most of the observation points at the head, crest and tail of the geomorphological structures, the 2nd order model was the most frequent model. Frequencies ranged from 0.51 to 0.76. At these positions 0.06 – 0.24 % of all daily amplitude ratio profiles could be described by the 1st order model (Fig. 2.6b). If the 1st order model was identified as the best supported model, the AICc of the second order model was showing it to also be a reasonably fitting model. Thus, the magnitude of the 2nd order in the polynomial (min = -0.26, max = 0.92) provides good information on the exchange flow deviation, even if it is not the best supported model. For all profiles characterised by the 2nd and 3rd order polynomial a_2 significantly differed from zero; i.e. the river-GW exchange flux at the head, crest and tail of the geomorphological structure significantly deviated from the one-dimensional vertical flow. Subsurface flow was characterised by a significant horizontal flow component. Such a non-vertical flow field violates assumptions required of standard 1D analytical methods and would influence vertical velocity estimates if not considered. Lautz (2010) and Roshan et al. (2012) demonstrated that errors in vertical flux estimates increase with the magnitude of a horizontal flow component (i.e. overestimation for losing condition). Cuthbert and Mackay (2013) highlighted that the degree of non-uniformity in the flow field (convergence/divergence) is the key control rather than non-vertical flow perse. They found that the largest discrepancy between 1D and 2D fluxes occurred where the non-uniformity in the flow field was greatest.

For the observation points at the head and tail of the meander (Fig. 2.2), the third order model was the most frequent model (0.76/0.63), fitting the $ln(AR_z(t))$ best (Fig. 2.6b). If the third order model was identified as best supported model the 2nd and 3rd order coefficients significantly differed from zero. The average depths of the point of inflection

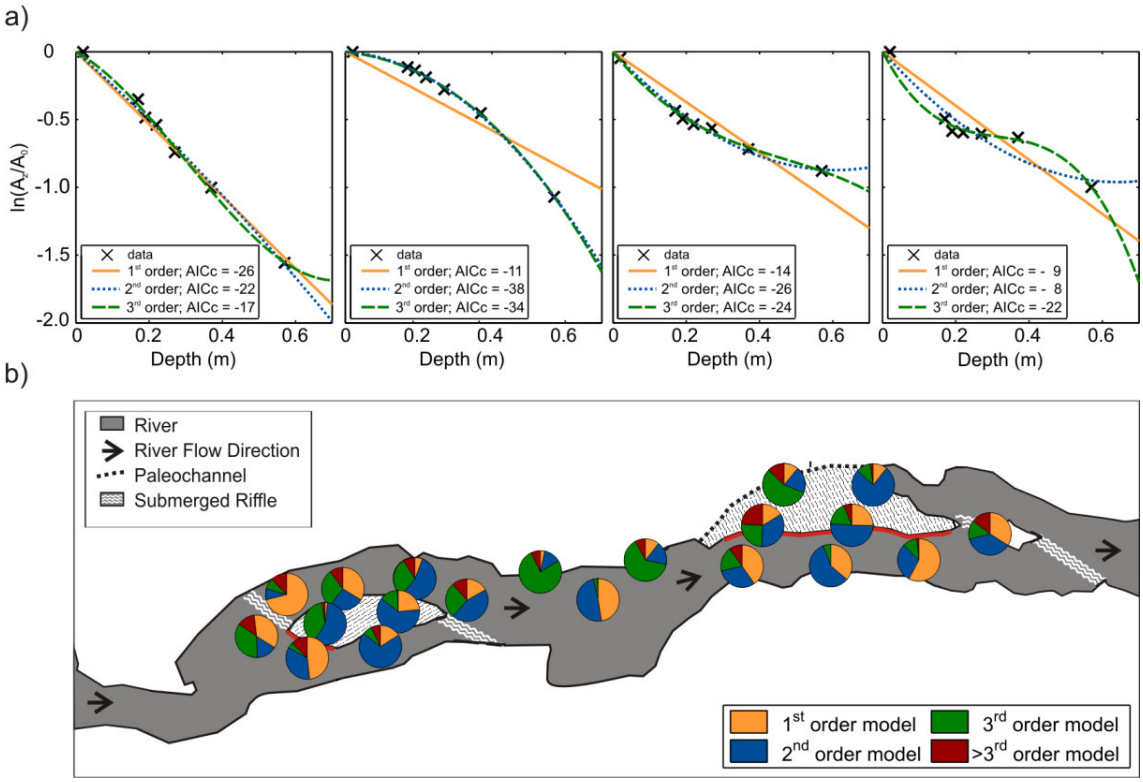

Figure 2.6: (a) Four experimental amplitude ratio profiles for the head of the gravel bar, fitted model set and corresponding performance measures; shown is the Akaike Information Criterion with corrections for finite sample size (AICc) and (b) schematic showing relative frequency of best supported model for all observation points for the observation period. Position of the pie diagrams correspond to the measurement location.

of the fitted polynomial at the head and tail of the meander were 0.40 m (STD = 0.12 m) and 0.43 m (STD = 0.14 m), respectively. This subsurface flow geometry was caused by the presence of a highly permeable layer in these profiles. The strongest vertical water flows at the head and tail of the meander were located at depths of about 0.40/0.43 m ± 0.12/0.14 m below the riverbed, respectively. These findings agreed with previous observations in heterogeneous riverbeds, which showed that riverbed layering creates zones with higher vertical exchange fluxes through zones of higher hydraulic conductivity (Lautz et al., 2010; Salehin et al., 2004). The analysis presented here allows easy identification and location of such preferential exchange patterns without a detailed knowledge of the subsurface hydraulic conductivity (i.e. $a_3 \neq 0$).

Only a minor part of the amplitude ratio profiles was not fitted well with the models of lower complexity of $n \leq 3$ (Fig. 2.6b). In these cases higher order models were needed to show a reliable fit indicating complex patten in the decrease of $ln(AR_z(t))$ with depth. Such complexity was most likely introduced by transient exchange flux and associated temperature signal non-stationarity (cf. Appendix 2.C).The results highlight the fact that models of different complexity can be clearly ranked, allowing full consideration of the best supported model in terms of model residuals and model complexity.

Minimizing the AICc for model selection is easy to assess and interpret. Evidence ratios of LRT allow a formal test of the evidence of alternative models. The model selection provides the shape of $ln(AR_z(t))$ and the optimised shape parameter (a_2). Both are related to river-GW exchange flow deviation from the one-dimensional vertical direction.

2.4.4 Spatial patterns of river-GW flow deviation

To identify the spatial pattern in subsurface flow geometry, we applied a hierarchical time series clustering to the time series of a_2. The polynomial parameter a_2 is defined as a measure quantifying the deviation from the one-dimensional vertical flow even if the third order polynomial was identified as the best supported model ($a_3 \neq 0$). The resulting dendrogram displays two main clusters (Fig. 2.7). The first main cluster included all observations located at the thalweg and the head of the geomorphological features,

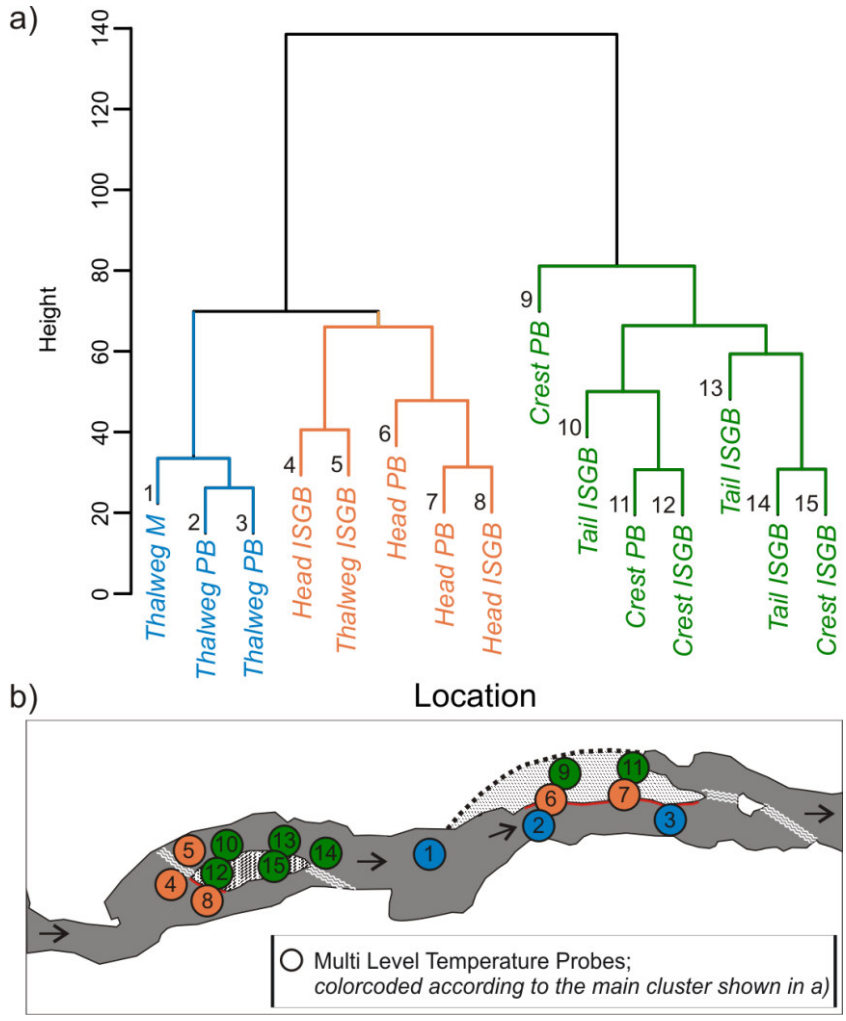

Figure 2.7: (a) Cluster Dendrogram, y-axis showing the intergroup distance at which the time series were combined into a single cluster. (b) Schematic showing the distribution of the main clusters at the study site.

whereas the second included all observations at the crest and the tail of the geomorphological features. Further subclasses were not well separated from each other. Common clustering techniques such as hierarchical clustering, k-means and density-based clustering were tested to identify spatial structures. All methods applied provided identical clustering results.

The clustered time series clearly differed as to their spatial position along the geomorphological structures. Observations located at the thalweg and at the head of the geomorphological structures clearly diverged from observations at the crest and tail of the geomorphological structures. Differences between observations at the same relative position (head, crest and tail) along the geomorphological structure were of minor importance and partly mix in different sub-clusters. For the left cluster, representing the thalweg and head of the geomorphological structures, a subdivision was possible with the exception of one observation at the thalweg close to the in-stream gravel bar (point 5, Fig 2.7b). The difference might result from that point not being located in a completely flat part at the thalweg. Furthermore, it might belong to a long, stretched, submerged riffle, presumed less relevant during installation. In contrast, no clear subdivision of the right cluster between crest and tail locations was possible.

These results highlight that the geometry of subsurface water flow clearly differed between the relative locations of the observation points along the geomorphological structures. Points where river water infiltrates into the riverbed at the thalweg and at the head of the geomorphological structures can be clearly separated from points at the crest and tail of the geomorphological structures. These findings agree with the numerical investigations of Trauth et al. (2015) who applied multiple steady state three-dimensional Computational Fluid Dynamics simulations for several steady state scenarios of stream discharge for the same in-stream gravel bar. Their simulations resulted in identical spatial patterns of hyporheic infiltration and exfiltration locations at the riverbed around the in-stream gravel bar and losing conditions within the river channel (Trauth et al., 2015).

2.4.5 Temporal dynamics of river-GW flow deviation

The temporal dynamics of the subsurface flow geometry was influenced by the river level. Figure 2.8 shows the logarithmic relation between river level and flow deviation from the one-dimensional direction quantified by a_2. The corresponding model accuracy is presented in Figure 2.8. Also the observation points at the head and the crest of the geomorphological structures show that logarithmic relation as in Fig. 2.8a with R^2 ranging between 0.6 and 0.9. No significant relationship was found between hydraulic gradients and a_2. Thus, the river level, determining the lateral hydraulic gradient across the geomorphological structures, was the main driver for the subsurface flow geometry.

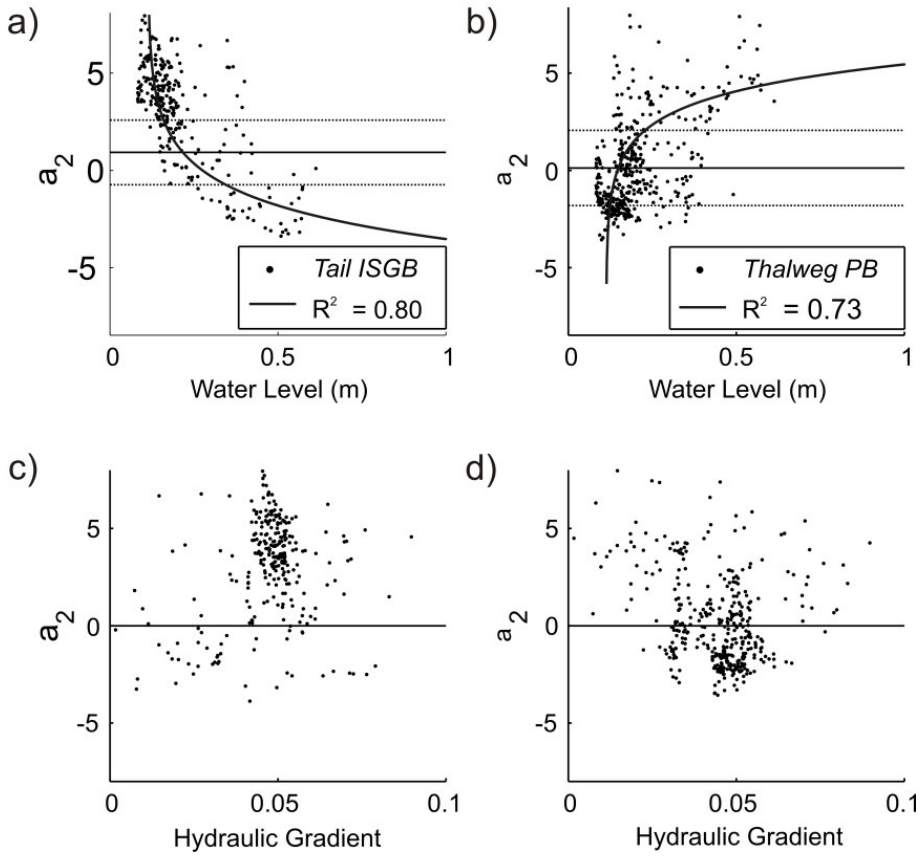

Figure 2.8: Scatterplot of water level vs. deviation of river-GW exchange from the one dimensional vertical direction (a_2) with optimized logarithmic model (a, b) and scatter plot of hydraulic gradient vs. a_2 (c, d) for one observation point at the tail of the in-stream gravel bar (ISGB) (a, c) and at the thalweg of the point bar (PB) (b, d).

For most periods, the observation points at the thalweg were characterised by one-dimensional vertical fluxes ($a_2 \sim 0$, Fig. 2.8). All observation points at the head, crest and tail of the geomorphological structures were characterised by hyporheic exchange flux ($a_2 > 0$; cf. Fig. 2.3a) as long as the river level was below 0.2 m (Fig. 2.8). With decreasing a_2 the vertical flow component increases as a result of changes in the in-/exfiltration areas of the hyporheic flow cell with respect to the observation point. With increasing river levels (increasing lateral hydraulic gradients), the flow system changed to strong horizontal advective fluxes through the riverbed, limiting the penetration depth of the daily temperature signal. ($a_2 < 0$; Fig. 2.3b). Parts of geomorphological structures more than 0.17 m below the water table were characterized by upwelling fluxes from the groundwater or static water (amplitudes close to zero).

These flow patterns go along with the relationship found in 2.4.2: formation of a distinct hyporheic flow cell across the geomorphological structures as well as a river level-dependent subsurface flow regime. River water infiltrates at the head, flows through the point bar / in-stream gravel bar and exfiltrates back to the secondary river channel at the tail of the structures. For all locations, the horizontal flow component dominates. The

hyporheic flow cell develops independently of the vertical hydraulic gradient (losing condition) and remains persistent over time until the geomorphological structure becomes submerged. The flow system changes from a distinct hyporheic flow cell across the point bar / in-stream gravel bar to a dominant losing condition with a significant vertical flow component in the riverbed.

2.5 Conclusions

In this paper, we developed a methodology to analyse the geometry of subsurface water flux using vertical riverbed temperature profiles. Beyond the one-dimensional vertical water flow in the riverbed sediment, major flow patterns could be identified. The deviation from the one-dimensional vertical flow and thus the magnitude of horizontal water flux was quantified by fitting the parameter (a_2) of a 2nd order polynomial to the observed amplitude ratios. The amplitude ratios were directly extracted from measured riverbed temperatures. The more the river-GW flux deviated from the one-dimensional vertical flow direction, the greater the non-linearity in the amplitude ratios and the higher the absolute value of the 2nd order parameter a_2. The presented framework has great potential to be able to automatically check for significant deviations from the one-dimensional vertical flow direction (i.e. $a_2 \neq 0$) before applying standard analytical methods to estimate magnitudes of subsurface water fluxes (flow velocity). It furthermore could be used to prove the effect of river restoration activities like the artificial introduction of geomorphological structures to enhance hyporheic exchange.

We applied this approach over a two-year period, covering a broad range of hydrological conditions with peak discharges of up to a hundred times the minimum discharges, in a losing reach of a gravel bed river. We systematically evaluated the subsurface flow geometry in riverbed sediments, as well as the spatial patterns and temporal dynamics of river-groundwater exchange flux around characteristic in-stream geomorphological structures. The results highlight the fact that river groundwater exchange flux at the head, crest and tail of geomorphological structures significantly deviated from the one-dimensional vertical flow, having a significant horizontal advective component. These spatial patterns of water flow persisted as long as the geomorphological structures were not completely submerged. The penetration depth of surface water into the riverbed sediments strongly depended on river level.

The presence of horizontal advective water and the associated heat flux within the shallow riverbed creates unique environments with potential implications for the spatial and temporal dynamics of biogeochemical processes and related reaction kinetics, which should be addressed in future work.

APPENDIX 2.A: Operation time of pressure and temperature devices between June 2011 and July 2013

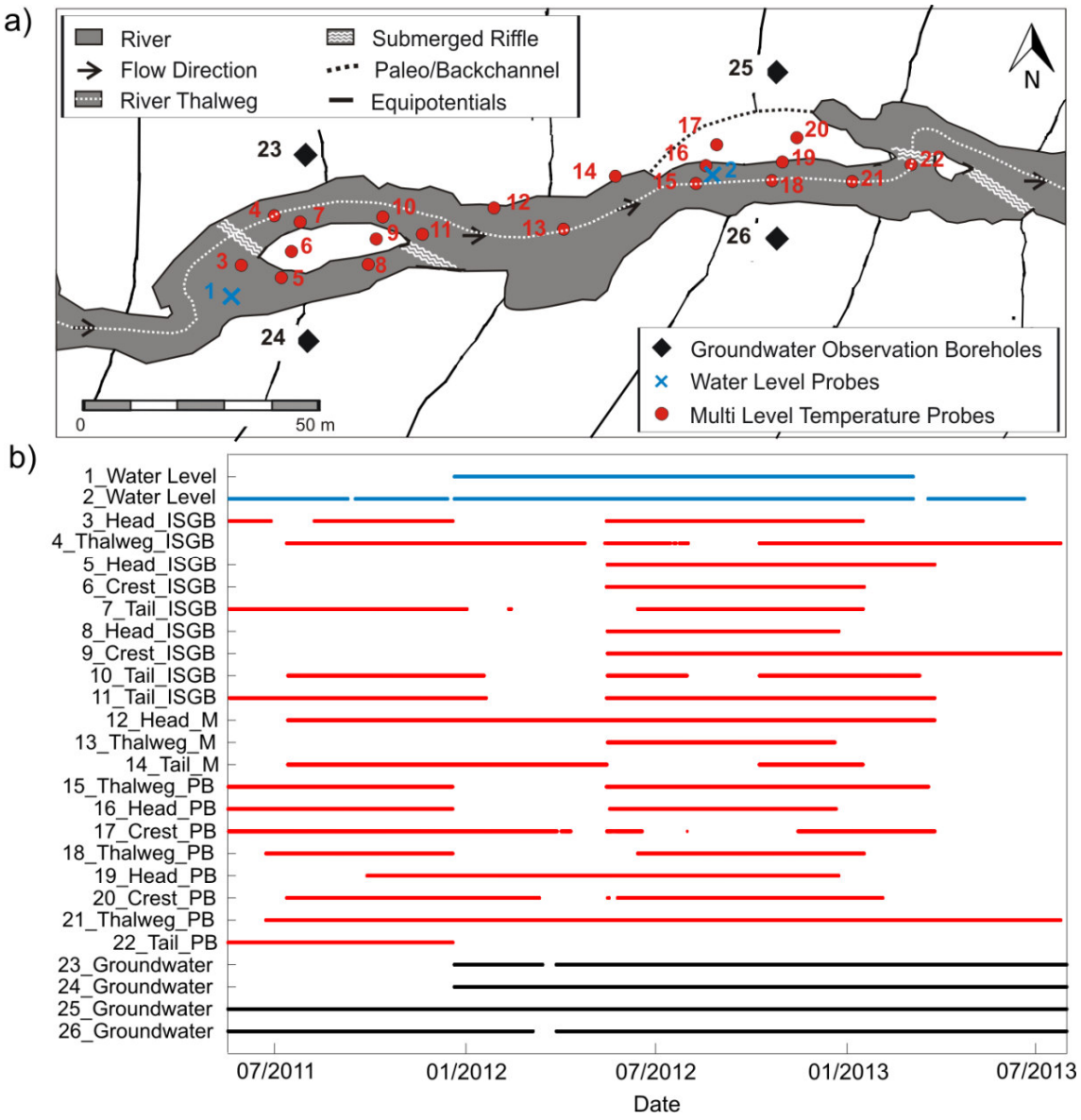

Figure 2.A1: (a) Schematic showing experimental infrastructure with water level recorders, Multi Level Temperature Probes and groundwater observation boreholes (for identical assignment, each sensor category is numbered from left to right) and (b) schematic showing the time of operation of each sensor free from defects or maintenance (the given numbers correspond to the specific location given in (a)).

APPENDIX 2.B: Relation between polynomial coefficient a_2 and magnitude of horizontal subsurface flow

To validate the relationship between subsurface flow geometry and the shape parameter of the second order polynomial (a_2) we used transient 2D forward numerical simulation of coupled water flow and heat transport in HydroGeoSphere (Brookfield et al., 2009, Therrien et al., 2010). The numerical model follows the setup presented in Cranswick et al. (2014), to numerically simulate surface water groundwater exchange fluxes. The model domain was 20 m wide (x-direction) and 4 m deep (z-direction). The 2D horizontal/vertical mesh discretisation was 0.1 m/0.02 m. The Hydraulic and Thermal Parameters Used in 2D numerical simulation are listed in Table 2.B1.

Table 2.B: Hydraulic and thermal parameters used in 2D numerical simulation.

Parameter	Value	Unit
Hydraulic conductivity	3.5×10^{-04}	m s^{-1}
Porosity	0.35	(-)
Dispersivity horizontal/vertical	0.01/0.001	m
Specific heat capacity of solid	1600	J kg^{-1} °C^{-1}
Thermal conductivity of solid	2.4	W m^{-1} °C^{-1}
Bulk density	1800	kg m^{-3}

2.B1 Hyporheic exchange

Flow boundaries were assigned as the constant flux boundary at the top of the domain from x = 0 to x = 6.5 m (q_SFW_{in}) and from x = 13.5 m to x = 20.0 m ($q\_SFW_{out} = - q\_SFW_{in}$). A time variable temperature was specified on top of the domain using a sinusoidal diel temperature variation with a mean temperature of 12 °C and an amplitude of 3 °C. All other boundaries are no-flow. An initial model set was designed to simulate hyporheic exchange flux. Therefore, q_SFW_{in}/q_SFW_{out} were set as 1 m^3 d^{-1} (Fig. 2.B1); 0.25 m^3 d^{-1}, 0.5 m^3 d^{-1} and 2 m^3 d^{-1}.

Synthetic temperature observations were exported every 0.5 m (x-direction) at depths (z-direction) of 0.00 m, 0.05 m, 0.20 m, 0.22 m, 0.25 m, 0.30 m, 0.40 m and 0.60 m. Synthetic temperature observations were used to generate the Amplitude Ratio Profiles, which were evaluated using the presented model set. The derived shape parameter a_2 (describing the curvature of the second order polynomial) was compared to the normalized difference between the horizontal and vertical flux $(v_x - v_z) / \max(v_x - v_z)$, whereby positive values indicate the dominance of the vertical flow component and negative values indicate the dominance of the horizontal flow component. The comparison between polynomial parameter a_2 and the normalized difference between horizontal and vertical flux is shown in Figure 2.5a for all simulated q_SFW_{in}/q_SFW_{out}.

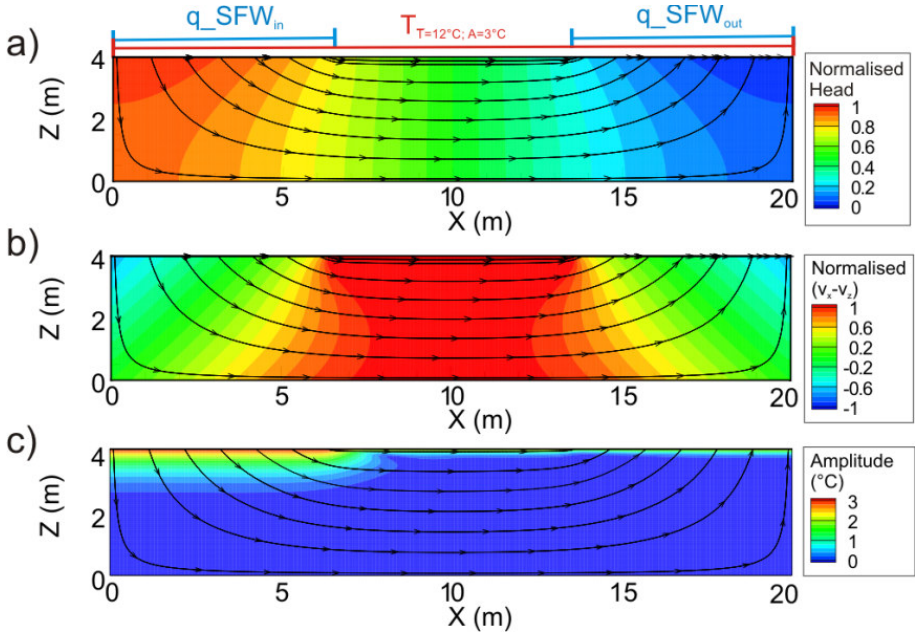

Figure 2.B1: (a) Calculated flow paths from numerical forward simulation in HydroGeoSphere showing hyporheic exchange (constant upper boundary q_SFW_{in}/q_SFW_{out} of 1 m^3 d^{-1} and sinusoidal temperature variation). Simulated and normalized hydraulic heads show the drop in hydraulic head from the inflow to the outflow boundary.

(b) Normalised difference between horizontal (v_x) and vertical (v_z) flow velocity, showing the dominance of the vertical flow component at the sides of the inflow and outflow boundaries, whereas the horizontal flow component is dominant at the centre of the hyporheic flow cell.

(c) Simulated amplitudes showing a deeper penetration of the temperature signal at the inflow boundaries and a shallow penetration of the temperature signal at the centre and the outflow of the hyporheic flow cell.

2.B2 Dominant horizontal flux parallel to the surface

For a second model set, the constant flux boundaries were assigned at the sides of the domain as 12 m^3 d^{-1} (Fig. 2.B2); 1 m^3 d^{-1}, 3 m^3 d^{-1}, 6 m^3 d^{-1}, 6 m^3 d^{-1}, 12 m^3 d^{-1} , 24 m^3 d^{-1}; to simulate dominant horizontal flux parallel to the surface (top boundary) with significant groundwater contribution. The high exchange flux was chosen according to field estimates of water flux across the observed, partly submerged geomorphological structures. A time-variable temperature was specified on top of the domain ($z = 0$ m) using a sinusoidal diel temperature variation with a mean temperature of 12 °C and an amplitude of 3 °C and a constant temperature of 8 °C was assigned to the left side of the domain ($x = 0$ m). All other boundaries were no-flow. Simulated temperatures were exported every 1 m (x-direction, from $x = 3$ m to $x = 8$ m) at depths (z-direction) 0.00 m, 0.05 m, 0.20 m, 0.22 m, 0.25 m, 0.30 m, 0.40 m and 0.60. Processing of the temperature data was as described in B.1. The comparison between polynomial parameter a_2 and the magnitude of horizontal flux is shown in Figure 2.5b for all simulated q_SFW_{in}/q_SFW_{out}.

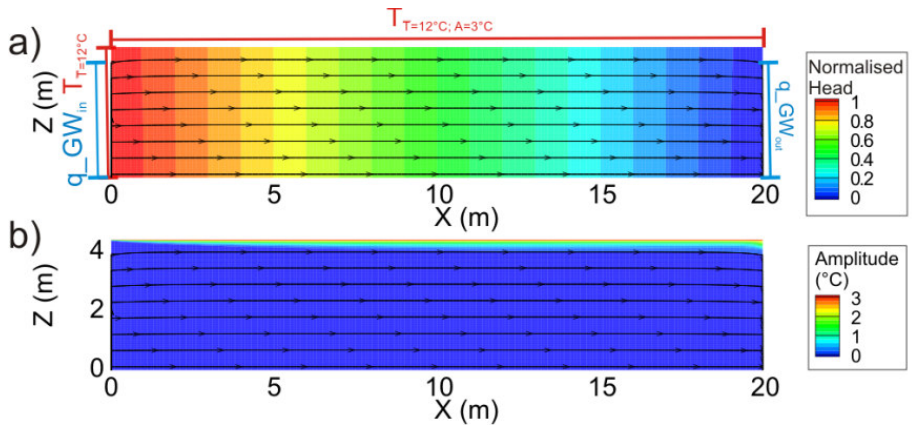

Figure 2.B2: (a) Calculated flow paths from numerical forward simulation in HydroGeoSphere showing horizontal water flux parallel to the surface (constant side boundary q_GW_{in} and q_GW_{out} of 12 m^3 d^{-1} and sinusoidal temperature variation on top of the domain). Simulated and normalized hydraulic heads show the drop in hydraulic head from the inflow to the outflow boundary.

(b) Simulated amplitudes showing a shallow penetration of the temperature signal and no variation of simulated temperatures at higher depths due to the high vertical exchange flux and heat transport.

APPENDIX 2.C: Influence of transient exchange flux and associated temperature signal non-stationarity on $ln(A_z/A_0)$ profiles

To investigate the extent to which rapid changes in the vertical water flux, and associated temperature signal non-stationarity, introduce an erroneous temporal spreading of estimated advective flow velocities (using the 1D analytical method), we followed the method of Rau et al. (2015). They found that rapid changes in exchange flux can introduce errors of up to 57 % in velocities and artefacts spanning +- 2 days compared to 1D analytical estimates. These findings highlight the sensitivity of subsurface temperatures to rapid changes in vertical water flux, which then also have the potential to cause significant changes in AR from linearity along with depth. We numerically simulated the subsurface temperature response to rapid changes in vertical flow velocities (all boundary conditions are set equal to those used in Rau et al. (2015)) to show the influence of transient exchange flux and associated temperature signal nonstationarity on $ln(A_z/A_0)$ profiles.

HydroGeoSphere (Brookfield et al., 2009, Therrien et al., 2010) was used for the transient (quasi) 1D forward numerical simulation of coupled water flow and heat transport. The model domain was 1 m wide (x-direction) and 30 m deep (z-direction). The horizontal/vertical mesh discretisation was 0.5 m/0.02 m. The hydraulic and thermal parameters used in the numerical simulation are listed in Appendix 2.B, Table 2.B.

A time-variable temperature was specified on top of the domain (z = 0 m) using a sinusoidal diel temperature variation with a mean temperature of 20 °C and an amplitude of 3 °C, and a constant temperature of 20 °C was assigned to the bottom of the domain (z = 30 m). The initial temperature condition was set to 20 °C across the whole model domain. Transient flow boundaries were assigned at the top and bottom of the domain. Each simulation was conducted for 30 days, with a constant exchange flux assigned to the first 10 days, followed by a step change in exchange flux for another 20 days. The step change from 0 m d^{-1} to -0.01 m d^{-1}, -0.1 m d^{-1}, -0.5 m d^{-1}, -1.0 m d^{-1} and -5.0 m d^{-1} was applied at eight different times of the specified day at 0, +3 h, +6h, +9h, +12 h, +15 h, +18 h and +21 h relative to the harmonic boundary (for details of the model set-up, cf. Rau et al. (2015)).

Synthetic temperature observations were exported depths (z-direction) 0.00 m, 0.05 m, 0.20 m, 0.22 m, 0.25 m, 0.30 m, 0.40 m and 0.60 m. Synthetic temperature observations were used to generate the Amplitude Ratio Profile and thus to evaluate the influence of transient exchange flux on $ln(A_z/A_0)$ profiles (Fig. 2.C1).

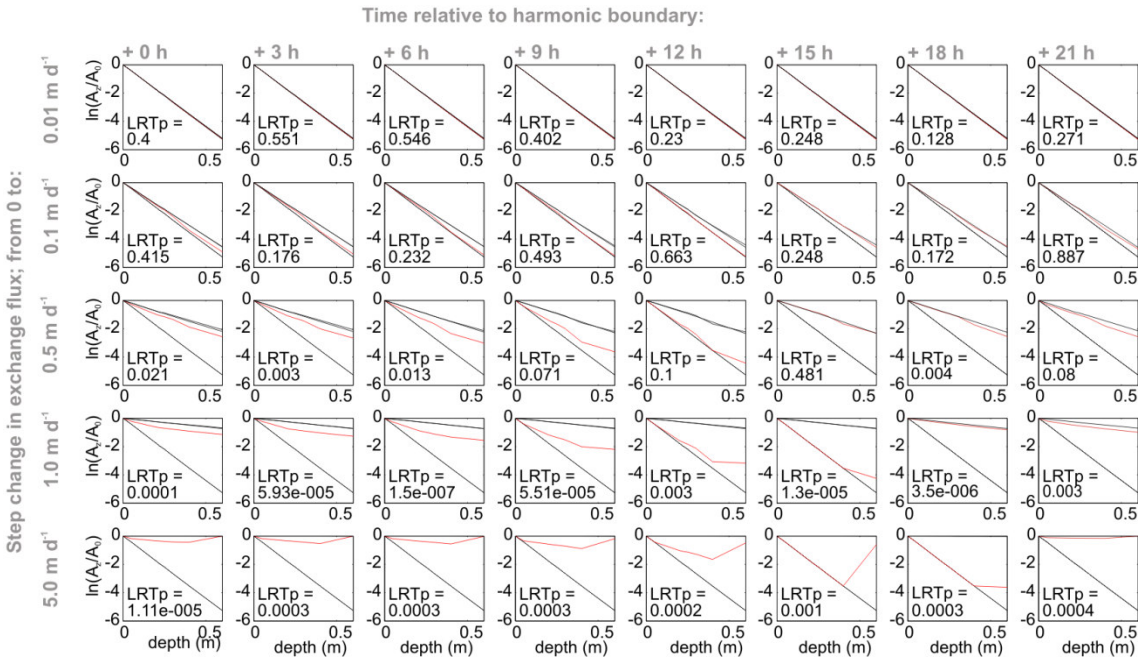

Figure 2.C1: Amplitude ratio profiles of days 8 - 12 for step change in exchange flux from 0 m d^{-1} to 0.01 m d^{-1}, 0.1 m d^{-1}, 0.5 m d^{-1}, 1.0 m d^{-1}, 5.0 m d^{-1} (rows, exchange flux is in downward direction) applied at eight different times of the specified day – in 0, +3 h, +6h, +9h, +12 h, +15 h, +18 h, +21 h relative to the harmonic boundary (columns). The most affected $ln(A_z/A_0)$ occuring on day 10 or 11 (depending on the time when the step change was applied and exchange flow direction) is colored in red. The Likelihood Ratio Test test p-value (LRTp) for comparing the performance of the 1st and 2nd order models. An LRTp < 0.05 provides evidence for the complex model against the reduced model, e.g. that the more complex model fits the data significantly better.

For all simulations with step changes in exchange velocity <= -0.1 m d^{-1} the 1^{st} order polynomial (linear case) was clearly identified as the best supported model with respect to model residuals and model complexity. For step changes in exchange velocity >= -0.5 m d^{-1} higher order polynomials (5^{th} – 6^{th} order) were identified as the best supported model. Thus, only these 5^{th} – 6^{th} order polynomials provide a reliable fit to the complex $\ln(A_z/A_0)$ profiles effected by high step changes in exchange velocity.

These results highlight the fact that transient exchange flux and associated temperature signal non-stationarity have a significant impact on $ln(A_z/A_0)$ profiles. However, these impacts on $ln(A_z/A_0)$ profiles can only be described by 5^{th} – 6^{th} order polynomials. As long as the $ln(A_z/A_0)$ profile is better described by the 1^{st} – 3^{rd} order polynomials, we assume these profiles to be affected by continuous changes in the subsurface flow field and not affected by high step changes in exchange velocity.

3 Estimation of vertical water fluxes from temperature time series by the inverse numerical computer program FLUX-BOT

An article with equivalent content has been published as: Munz M and C. Schmidt (2017), Estimation of vertical water fluxes from temperature time series by the inverse numerical computer program FLUX-BOT, Hydrological Processes, 31:2713–2724. https://doi.org/10.1002/hyp.11198.

Abstract

The application of heat as a hydrological tracer has become a standard method for quantifying water fluxes between groundwater and surface water. The typical application is to estimate vertical water fluxes in the shallow subsurface beneath streams or lakes. For this purpose, time series of temperatures in the surface water and in the sediment are measured and evaluated by a vertical 1D representation of heat transport by advection and conduction. Several analytical solutions exist to calculate the vertical water flux from the measured temperatures. While analytical solutions can be easily implemented, they are restricted to specific boundary conditions such as a sinusoidal upper temperature boundary. Numerical solutions offer higher flexibility in the selection of the boundary conditions. This, in turn, reduces the effort of data preprocessing, such as the extraction of the diurnal temperature variation from the raw data. Here, we present software to estimate water fluxes based on temperatures- FLUX-BOT. FLUX-BOT is a numerical code written in MATLAB that calculates vertical water fluxes in saturated sediments based on the inversion of measured temperature time series observed at multiple depths. FLUX-BOT applies a centered Crank-Nicolson implicit finite difference scheme to solve the one-dimensional heat advection-conduction equation. FLUX-BOT includes functions for the inverse numerical routines, functions for visualizing the results as well as function for performing an uncertainty analysis. We present applications of FLUX-BOT to synthetic and to real temperature data to demonstrate its performance.

Keywords: Surface water-groundwater interaction, Heat tracing, Temperature time series, Vertical water flux, Numerical solution

3.1 Introduction

Heat as a hydrological tracer has become a standard tool for quantifying water fluxes between groundwater and surface water. Most studies applying heat as a tracer conceptualize heat transport at the groundwater- surface-interface (GWSI) as a one-dimensional process, where the observed temperatures are used to determine vertical water fluxes. Because temperatures can be easily measured over time with self-contained temperature loggers, heat tracing methods are capable of estimating vertical water fluxes over time.

The most common heat signal that is traced in the subsurface is diurnal temperature variations, typically represented as sine functions, which are used as upper boundary condition in analytical solutions (Stallman, 1965; Hatch et al., 2006; Keery et al, 2007). Recent extensions to these analytical solutions allow the inclusion of the entire frequency spectrum into the estimation procedure (Wörman et al., 2012; Vandersteen et al., 2015). The processing and analysis of temperature time series based on analytical solutions have been implemented in relatively comprehensive codes such as Ex-Stream (Swanson and Cardenas, 2011) and in the code VFLUX (Gordon et al., 2012). A newer version (VFLUX 2, Irvine et al., 2015) includes analytical solutions that use both the amplitude ratio and the phase shift of the temperature signal simultaneously (McCallum et al., 2012; Luce et al. 2013).

Analytical methods can be relatively easy implemented but are limited to a functional representation of the boundary conditions. Temperature time series in the surface water can exhibit irregular patterns, arising from rain storms and associated flood events, snow melt etc., and do not follow a regular diurnal pattern that can be approximated with a sine curve. Under such conditions the application of a numerical heat transport model may be favourable because of their flexibility in terms of boundary conditions. There are several numerical model codes that simulate heat transport in porous media (e.g. VS2DH, HydroGeoSphere, and FEFLOW) but these advanced modelling frameworks may not be readily accessible, particularly for inexperienced users to routinely infer water fluxes between surface water and groundwater. There exist only a few one-dimensional numerical codes specifically developed for simulating and inverting vertical temperature profiles (Lapham, 1989; Voytek et al., 2013). Voytek et al. (2013) developed the free, stand-alone GUI 1DTempPro, which is based on the 2D Code VS2DH (Healy and Ronan, 1996) to estimate one vertical fluid flux for the given temperature time series based on a manual parameter optimization. 1DTempPro has been augmented to include automated parameter estimation, layer heterogeneity, and time-varying fluid flux estimation (Koch et al., 2015). However, the functionality of 1DTempPro to estimate variable fluid flux requires manual adjustment of fluid flux with time by point and

click via a simple graphical interface or alternatively initial estimates of time-varying exchange flux (Koch et al., 2015).

The limited applicability of analytical solutions when the required boundary conditions are not met and the lack of numerical models to process temperature time series without manual adjustments or initial estimates of the unknown time-varying exchange flux was the motivation to develop FLUX-BOT. The concept of FLUX-BOT was inspired by Lapham's pioneering work (Lapham, 1989), which applied a numerical solution to the 1D heat advection-conduction equation in a forward way. Such a numerical approach offers flexibility in the boundary conditions, the fully automated processing of vertical water flux varying in time and corresponding uncertainty estimates which are crucial for comparing vertical exchange fluxes in space and time. This, in turn, reduces the effort of data pre-processing such as the extraction of the diurnal temperature variation from the raw data.

In this paper we present and test the computer program FLUX-BOT which is written in MATLAB. FLUX-BOT solves the one-dimensional heat advection-conduction equation on a finite difference subsurface domain. Time series of vertical water fluxes are inverted from observed sediment temperatures. We demonstrate the capabilities and the workflow of FLUX-BOT on synthetic examples with known fluxes and on real world case studies comprising temperature profiles with many harmonic, trend, and noise components. FLUX-BOT includes functions for the inverse numerical routines, functions for visualizing the results as well as a function to perform an uncertainty analysis.

3.2 Methods

3.2.1 The program

FLUX-BOT is a collection of functions written in MATLAB R2010a (The MathWorks, Inc., Natick, MA) that calculates vertical water fluxes in saturated sediments based on the inversion of measured temperature time series. In principle, FLUX-BOT should be compatible with GNU Octave, although it has not been tested. The one-dimensional heat advection-conduction equation is solved applying the cell-centered Crank-Nicolson implicit finite difference scheme. FLUX-BOT finds the vertical water flux that minimizes the sum of squared differences between measured and modelled temperatures over a user-defined time period. The advantages and limitations of FLUX-BOT are summarized in Table 3.1.

FLUX-BOT parameter setting and execution is done via the MATLAB Command Window within the main script (*fluxbotscript_yourexample*; example files are provided at https://bitbucket.org/flux-bot/flux-bot, see Data and Code availability), passing all variables and instructions to the incorporated functions without any further user input. Optionally, the program can be used solely for data post processing, e.g. data visualization and uncertainty analysis. Figure 3.1 shows an execution flowchart underlying the FLUX-BOT program. Detailed instructions to run FLUX-BOT are provided in the user manual (https://bitbucket.org/flux-bot/flux-bot).

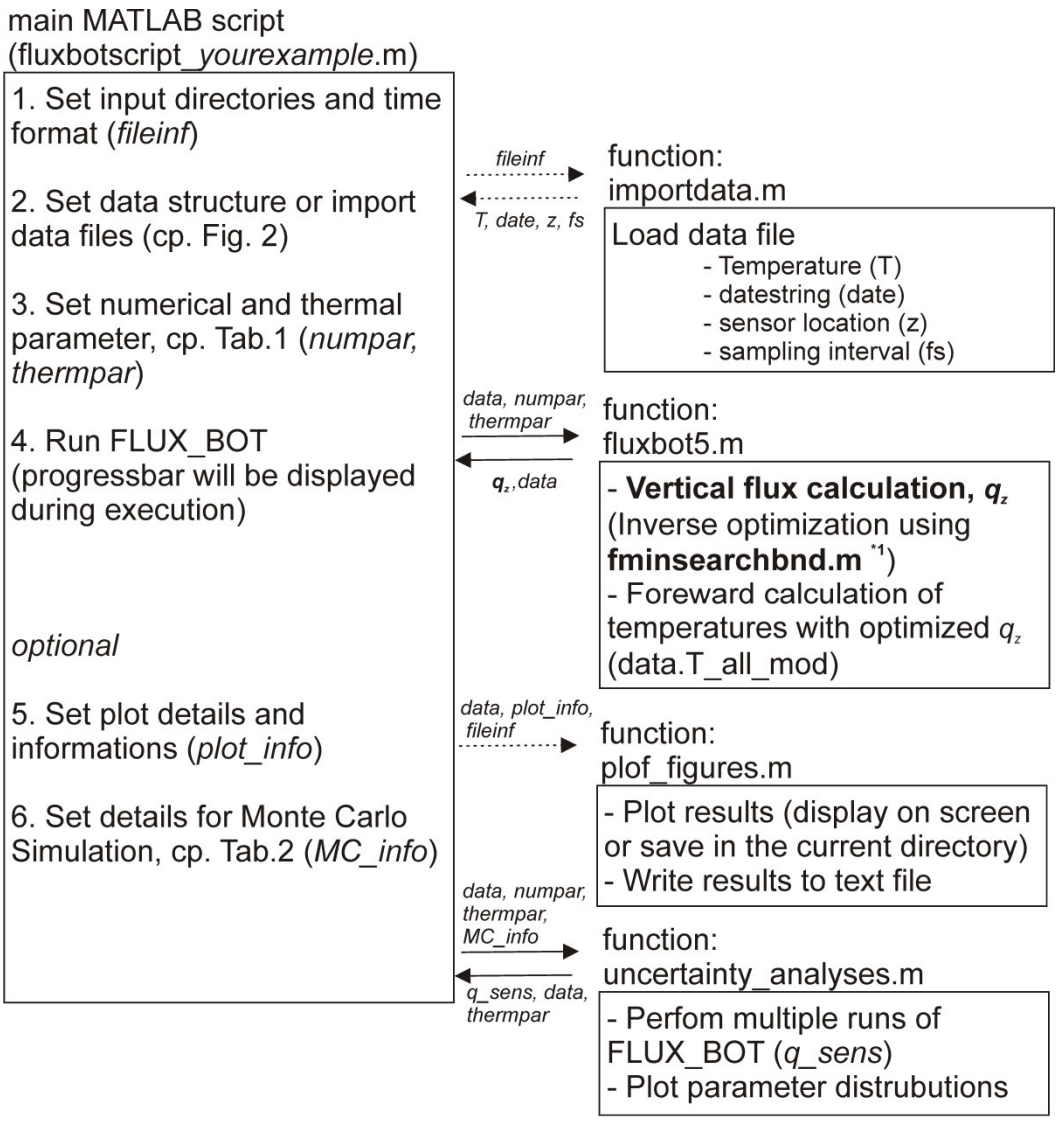

*1 bounded optimization implementing the Nelder-Mead method (D'Errico, 2006)

Figure 3.1: FLUX-BOT program execution flowchart, highlighting main parameter setting and data handling between involved MATLAB functions.

Table 3.1: Main advantages and disadvantages of the FLUX-BOT model

Advantages	Disadvantages / Limitations
Flexibility in the boundary conditions	At least three measuring depths are required [*1]
Minimal effort for preprocessing, e.g. filtering	A single vertical flux is estimated for the entire domain [*2]
The goodness of fit can be derived immediately by comparing measured and modeled temperatures	
Handy evaluation of parameter uncertainty (uncertainty bounds)	

[*1] where the shallowest and deepest measuring depths serve as boundary conditions
[*2] standard analytical methods are based on the analysis of pairs of temperature sensors

3.2.1.1 Vertical water flux calculation

Heat transport at the GWSI, conceptualized as water saturated porous medium, can be described by the 1D advection-conduction equation as proposed by Stallman (1963):

$$\frac{K_{fs}}{\rho c}\frac{\partial^2 T}{\partial z^2} - q_z \frac{\rho_f c_f}{\rho c}\frac{\partial T}{\partial z} = \frac{\partial T}{\partial t} \tag{3.1}$$

where K_{fs} is the thermal conductivity of the saturated sediment (Js^{-1} m^{-1} °C^{-1}), T is the measured temperature (°C) at depth z (m) (positive = downward); t is time (s); q_z is the vertical Darcy flux (L m^{-2} d^{-1}) (positive = downward); ρc is the volumetric heat capacity of the solid-fluid system. ρc can be written as $\rho c = n\rho_f c_f + (1-n)\rho_s c_s$, where $\rho_f c_f$ is the volumetric heat capacity of the fluid $\rho_s c_s$ is the volumetric heat capacity of the solids (J m^{-3} °C^{-1}) and n is the porosity (-). The magnitude and direction of q_z is a result of Darcy flow, which is controlled by the hydraulic conductivity as the product of the hydraulic conductivity and the total head gradient. In the case of a q_z of zero, Eq. 3.1 reduces to the Fourier equation of heat conduction.

In FLUX-BOT, Eq.3.1 is solved numerically by a cell-centered, finite difference Crank-Nicolson numerical scheme. With this, FLUX-BOT calculates the temperatures in each cell for a given, constant q_z and time-varying upper and lower temperature boundary conditions over a certain time increment (time window with specified window length). In order to perform the inverse modelling, and estimate q_z from the observed temperatures, the derivative-free Nelder-Mead simplex optimization method, as implemented in MATLAB, is applied (Lagarias et al., 1998). The optimization for q_z is not carried out for each observation but for a time window, where q_z is assumed to be constant. If the optimization would be performed for each observation, changes in the observed temperatures, i.e. arising from the diurnal temperature cycle, would be treated as a change in q_z

which could not be distinguished from a real change in vertical Darcy flux. A typical choice of the window length would be 24 h, where the effect of the diurnal temperature variation would be effectively excluded from the estimation of q_z (quasi steady state temperature condition). In FLUX-BOT the first estimate of q_z is performed for a time window (temperature subset) beginning at the user defined initial time of the temperature time series. Then the time window is shifted forward; that is, excluding the first temperature data points of the series and including the next temperature data points following the original subset in the series. This process is automatically repeated over the entire data series, providing time varying flux estimates (constant for each time window) across the entire temperature time series. To obtain a constant q_z over a certain time window, the objective function to be minimized (E) is represented by:

$$E = \sum_{l=1}^{wl} \sum_{j=1}^{n_z} \left[T_{jl}^{OBS} - T_{jl}^{SIM} \right]^2 \tag{3.2}$$

where T_{jl}^{OBS} and T_{jl}^{SIM} are the measured and simulated sediment temperatures at depth j over observation depths n_z and for a time window, wl, of length l.

To run FLUX-BOT, an individual input of the volumetric heat capacity and the thermal conductivity of the saturated sediment and temperature time series with the corresponding depth information is necessary (Fig. 3.2). Table 3.2 provides parameters to control the cell size of the numerical mesh, the termination tolerance for the optimization algorithm, the window length and the amount of overlap between the windows. In order to avoid too strong fluctuations in the estimated q_z, a maximum rate of change ('*Slope*') of the estimated q_z between subsequent windows can be specified. All parameters and out-

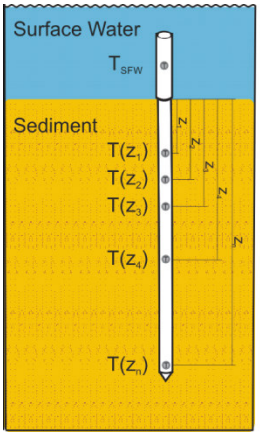

Time	0	z_1	z_2	z_3	z_4	....	z_n
t_1	$T_{SFW}(t_1)$	$T(z_1,t_1)$	$T(z_2,t_1)$	$T(z_3,t_1)$	$T(z_4,t_1)$	....	$T(z_n,t_1)$
t_2	$T_{SFW}(t_2)$	$T(z_1,t_2)$	$T(z_2,t_2)$	$T(z_3,t_2)$	$T(z_4,t_2)$	....	$T(z_n,t_2)$
....	....	....	....	....	....	....	....
t_m	$T_{SFW}(t_m)$	$T(z_1,t_m)$	$T(z_2,t_m)$	$T(z_3,t_m)$	$T(z_4,t_m)$	....	$T(z_n,t_m)$

e.g.:

Time	0	0.15	0.20	0.25	0.35	0.55
01.01.2011 00:00:00	15.71	16.22	16.05	16.05	15.95	15.88
01.01.2011 00:10:00	...	...	...	...	...	...

Figure 3.2: (Left) Typical design of a Multi-Level Temperature Probe showing one temperature sensor installed in the surface water and five temperature sensors installed in the saturated sediment. (Right) Corresponding temperature input file for FLUX-BOT.

puts are described in detail in the FLUX-BOT user manual. If FLUX-BOT execution terminates successfully, the individual results of FLUX-BOT are returned to the MATLAB main menu as a data matrix of time (median time of the time window) and q_z, as well as data structures containing the simulated temperatures for each time step and each temperature sensor.

If option to visualize the FLUX-BOT results is selected prior to model run the optimized time series of q_z (L m^{-2} d^{-1}) the time series of observed and simulated temperatures as well as the temperature residuals, and a scatter plot of observed versus simulated temperature are displayed. The scatter plot includes the 1:1 line and the goodness of fit measures from the Root Mean Square Error (RMSE), Nash-Sutcliffe-Efficiency (NSE) and Correlation Coefficient (CC) for each temperature sensor not used as model boundary condition.

Table 3.2: FLUX-BOT input parameters to calculate vertical darcy velocities

Parameter	Value	Unit	Description	Requirements
rc	3.76×10^{6} *^ / 3.2×10^{6} ^	$Jm^{-3}°C^{-1}$	Vol. heat capacity of the saturated sediment	Positive integer
rfcf:	4.18×10^{6}	$Jm^{-3}°C^{-1}$	Volumetric heat capacity of water	Positive integer
kfs	1.58*' / 2.58^	$Js^{-1}m^{-1}°C^{-1}$	Thermal conductivity of the saturated sediment	Positive integer
dz	0.005	m	Vertical mesh width	Specific portion of *z* (at least ½)
wl	24	h	Length of time window for T optimisation	Depends on variability in T
R	24	h	Time shift of moving window for subsequent q_z estimates	For continuous q_z estimations R <= wl
Qzi	-2.3×10^{-5} * / 1.7×10^{-5} ^ / 3.5×10^{-5} ‘	L m^{-2} d^{-1}	Initial estimate of vertical Darcy velocity	Sufficient close to the real solution
Slope	10	-	Max change in q_z for subsequent time windows	Positive integer
tol	10^{-6}	-	Termination tolerance for fminserach	Standard value = 10^{-6}

* Generic Test case, synthetic temperature data
^ Real data test case, sandbox experiment
‘ Real data test case, riverbed temperatures

3.2.1.2 Sensitivity and uncertainty analysis

The FLUX-BOT program suite contains two additional functions to perform global sensitivity and uncertainty analysis. The aim of the sensitivity analysis was to identify

which input parameters significantly influence the estimate of q_z. The uncertainty analyses were used to assess the variability in estimated q_z in relation to the uncertainties in estimating the input parameters. To systematically vary the FLUX-BOT input parameters we used Monte Carlo sampling of 1000 points in the feasible parameters space, drawn from a multivariate normal distribution. Tested parameters are: heat capacity and thermal conductivity of the saturated sediment, sensor spacing, and temperature sensor accuracy. It has been recognized that uncertainties in thermal parameters and inaccuracy of temperature measurements and its spatial location can lead to large relative errors in the velocity estimates in particular for low flows (Constantz et al., 2003; Shanafield et al., 2011). Thermal parameters are rarely measured in streambed studies and most authors use literature values for thermal variables (e.g. Stonestrom and Blasch, 2003; Rau et al., 2014). An error in sensor spacing (likely up to 0.02 m) can occur as a result of incorrect installation of single temperature sensors or piezometers (Shanafield et al., 2011). Such depths errors do not occur if pre-assembled sensor arrays are applied. When the surface water temperature is used as upper boundary, the depths of streambed sensors below the streambed and therewith the sensor spacing might change over time because of erosion or accretion of sediment. Many different types of sensors can be used to collect temperatures over time. Varying the temperatures actually tests the sensitivity and uncertainty of the vertical flux estimates towards the uncertainty in temperature measurements. This uncertainty is a result of both the sensor precision and the sensor accuracy. Precision is a random error in measured temperature (the deviation from the mean of repeated measurements) whereas the accuracy is the systematic error between different temperature sensors. The accuracy of temperature sensors generally ranges between <0.01 °C for thermistor probes connected to advanced data loggers to up to 1.0 °C for some individually deployed ibutton thermistors and loggers (Shanafield et al., 2011). The accuracy of the Multi Level Temperature Stick (Umwelt und Ingenieurtechnik GmbH, Dresden, Germany) used in the application examples was 0.1 °C. Because the estimation procedure includes a temperature time series of about one day (144 data points) the estimated water flux should be rather insensitive to random errors while a systematic deviation from the true temperature potentially introduces errors in temperature based vertical flux estimates.

Using Monte Carlo sampling, the whole range of input parameters can be considered and varied at the same time. Optionally, Monte Carlo sampling can be run in parallel to make use of several processor cores in order to reduce overall computation time. If the functions should be run in parallel, user input of the number of cores available and the estimated run time of the FLUX-BOT routine is required.

Sensitivity Analysis

Parameter sensitivity was evaluated by applying the Regional Sensitivity Analysis (RSA) technique originally proposed by Hornberger and Spear (1981). The RSA evaluates the impact of changes in the model input parameters on the model output of interest, the vertical flow velocity. To conduct the RSA, FLUX-BOT was run 1000 times with the parameter sets created by the Monte Carlo sampling, drawn from a multivariate normal distribution. The sampled parameter population was partitioned into behavioural and non-behavioural subsamples. "Behavioural" means that a specific parameter set produced a vertical flux estimate (behaviour) that was within a certain flux tolerance (Saltelli et al., 2008). The categorisation into behavioural and non-behavioural was based on the Root Mean Square Error of synthetic/measured vs. estimated vertical flow velocities on a daily time interval. The magnitude of the RMSE was manually defined in a way that 10 % of all Monte Carlo simulations were classified as behavioural. This categorisation was than mapped back onto the input parameter population, each of which was thus also partitioned into behavioural and non-behavioural subsamples. For each of the four parameters tested, the cumulative distribution functions for the two subsamples were computed. A separation between the behavioural and non-behavioural cumulative distribution indicates that the tested parameter is sensitive, i.e. has an effect on the estimated vertical flux (Wagener et al., 2007; Saltelli et al., 2008). The significance of the effect each parameter has on the model output was estimated by the Smirnov two-sample test with a significance level of 0.1. The higher the value of the test statistics (d-stat), the more important the input parameter is in driving the behaviour of the model (Saltelli et al., 2008). RSA was performed for the synthetic test case and the sand box experiment where the true vertical fluxes were known or independent vertical flux measures were available.

Uncertainty analysis

To conduct the uncertainty analysis, FLUX-BOT was run 1000 times with the parameter sets created by the Monte Carlo sampling, with the uncertain input parameters assigned by multivariate uniform parameter distributions. Uncertainty bounds around the mean flux estimates through time were calculated as two times the standard deviation (2σ) of the 1000 FLUX-BOT realisations. The uncertainty bounds represent the uncertainty in a calculated vertical flow velocity due to the often unknown (uncertain) input parameters. All input parameters tested were uncorrelated, so that the selected values for each realisation are unrelated. This provides a standard procedure to compare different flux estimates (in space and time) and check whether they significantly differ from each other or not (Saltelli et al., 2008). Uncertainty analysis was performed for all presented test cases.

3.3 FLUX-BOT application and evaluation

To test the implementation of the numerical scheme and the functionality of FLUX-BOT we applied FLUX-BOT to three synthetic and real-data test cases. All test cases contained complex temperature signals containing many harmonic and trend components as well as a noise component.

3.3.1 Synthetic test case

3.3.1.1 Synthetic temperature data

Synthetic temperature profiles where generated using forward numerical simulation of the fully coupled water flow and heat transport model HydroGeoSphere (Brookfield et al., 2009; Therrien et al., 2010). The numerical model domain was 1 m wide (x-direction) and 30 m deep (z-direction). The horizontal/vertical mesh discretisation was 0.5 m/0.02 m. Common hydraulic and thermal parameters for gravelly to sandy material were used in the numerical simulations as rc = 3.76 × 10^6 J m^{-3} $°C^{-1}$, kfs = 1.58 J s^{-1} m^{-1} $°C^{-1}$, porosity = 0.3, hydraulic conductivity = 3.5 × 10^{-4} m s^{-1} (Stonestrom and Blasch, 2003).

A time-variable temperature boundary condition having multiple frequencies was specified on top of the domain (z = 0 m) using a synthetic temperature signal composed of a sum of multiple sinusoidal time series (daily and seasonal) and a gaussian random noise (Fig. 3.3). At the bottom of the domain (z = 30 m), a constant temperature of T_{mean} = 8 °C was assigned. The initial temperature condition was set to a uniform distribution of 8 °C across the whole model domain. Transient flow boundaries were assigned at the top and bottom of the domain. Exchange flux was incrementally increased from -2000 to 2000 L m^{-2} d^{-1} in steps of 100 L m^{-2} d^{-1}, each lasting 5 days. Positive values indicate downward water flux.

The simulated, synthetic temperatures were exported at depths of 0.01 m, 0.06 m, 0.11 m, 0.21 m, 0.23 m, 0.26 m, 0.31 m, 0.41 m and 0.61 m (Fig. 3.3). These depths correspond to a typical design of Multi Level Temperature Probes, as in Munz et al. (2016). The resulting temperature time series were then processed by FLUX-BOT using the same physical parameters (Table 3.2) as program input. FLUX-BOT was applied to the data set using different time windows in the range between 6 h and 72 h. The corresponding data files, scripts and functions are available at https://bitbucket.org/flux-bot/flux-bot.

3.3.1.2 Results

Figure 3.3 shows an example of the synthetic and simulated temperatures. The synthetic temperature signal at z = 0 was dominated by the daily temperature component over seasonal temperature component and white noise. The daily signal-to-noise ratio (calculated as $\frac{mean\ of\ daily\ Amplitudes}{\sigma\ of\ random\ noise}$) was 1.75. Figure 3.4a illustrates the estimated vertical flow velocity from FLUX-BOT relative to the initially defined, synthetic flow velocity. The flow velocity estimated with FLUX-BOT accurately matched the synthetic flow velocity. The estimated and synthetic temperatures were also in good agreement (Fig. 3.4b).

The highest deviation between synthetic and estimated vertical flow velocity occurred in the range between 100 to 300 L m^{-2} d^{-1}, with a difference of up to 70 % of the synthetic flow velocity. These inaccuracies were caused by the specific temperature conditions during this period, when the surface water temperature equals the groundwater temperature and when daily temperature amplitudes were low (Fig. 3.3); that is, neither substantial temporal nor spatial temperature variations occur in the subset (time window length equal to one day) of the temperature time series. Surface water and groundwater temperatures typically converge for certain time periods during spring and autumn in moderate climates. During these periods also the daily temperature amplitudes in the surface water might diminish, especially for heavily clouded condition and extreme discharges.

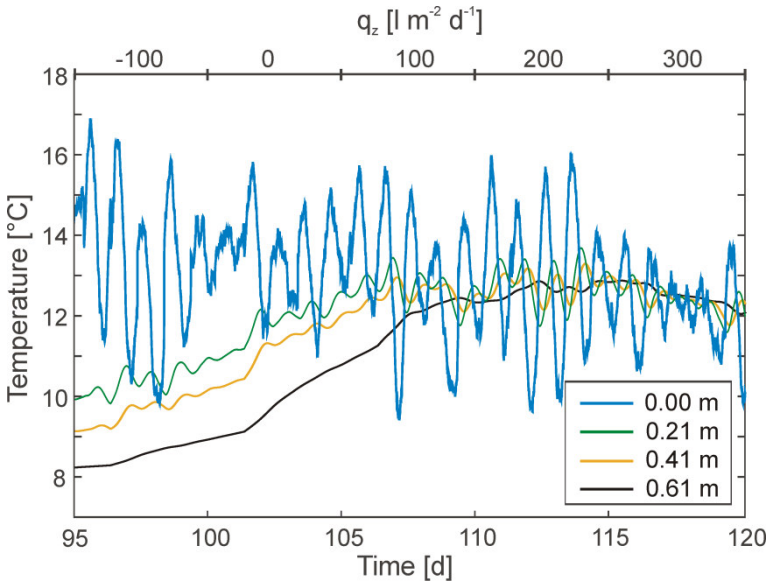

Figure 3.3: Example of synthetic temperatures at z = 0.0 m, 0.21 m, 0.41 m and 0.61 m for exchange flux between -100 L m^{-2} $d^{-1}$and 400 L m^{-2} d^{-1} (positive downward), each lasting for 5 days. The temperature at z = 0.0 m was specified by a sinusoidal, seasonal temperature cycle with a mean Temperature of 8 °C and a temperature Amplitude of 6°, a sinusoidal, daily temperature cycle with zero mean and randomly chosen temperature Amplitude between 0 and 3 °C and random noise component.

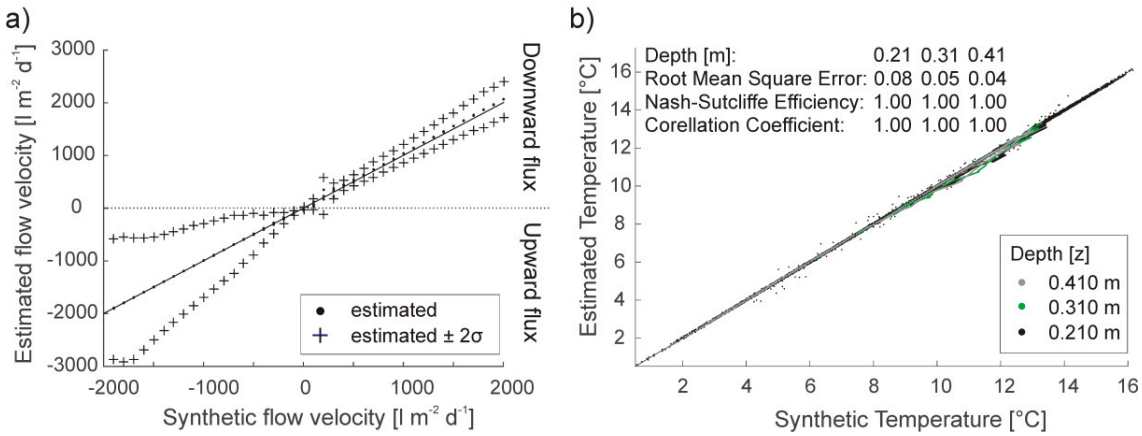

Figure 3.4: (a) Scatter plot comparing synthetic flow velocity vs. estimated flow velocity including the calculated confidence intervals and (b) scatter plot comparing synthetic vs. estimated temperatures.

The synthetic case results also demonstrated that the selected length of the time window (window size) for the optimization can have a significant influence on the estimated vertical flow velocity. Long-time windows potentially resulted in a loss of information on the temporal behaviour of q_z. Minimum window size should not be smaller than 24 h where the surface temperature is at quasi steady state. The use of time windows smaller than 24 h resulted in substantial deviations between synthetic and estimated flow velocities (Table 3.3). Calculated q_z for time windows smaller than 24 h strongly fluctuated around the estimated daily vertical water flux. This increasing mismatch was clearly reflected by an increase in the mean square error between the synthetic and estimated temperatures (Table 3.3). An increase in the window length to 72 h resulted in an increase in the RMSE between the synthetic and estimated q_z. The step change in q_z appears smoothed in the estimations, increasing the deviation between synthetic and estimated vertical flow velocity. Despite the decreasing accuracy between synthetic and estimated q_z the RMSE between synthetic and estimated temperature decreased.

Table 3.3: Calculated root mean square error (RMSE) between the synthetic and estimated exchange flux (q_z) based on a daily time interval and temperature (T) based on a 10 min time interval and model run time applying a range of window lengths to FLUX-BOT.

Window length (h)	RMSE between synthetic and estimated q_z (L m^{-2} d^{-1})	RMSE between synthetic and estimated T (°C) at z=0.26 m	Run time (s) [*1]
72	82	0.07	623
24	**33**	**0.08**	**224**
12	88	0.10	244
6	117	0.17	284

[*1] using an Intel 2.67 Ghz processor

The better fit in terms of RMSE between synthetic and estimated temperatures for higher window length is an effect caused by the increasing number of data points were included for the temperature optimization and the termination tolerance for the optimization remained equal. Thus the overall accuracy between synthetic and estimated temperatures slightly increases as more temperature data points were included in the optimization process.

3.3.1.3 Sensitivity and uncertainty analysis

To evaluate the influence of the most relevant input parameters on the estimates of the vertical flow velocity we conducted the Regional Sensitivity Analysis. The parameter space for the most uncertain parameters/variables was defined according to Table 3.4. The results highlight that volumetric heat capacity and thermal conductivity had a significant impact on the vertical flux estimates of FLUX-BOT (Fig. 3.5). The sensitivities in the location of each sensor and potential temperature offsets had negligible effects on the flux estimates. The subsets had the same distribution, meaning that each input factor is equally likely to produce behavioural or non-behavioural model realisations.

The behavioural cumulative distribution function for the volumetric heat capacity and the thermal conductivity is steepest in the central part, indicating that the mean values of these model input parameter were more likely to produce behavioural model realisations (Fig. 3.5). The extreme values should be avoided in order to produce behavioural model realisations. The overall effect of the volumetric heat capacity (Smirnov two-sample test statistics (d-stat) = 0.34) on the behavioural model realisations was larger compared to the thermal conductivity (d-stat = 0.27). No correlation was found between thermal conductivity and volumetric heat capacity in producing behavioural model realisations (CC = -0.03).

Table 3.4: FLUX-BOT input parameters to perform sensitivity and uncertainty estimation. Further input parameter are similar to those defined for the main FLUX-BOT function.

Parameter	Value	Unit	Description
Num_sens_run	1000	-	Number of Monte Carlo model simulation to perform
Rc_error*	0.5×10^6	$Jm^{-3}°C^{-1}$	Uncertainty estimate for the volumetric heat capacity
Kfs_error*	0.3	$Js^{-1}m^{-1}°C^{-1}$	Uncertainty estimate for the thermal conductivity
***T_error**^*	0.05	°C	Uncertainty estimate for the Temperature
***z_error**^*	0.01	m	Uncertainty estimate for the sensor location

* The parameter space is defined as normal distribution with a given mean and the standard deviation equal to the given uncertainty

^ The parameter space is defined as normal distribution with mean = 0 and standard deviation equal to the given uncertainty estimate (independent for each temperature time series and each depth). These uncertainties are than added to the specific temperature time series and to the specific sensor location)

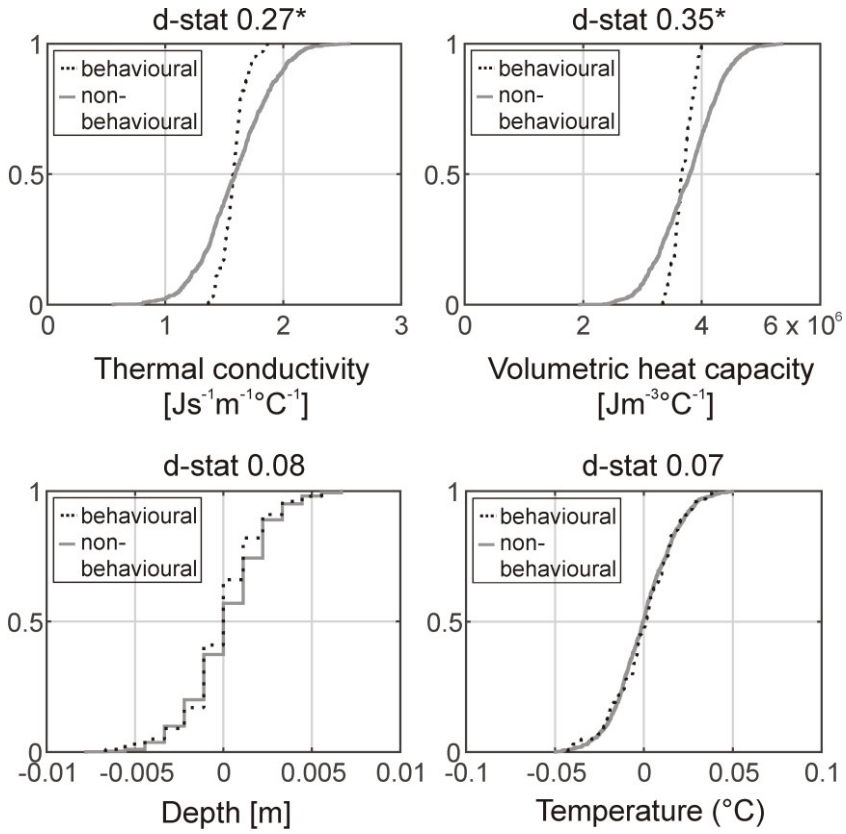

Figure 3.5: Regional Sensitivity Plot (RSA) for FLUX-BOT input parameter (a) volumetric heat capacity, (b) thermal conductivity, (c) depth and (d) temperature showing the cumulative distribution function for all behavioural (dotted line) and non-behavioural (straight line) model realisations. The spreading between both lines is a visual measure of FLUX-BOT sensitivity to the respective input parameter. The objective function is RMSE based on a daily time interval.

The estimated uncertainty bounds for the synthetic test case are shown in Fig. 3.4. The uncertainty bounds highlight the extent to which estimated vertical flow velocities were affected by variation in the thermal properties of sediments and accuracy of the temperature sensor and positioning. The uncertainty bounds (ub) were smallest for moderate vertical exchange fluxes between -500 L m^{-2} d^{-1} (lower ub = -670 L m^{-2} d^{-1}, upper ub = -317 L m^{-2} d^{-1}) and +500 L m^{-2} d^{-1} (lower ub = 398 L m^{-2} d^{-1}, upper ub = -630 L m^{-2} d^{-1}). The uncertainty in exchange fluxes was highest for high upward fluxes (-1500 L m^{-2} d^{-1}) with percental deviation of uncertainty bounds form the median of ± 45 %, successively decreased for moderate exchange fluxes (-500 L m^{-2} d^{-1}/ +500 L m^{-2} d^{-1}) to ± 35 %/23 %, and was lowest for high downward fluxes (+1500 L m^{-2} d^{-1}) with percental deviation of only ± 15 %.

3.3.2 Real data test cases

3.3.2.1 Sand box experiment (Munz et al., 2011)

The results highlight that FLUX-BOT accurately reproduces the measured flux, especially for low to moderate exchange fluxes, typical of hyporheic exchange (Fig. 3.6). The execution time for the time series of 96 days recorded with a 15 min interval was 65 s (Intel 2.67 Ghz processor) using the default parameterisation (Table 3.2). The root mean square error between measured and estimated vertical flow velocity was 0.18. The RMSE was slightly better than the RMSE of 0.21 derived for vertical flux estimation based on the Keery evaluation method (Munz et al., 2011). The large offset between measured and simulated values during high downward flow condition, between day 83 to day 86 (660 L m^{-2} d^{-1}), were comparable to those of the Keery and Hatch methods (Munz et al., 2011). For this period the experimental measurement of exchange flux seems to be inaccurate. There was a good match between simulated and observed temperatures over the whole simulation period (RMSE(at z = 0.07 m) = 0.26).

3.3.2.2 Sensitivity and uncertainty analysis

The parameter space for the most uncertain parameter/variables was defined in the same way as the synthetic test case (Table 3.4). Again, the results of the RSA highlight that two (volumetric heat capacity and thermal conductivity) out of the four tested input parameters had a significant impact on the vertical flux estimates of FLUX-BOT. Uncertainties in the location of each sensor and potential temperature offsets had negligible effects on the flux estimates (d-stat < 0.1). The overall effect of the thermal conductivity (d-stat = 0.27) in producing non-behavioural model realisations was comparable to the effect of the volumetric heat capacity (d-stat = 0.29). A slight correlation (CC = 0.38)

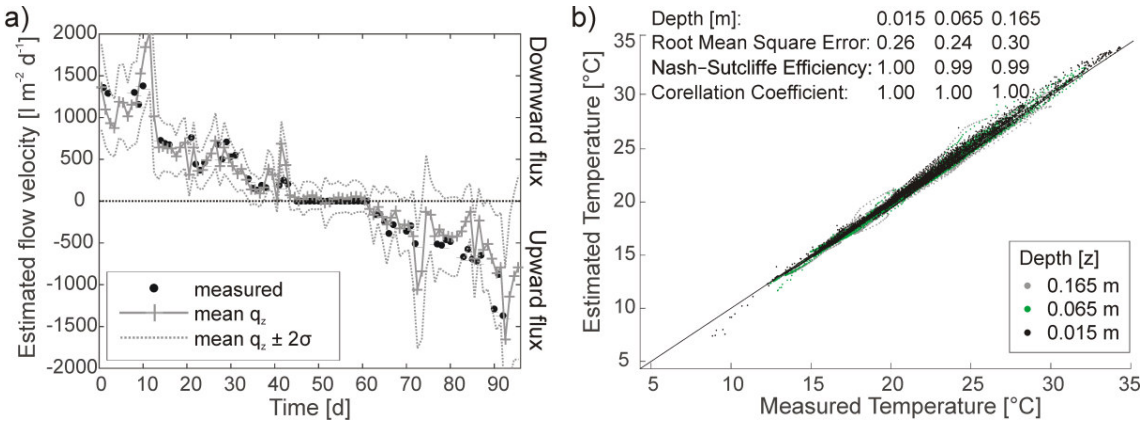

Figure 3.6: (a) Measured and estimated flow velocities based on vertical temperature profile of controlled hydrological conditions in a sand box experiment and (b) scatter plot comparing synthetic vs. estimated temperatures with the 1:1 line.

was found between thermal conductivity and volumetric heat capacity in producing behavioural model realisations. The estimated uncertainty bounds for the sand box experiment are shown in Fig. 3.6. The general patterns of uncertainty were comparable for those described for the synthetic test case. We observed highest uncertainty especially for the upward fluxes.

3.3.2.3 Riverbed data (Munz et al., 2016)

The Riverbed data case further illustrates the capabilities of the FLUX-BOT model. The temperature profile was measured at the thalweg of the Selke River (Munz et al., 2016). The data were measured over a period of two years with a resolution of 10 min and includes a wide range of temperature conditions (Fig. 3.7). Exchange flux between river and groundwater was shown to be predominantly downwelling vertically along the temperature profile (Munz et al., 2016). Common thermal parameters for gravelly to sandy material were used for the FLUX-BOT application, as listed in Table 3.2. The parameter space for the most uncertain parameter is defined according to Table 3.4. The corresponding data files, scripts and functions are available at https://bitbucket.org/flux-bot/flux-bot.

3.3.2.4 Results

The estimated flow velocity and corresponding temperature residuals (for a selection of sensors not used as FLUX-BOT boundary conditions) are illustrated in Fig. 3.8. FLUX-BOT execution time was 47 min (Intel 2.67 Ghz processor) using the default parameterisation (Table 2). The Root Mean Square error between simulated and estimated temperatures ranged between 0.10, at a depth of 0.05 m, and 0.22, at a depth of 0.25 m. The RMSE increased continuously with increasing depth. The estimated uncertainty bounds

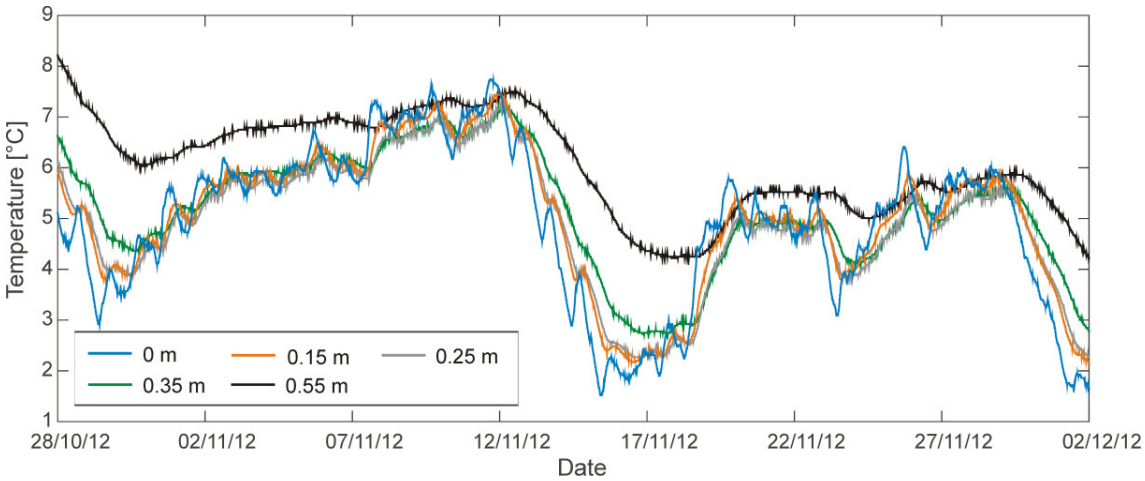

Figure 3.7: Example of measured temperature time series in the riverbed of a lowland river from 28/10/2012 to 02/12/2012. Corresponding vertical flow velocities are shown in Fig. 3.8 (yellow shaded).

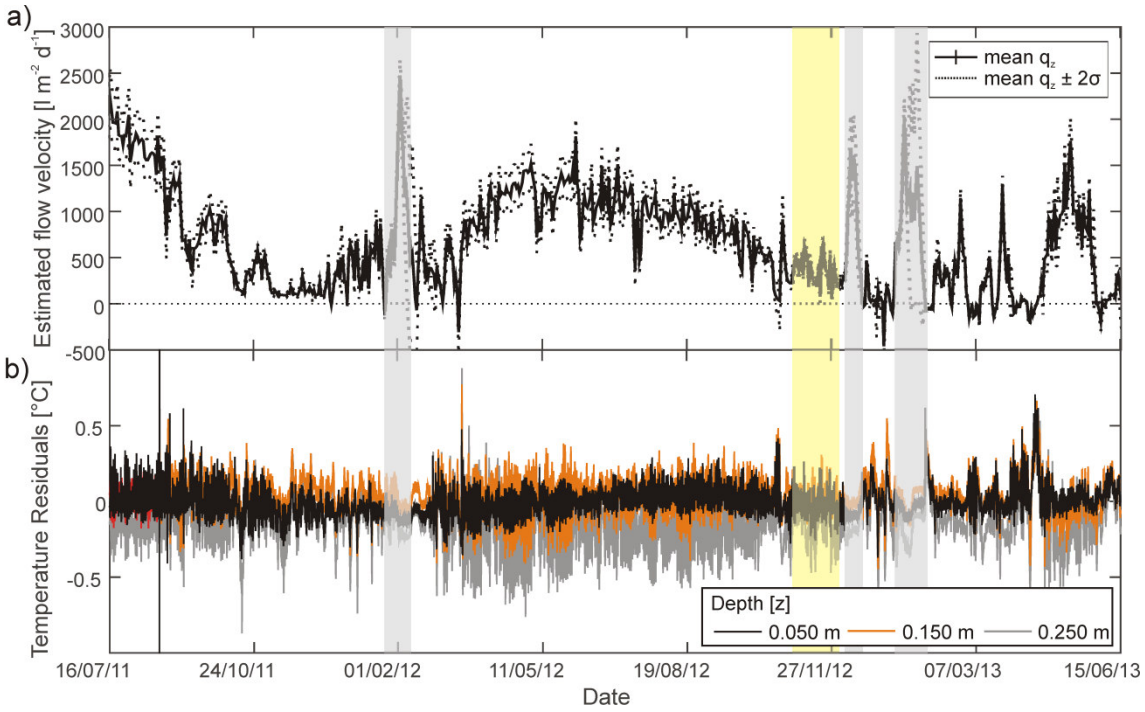

Figure 3.8: (a) Estimated flow velocities based on vertical temperature profile of a lowland river and (b) temperature residuals for the observation period from 16/07/2011 to 15/06/2013. Gray shaded areas highlight times when boundary condition of FLUX-BOT model where not matched (temperatures of the entire riverbed were close to 0, i.e. no temperature gradient in the riverbed). Yellow shaded area corresponds to temperature time series shown in Fig. 3.7.

for q_z are shown in Fig. 3.8. The uncertainty in estimated vertical flow velocity was small throughout the whole time period. These results highlight the robust vertical flux calculation of FLUX-BOT for a wide range of temperature boundary condition (Fig. 3.7; z = 0 and z = 0.55 m). GWSI flux at the study side exhibit a clear seasonal cycle with exchange velocities up to 2000 L m^{-2} d^{-1} during the summer months, when groundwater levels were at a minimum, and near 0 L m^{-2} d^{-1} in the winter months, when groundwater levels were highest. GWSI flux reached peak values for short periods in May/June 2013 during a major river flood event (Munz et al., 2016).

3.4 Discussion

3.4.1 FLUX-BOT

FLUX-BOT applies a cell-centered, finite difference Crank-Nicolson numerical scheme (CNs) to solve the one-dimensional heat advection-conduction equation. The CNs is unconditionally stable i.e. the numerical stability of the solution is independent of the time step size. Thus the CNs yields a computational, numerical scheme that is robust to choices of ∂t and ∂z (Hinkelmann, 2005).

The spatial resolution of the CNs was found to have a significant impact on the vertical flux estimation with FLUX-BOT. In general, increasing the spatial resolution (*dz*), i.e. the number of computational cells, also increases the accuracy of the numerical solution (by decreasing the spatial truncation error). The dependence of the FLUX-BOT solution on the spatial resolution can be easily tested by running the model with two different spatial resolutions and calculating the flux residuals of both model results. The best solution is achieved if the magnitude of flux residuals does not reduce with a further increase in the spatial resolution. However the applied spatial resolution of dz = 0.005 m was sufficiently fine to provide accurate flux estimates for all conducted test cases.

FLUX-BOT includes the entire frequency spectrum of the temperature time series into the estimation procedure using all information contained in the temperature time series. Furthermore FLUX-BOT allows a flexible set up of the temporal resolution for the estimation of vertical flow velocity.

The conducted test cases highlight the ability of FLUX-BOT to accurately calculate time-variable vertical exchange fluxes. The presented approach does not require elaborate pre-processing of the observed temperature data, eliminating one major, time consuming and non-trivial step when applying common analytical solutions. Temperature time series often contain periods where it is almost impossible to extract specific temperature characteristics using automated procedures. In particular, extracting of the frequency of interest by filtering or finding good fits of static sine function to the raw time series makes it challenging to apply automated peak detection and filtering procedures (Gordon et al., 2012). FLUX-BOT can be easily applied to temperature time series even if no daily (sinusoidal) temperature oscillation could be extracted from the raw data. The problems incurred with non-sinusoidal raw temperature time series and how they can be processed with state of the art methods are intensively discussed in Gordon et al. (2012).

FLUX-BOT allows flexible set-up of the temporal resolution, from daily to long term estimations, of vertical flow velocity. By using overlapping windows, q_z can be calculated continuously at a high temporal resolution. Strong overlapping cause longer calculation times for a temperature time series, but still, FLUX-BOT remains a handy and flexible tool for such circumstances. The use of time windows smaller than 24 h introduces artificial effects to the estimation of q_z due to the diurnal temperature variation (violation of the quasi steady state boundary condition). FLUX-BOT can be easily applied to a broad frequency spectrum beyond the diurnal signal commonly used for flux calculations. The synthetic temperature signal used as upper boundary condition for the synthetic test case was dominated by the daily temperature signal and relatively low noise. The resulting signal to noise ratio was 1.75. Comparable, accurate exchange flux estimates with FLUX-BOT were also achieved with synthetic temperature time series

with signal to noise ratios < 1, indicating the noise component (frequency > one day) dominates. Thus the FLUX-BOT method does not depend on the dominance of the daily temperature signal and can be successfully applied to very noisy temperature time series. On the other hand, lower signal frequencies (e.g. inner annual temperature variations in a weekly to monthly scale dominant in saturated sediments below larger rivers and lakes) could by easily evaluated with FLUX-BOT by increasing the window size. Even if no temperature variation is observed at the sediment water interface, FLUX-BOT remains a handy tool to calculate vertical water fluxes so as long as temperature differences along the profile exists. However, FLUX-BOT depends on temperature differences with time and depth that are a function of q_z. If temperatures would be uniform and constant throughout the domain, they would be independent of q_z and thus no active heat tracing technique would work.

A drawback for the numerical evaluation of temperature profiles is the spatial domain of the calculated vertical flux. Whereas pairs of sensors were sufficient to apply common analytical methods FLUX-BOT only calculates a single vertical flux for the entire domain. At least three sensors are necessary to drive the model, with the upper- and lower temperature time series serving as the boundary conditions. The remaining temperatures are used for the inverse optimization of q_z. Hence, if the temperature profile contains more than four temperature sensors, sequential flux calculation is possible for subprofiles (several depths). Given that most field studies using streambed temperatures to quantify GWSI fluxes setup a high vertical temperature resolution using more than four temperature sensors per profile, limitation by this drawback should be minimal. In general we recommend a high vertical spatial resolution of temperature sensors when temperature profiles should be used to calculate vertical exchange flux.

All case studies presented here show high comparability between simulated and observed temperatures in the saturated sediment, with RMSE ranging between 0.01 °C and 0.26 °C. These results highlight the accuracy of the implicit finite difference approximation. The RMSE for the synthetic test case was equal for all depths illustrating the capabilities of FLUX-BOT to correctly simulate subsurface temperatures when GWSI exchange fluxes were purely vertical. The RMSE increased from shallow toward greater riverbed depths for the riverbed test case, where higher flow complexity and streambed heterogeneity is expected compared to the other test cases. For the riverbed test case the RMSE was generally lower during winter, when absolute temperatures and temperature dynamics (daily to weekly) were the smallest.

The evaluation of the simulated and observed temperatures (Figs. 3.4, 3.6) and temperature residuals (Fig. 3.8) gives a direct indication of the accuracy of vertical water flux estimates and hence on the validity of the underlying assumptions namely spatially homogeneous, vertical flux. Periods when the deviation was high corresponded to inaccu-

rate flux estimates. The calculation of quality criteria for each analysed window is a major advantage of the presented method compared to common analytical approaches where the quality of the flux estimate remains unknown.

3.4.2 Sensitivity and uncertainty analysis

The Regional Sensitivity Analysis was performed for the synthetic test case and the sand box experiment where the true vertical fluxes were known or independent vertical flux measures were available. However, in most field studies such independent flux measures would not be available. In this study we use the RSA as a tool for model structure evaluation, providing a basis for estimating the precision of parameters required to obtain reliable flux estimates. The RSA results illustrate where additional effort should be placed to reduce uncertainty, for example, by improving the quality of the input parameter (heat capacity, thermal conductivity of the saturated sediment, sensor spacing, and temperature sensor accuracy) (Wagener and Kollat, 2007). The magnitude of the Smirnov two-sample test statistics directly quantifies the effect that model input parameters have on the estimated vertical flow velocity.

The Regional Sensitivity Analysis highlights the sensitivity of FLUX-BOT's vertical flux estimates to heat parameters compared to its robustness to uncertainties in the temperature sensor accuracy and the sensor spacing. Existing sensitivity studies, based on the established analytical solutions (Hatch et al., 2006; Keery et al, 2007), found that uncertainties in thermal parameters and inaccuracy of temperature measurements and its spatial location can lead to large errors in the velocity estimates in particular for low flows (Constantz et al., 2003; Shanafield et al., 2011; Munz et al., 2011). In contrast the FLUX-BOT method was not sensitive to inaccuracies in the sensor location and sensor accuracy. Furthermore the uncertainty in exchange flux estimated with the FLUX-BOT method was smallest for high downward fluxes and successively increased towards moderate and high upward fluxes. The uncertainty in thermal parameters has a stronger impact on the upward flux solution due to the strong dependence of observed thermal differences with depth on the parameters that control downward heat conduction.

In general, the calculated sensitivity (expressed by the Smirnov test statistics) clearly depends on the uncertainty assigned to the heat transport parameters but the general pattern remains consistent. Whereas the heat capacity varies little in nature (Gordon et al., 2012), the thermal conductivity of solids varies largely from 8.4 W m^{-1} $°C^{-1}$ in quartz minerals to 0.25 W m^{-1} $°C^{-1}$ in clay and furthermore depends on composition and connectivity of the sediment grains (Stonestrom and Blasch, 2003). That highlights the need for accurate quantification of thermal conductivity to derive representative vertical water fluxes with the FLUX-BOT method.

To account for statistical differences between different flux rates it is essential to estimate the confidence (uncertainty) intervals. They should be always given along with the estimated vertical flux. The FLUX-BOT program offers an automatic tool for the calculation of confidence intervals. In all case studies presented we observed lowest uncertainty in downward flow direction and highest uncertainty in upward flow direction.

3.5 Conclusions

In this study we presented a new computer code to numerically solve the one-dimensional advection-conduction equation to estimate vertical water fluxes from measured temperature profiles. Flexibility in the required boundary conditions allows for better representation of measured temperatures and, thus, enhances application to all natural temperature condition without the need of any data preprocessing (e.g. curve fitting, frequency analysis). This approach was implemented using the numerical code FLUX-BOT to automate the entire workflow to calculate vertical water fluxes from raw temperature time series. FLUX-BOT also contains functions for data and result visualization and uncertainty analysis. The accuracy and functionality of the FLUX-BOT program was demonstrated by three independent, synthetic and real data test cases. FLUX-BOT provides a handy and flexible tool to allow analysis of transient vertical exchange fluxes in saturated porous media using temperature profiles; easy to apply and not restricted in temperature boundary condition. The model application is simple and fast to apply to routinely measured temperature profiles over time.

Data and code availability

FLUX-BOT is distributed as open source code. The most up to date version can be downloaded from the Bitbucket web site (web-based hosting service for projects that use GIT version control, allowing to further augment and adapt the numerical code): https://bitbucket.org/flux-bot/flux-bot. Full documentation including a point by point instruction how to use FLUX-BOT and a detailed description of all functions, the data structure and the incorporated input and output instructions is provided alongside with the program.

4 Coupled long-term simulation of reach-scale water and heat fluxes across the river-groundwater interface for retrieving hyporheic residence times and temperature dynamics

An article with equivalent content has been published online as: Munz, M., S.E. Oswald, C. Schmidt (2017), Coupled long-term simulation of reach-scale water and heat fluxes across the river-groundwater interface for retrieving hyporheic residence times and temperature dynamics, Water Resources Research, 53, https://doi.org/10.1002/2017WR020667.

Abstract

Flow patterns in conjunction with seasonal and diurnal temperature variations control ecological and biogeochemical conditions in hyporheic sediments. In particular, hyporheic temperatures have a great impact on many temperature-sensitive microbial processes. In this study, we used 3D coupled water flow and heat transport simulations applying the HydroGeoSphere code in combination with high resolution observations of hydraulic heads and temperatures to quantify reach-scale water and heat flux across the river-groundwater interface and hyporheic temperature dynamics of a lowland gravel-bed river. The model was calibrated using temperature and hydraulic head observations in order to constrain estimates of the most sensitive model parameters. The magnitude and variations of the simulated temperatures matched the observed ones, with an average mean absolute error of 0.7 °C and an average Nash Sutcliffe Efficiency of 0.87. Our results indicate that non-submerged streambed structures such as gravel bars cause substantial thermal heterogeneity within the saturated sediment at the reach-scale. Individual hyporheic flow path temperatures strongly depend on the flow path residence time and the temperature gradient between river and groundwater. Variations in individual hyporheic flow path temperatures were up to 7.9 °C, significantly higher than the daily average (2.8 °C), but still lower than the average seasonal hyporheic temperature difference (19.2 °C). The distribution between flow path temperatures and residence times follow a power law relationship with exponent of about 0.32. Based on this empirical relation, we further estimated the influence of hyporheic flow path residence time and temperature on oxygen consumption.

Keywords: Transient Model, River-groundwater exchange, Heat transport, Hyporheic zone, Geomorphological structures, Oxygen consumption

4.1 Introduction

Flow and temperature patterns control ecological and biogeochemical conditions in hyporheic sediments (Findlay, 1995; Boulton et al., 1998; Krause et al., 2011). The infiltration of river water, solutes and thermal energy, into the subsurface and its delayed exfiltration back into the river has a major influence on the transport and transformation of nutrients (Boano et al., 2010; Zarnetske et al., 2012; Krause et al., 2013) and the thermal regime within the shallow streambed (Arrigoni et al., 2008; Sawyer et al., 2012). Temperature is recognized to control microbial processes in hyporheic sediments (Thamdrup and Fleischer, 1998; Acuna et al., 2008). Microbially mediated solute transformation rates in gravel bed rivers have been observed to vary by a factor of 10 for temperature differences of 10 °C (Vieweg et al., 2016). Intense groundwater upwelling furthermore has the potential to alter water column temperature (Briggs et al., 2013), which in turn affects biotic conditions within the river ecosystem.

Solute turnover of dissolved substances in the hyporheic zone has been shown to depend on residence times (Boano et al., 2010; Zarnetske et al., 2011; Marzadri et al., 2012). For instance, long residence times promote denitrification, because usually oxygen must first be sufficiently depleted before denitrification occurs (Trauth et al., 2015). Diurnal temperature variations in the stream water propagate into the hyporheic zone by heat advection and conduction. These variations are increasingly damped at increasing depths in the sediment (Arrigoni et al., 2008), and hence also with increased flow path lengths and residence times (Marzadri et al., 2013). Thus, we hypothesize that there is a coupled effect of residence times and hyporheic temperatures on solute processing in the hyporheic zone.

To study the spatial and temporal variability of water and heat flux in riverbed sediments, a broad range of experimental methods exist (e.g. Kalbus et al., 2006; Rau et al., 2014). Despite recent improvements in logger technology and measurement methods, the experimental approaches are limited to device-dependent temporal and spatial resolutions and to their ability to cover entire river reaches. In contrast, three-dimensional flow and heat transport models can be used to simulate the complex river-groundwater exchange and thermal transport process in river-riparian systems, spatially distributed and at a high temporal resolution (Brookfield et al., 2009; Nützmann et al., 2014; Karan et al., 2014).

The application of distributed, fully-integrated models requires the parametrization of the flow and heat transport equations. Improvements in model calibration have been made by coupling both temperature and pressure to constrain estimates of hydraulic and thermal properties (Doussan et al., 1994; Naranjo et al., 2012; Karan et al., 2014). Espe-

cially the streambed hydraulic conductivity and its spatial representation strongly affect simulated river-groundwater exchange, hyporheic flow paths and residence times across dune-like streambed structures (Salehin et al., 2004; Sawyer and Cardenas, 2009; Tonina et al., 2016) and along the river reach (Naranjo et al., 2012; Karan et al., 2014).

At any scale, the large number of input parameters for spatially distributed, fully-integrated models and their interactions is a challenge for an effective model parameterization. Thus, there is a strong need to identify the key parameters controlling hydrological and thermal processes, as well as a subset of parameters to be targeted in more computationally-intensive parameter estimation processes. Global sensitivity analysis, accounting for model non-linearity and parameter interactions, helps to prioritize the parameters to be included in subsequent parameter estimation and to identify the dominant processes within the study domain (Van Griensven et al., 2006; Saltelli et al., 2008; Srivastava et al., 2014).

The aim of this study was to investigate reach-scale hyporheic exchange fluxes as well as the associated hyporheic residence times and hyporheic temperatures and their influence on temperature-sensitive biogeochemical processes, such as hyporheic oxygen consumption, in the sediments of a gravel-bed river. We applied a transient 3D coupled water flow and heat transport model to simulate reach-scale water and heat flux across the river-groundwater interface and hyporheic temperature dynamics for a two-years' time-series of naturally occurring hydrological and thermal conditions. We conducted a global sensitivity analysis to understand the effect of model parameterization on the simulation results in order to effectively calibrate the fully-integrated model and prove the benefits of including temperature in addition to hydraulic heads for model parameterization of fully-integrated numerical models. On the basis of the calibrated and validated model and established particle tracking techniques, we quantified the temporal and spatial variations in hyporheic exchange flux, hyporheic residence times and hyporheic temperatures and identified their controlling factors. Furthermore, we used an empirical temperature relationship between the effective temperature and respiration rate to quantify the influence of hyporheic flow path residence time and temperature on hyporheic oxygen consumption. Our study improves the understanding of complex, reach-scale water and heat fluxes, as well as hyporheic temperature dynamics and their implications on temperature-sensitive biogeochemical processes.

4.2 Methods

4.2.1 Study site and data collection

The study site is located within the catchment of the Selke River, a third-order perennial river (MNQ = 0.23 $m^3 s^{-1}$, MQ = 1.51 $m^3 s^{-1}$, MHQ = 15.6 $m^3 s^{-1}$) in the northern part of the Harz Mountains in central Germany (51°43'39.9"N 11°18'53.2"E) as high-intensity test-site of a TERENO observatory (Wollschläger et al., 2017). The studied river reach is 250 m long, encompassing a variety of natural fluvial morphological structures, such as a point bar (27 m long and 3.5 m wide during base flow) and an in-stream gravel bar

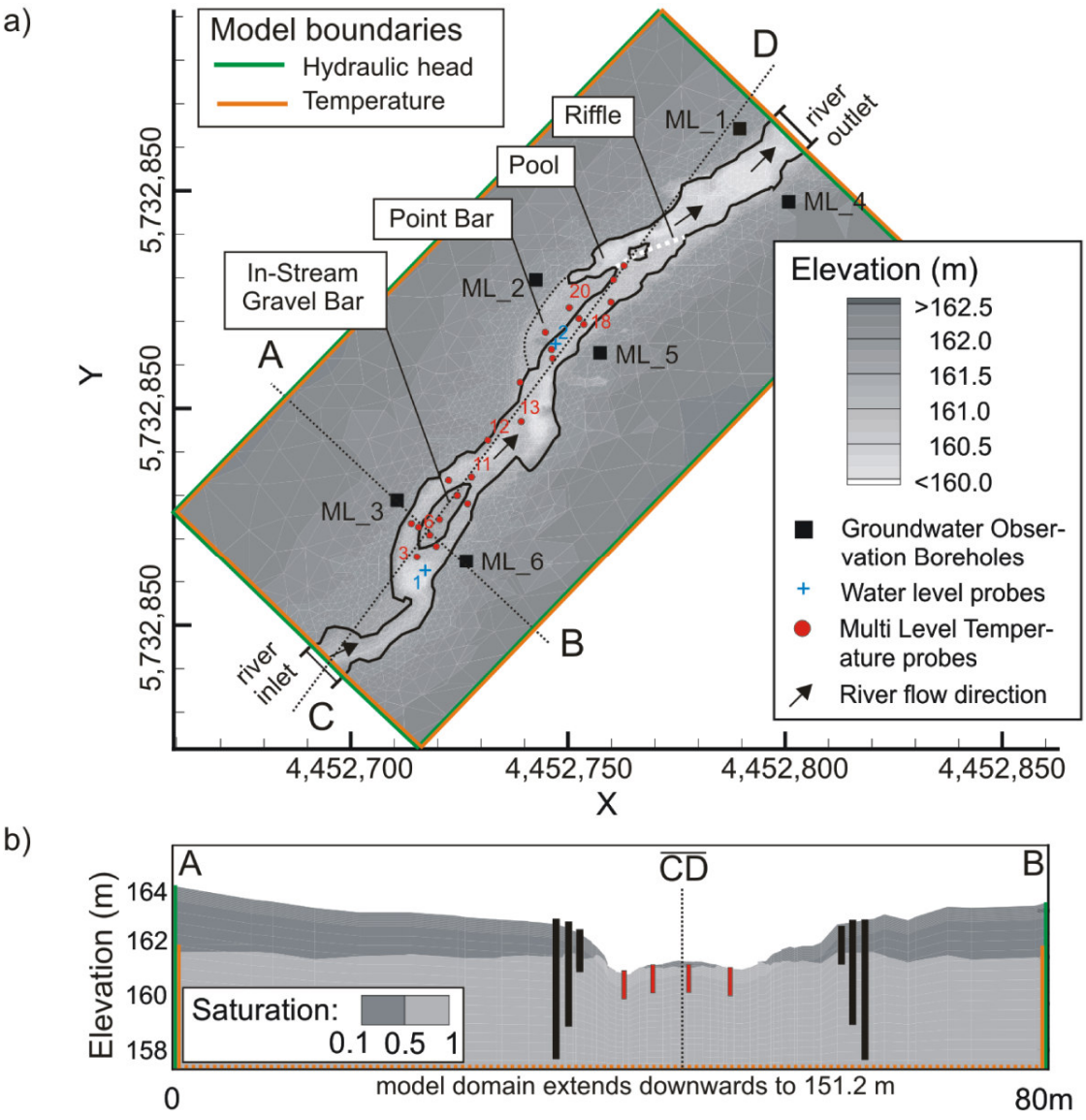

Figure 4.1: (a) Study site and model domain, showing experimental infrastructure, surface elevation, relevant geomorphological structures, and the finite element mesh (white-framed triangles). The black line indicates the river shape for discharges, here taken of 0.25 $m^3 s^{-1}$. (b) Cross-section through the model domain (A to B). The lower 6 meters of the model domain are not shown, because they are fully saturated and no observation boreholes extended to that depth range.

(20 m long and 6 m wide during base flow), which are typical for gravel bed rivers. The topography of the study site was surveyed using differential GPS in combination with a laser tachymeter (Trimble GPS R8), with 1633 data points. The local aquifer consists of up to 8 m-thick fluvial sediments, with grain sizes ranging from medium sands to coarse gravels underlain by less permeable clay and silt deposits which form the bottom of the alluvial aquifer. The studied river reach is characterized by overall losing conditions within the river channel, whereby the water flow direction within the streambed often has a strong horizontal flow component oblique to the riverbed interface (Munz et al., 2016). Patterns of hyporheic infiltration and exfiltration were observed at the streambed around the in-stream gravel bar (Trauth et al., 2015). The flow patterns within the gravel bar are highly variable in time, depending on the water level in the river (discharge) and the ambient groundwater flow direction (Trauth et al., 2015; Munz et al., 2016).

Continuous measurements of hydraulic heads and temperatures at different depths along the river bank (1.7 m, 2.7 m, 4.7 m) and within the river at a temporal resolution of 10 min were conducted over a two-year period from May 2011 until June 2013. Additionally, riverbed temperature profiles were recorded at 20 locations with seven points each in the depth interval 0 - 0.65 m below the streambed surface every 10 minutes using Multi Level Temperature Probes (Fig. 4.1). The vertical temperature profiles were measured along the thalweg, as well as at the head, crest and tail of the dominant fluvial morphological structures. A detailed description of the experimental setup, the temperature sensors and their operation times can be found in Munz et al. (2011; 2016).

4.2.2 Hydraulic conductivity

A detailed characterization of the hydraulic conductivity of the streambed and the aquifer is required to accurately simulate hydrological fluxes (Naranjo et al., 2012; Karan et al., 2014). Slug tests were carried out at 70 locations distributed across the river reach to estimate the horizontal hydraulic conductivity (K_h). Individual slug tests were conducted at four different depth intervals below the streambed surface (0 - 0.2 m, >0.2 - 0.4 m, >0.4 - 0.8 m, and >0.8 m) at the same location. We used 1.6 m-long piezometer pipes with a screened section of 0.05 m and an inner diameter of 0.0254 m. To estimate the hydraulic conductivity of the aquifer, slug tests were also carried out in the existing groundwater observation wells. We performed falling head slug tests by releasing water from an attached reservoir at the top of the piezometers until the piezometer was filled completely. The water level development in the piezometers was recorded with submerged pressure sensors (Levellogger Solinst Canada Ltd., Canada). Each test was repeated three times. The data was analysed using the case G, basic time lag equation from Hvorslev (1951). The calculated K_h were corrected to a reference temperature of 10 °C. Major measurement campaigns were conducted in September 2011 – 2013.

Streambed hydraulic conductivities were grouped based on observation year (2011, 2012, 2013), streambed depth (0 - 0.2 m, >0.2 - 0.4 m, >0.4 m - 0.8 m, and >0.8 m), and their relative location with respect to the geomorphological structures (head, crest, tail). The analysis of variance (MATLAB Statistics Toolbox) was used to test for differences of K_h in space and time, with the significance level chosen to be 0.05.

4.2.3 Integrated surface-subsurface flow and heat transport simulations

4.2.3.1 HydroGeoSphere model

The fully-integrated surface-subsurface flow and transport model HydroGeoSphere (HGS) includes simulations of water flow and heat transport (Therrien et al., 2010). HGS is a finite element code that solves Richard's equation for variable saturated flow in 3D. Surface water flow is simulated using the numerical solution of the diffusion-wave equation (an approximation of the Saint-Venant equations) together with Manning's equation. The Manning formula is an empirical formula estimating the average stream velocity depending on the streambed roughness (n). Details for the governing flow equations can be found in Therrien et al. (2010) and Brookfield et al. (2009).

The surface and subsurface model domain is coupled by the dual conductance concept (dual node approach), based on a first-order exchange coefficient (l_e) as a numerical parameter. The coupling flux was found to be insensitive to changes in the coupling length if the coupling length is selected lower than a site-specific threshold value, which should be defined on a case-by-case basis to ensure adequately converged results and avoid unrealistic model behavior (Ebel et al., 2009; Liggett et al., 2011).

4.2.3.2 Model setup (baseline model)

The dimensions of the model domain were 80 m x 250 m x 9 m (width, length, thickness; Fig. 4.1). The domain thickness was set according to the less permeable clay and silt deposits that form the bottom of the alluvial aquifer. A 2D triangular finite element mesh was generated for the top of the domain, representing the ground and riverbed surface (GRID BUILDER, McLaren, 2008). Element size was set to 10 m in the floodplain, but subsequently refined to 0.25 m in the riverbed. The generated 2D mesh was superimposed onto a 3D finite element mesh consisting of 28 model layers, with a vertical discretization of 0.05 m for the upper 12 layers, which increased to 0.4 m at the base of the 3D mesh, located at 151.2 m a.s.l. The whole model domain was discretized into approximately 250,000 elements. The chosen node spacing provided an adequate spatial resolution for representing riverbed topography, in order to capture steep hydraulic head

and temperature gradients, both horizontally and vertically. The surface topography of the domain was interpolated based on the riverbed and riparian floodplain DGPS survey with a high vertical resolution to the elevation map, including all locations of the numerical mesh nodes (Fig. 4.1).

The distribution of K_h in the streambed (0 - 0.8 m below the streambed surface) was defined based on conditional, sequential Gaussian simulation (SGS) with histogram reproduction (Hansen and Mosegaard, 2008) using the geostatistical MATLAB toolbox mGstat. In SGS, the measured hydraulic conductivities were transformed to standard Gaussian values and the semivariogram of the transformed data was estimated. Measured K_h values were replicated at their locations, and values at the remaining locations were randomly drawn from the conditional cumulative distribution function, defined by the kriging mean and variance. SGS preserved the mean and variance of the measured hydraulic conductivities. The aquifer (~0.8 m - 9 m) was divided into three zones of homogeneous K_h corresponding to the depth of the groundwater monitoring wells. Streambed and aquifer hydraulic conductivity was defined as homogeneous, but anisotropic (Table 4.1). The anisotropy ratio was obtained through calibration. All other state parameters were defined as homogeneous for the entire model domain (Table 4.1).

Table 4.1: Flow and transport parameters used for HydroGeoSphere simulations.

Parameter	Symbol	**Calibrated**	Min[*1]	Max[*1]	Unit
Hydraulic/Hydrodynamic – Porous Media					
Porosity	θ	**0.3**	0.2	0.4	(-)
Hydraulic conductivity (mean)	K_H mean	**2.30×10^{-3}**	0.1[*3]	10[*3]	m s^{-1}
Hydraulic conductivity (var)	K_H variance	**3.00×10^{-6}**	0.5[*3]	2[*3]	m s^{-1}
Hydraulic conductivity (range x/y direction)	K_H range	**23.8 / 5.8**	1 / 1	50 / 15	m
Anisotropy	K_H/K_V	**17**	1	100	(-)
Specific Storage	S_s	**10^{-4}**	-	-	m^{-1}
Longitudinal/transversal dispersivity	α_L	**0.1 / 0.01**	-	-	m^2 s^{-1}
Effective diffusion coefficient	D	**10^{-10}**	-	-	m^2 s^{-1}
Overland flow (Channel/Floodplain)					
Friction (roughness)	n	**0.022**	0.01	0.05	s $m^{1/3}$
Coupling length	l_e	**3.5×10^{-4}**	1×10^{-5}	1×10^{-2}	(-)
Thermal					
Thermal conductivity (sediment/water[*2])	λ_s/λ_w	**1.2 / 0.7[*2]**	1	5	W m^{-1} °C^{-1}
Heat capacity (sediment/water[*2])	C_s/C_w	**1330 / 4185[*2]**	1000	2500	J kg^{-1} °C^{-1}
Bulk density	ρ_b	**1350**	1200	2400	Kg m^{-3}

[*1] maximum parameter space, partitioned into 5 equidistant levels for the sensitivity analyses
[*2] baseline values (no calibration target)
[*3] factor multiplied by the initial value

A first estimate of the initial conditions for hydraulic head and temperature was based on interpolated field data. To determine a realistic initial condition, the transient model was run over a full seasonal temperature cycle as a spin-up period with the boundary condition from May 2011 to May 2012 (when hydrological and thermal regimes were comparable). The head and temperature distributions at the end of this one-year spin-up were used as updated initial conditions. According to the updated initial condition of the heads, the first-order exchange coefficient (l_e) was manually reduced until the exchange flux between surface and subsurface domain (coupling flux) became constant, as recommended by Liggett et al. (2011).

The transient simulation was carried out for the period from May 2011 to June 2013. The boundary conditions of the transient simulation were updated every hour based on hourly averaged measured hydraulic heads and temperatures. Boundary conditions were set as follows:

- **Prescribed hydraulic head** (Dirichlet) at the sides of the model domain. Based on measured hydraulic heads along the river and in the wider area of the floodplain (four observation wells outside the study site), the heads were linearly interpolated for each input time step and a specific hydraulic head was extracted at the location of each boundary node. These extracted hydraulic heads were extended homogeneously for the entire domain depth (green lines in Fig. 4.1).
- **Prescribed water flux** (Neumann) at the river inlet, based on discharge measurements at the nearby gauging station Meisdorf (51°41'29.1"N 11°17'02.2"E). Several manual discharge measurements at the study site have shown that the discharge at the gauging station is practically equal to the discharge at the domain boundary.
- **Critical-depth** boundary is applied at the river outlet, forcing the water depth at the boundary to be equal to the critical depth, and discharge to be calculated by the model.
- **Precipitation and potential evapotranspiration** applied to the surface. The precipitation was measured at the nearby climate station Aschersleben (51°43'33.6"N 11°30'39.6"E) of the German weather service DWD. Potential evapotranspiration was calculated based on measured climate conditions and crop vegetation (annual course of leaf area index) using the Penman Monteith equation.
- **No flow boundaries** were taken for the bottom of the model domain, representing the bottom of the alluvial aquifer.
- **Prescribed groundwater temperature** at the sides of the model domain, based on measured GW temperature at the flood plain. Based on hourly average borehole temperatures, vertical temperature profiles were interpolated for each simulation time step and assigned to the boundary nodes (orange lines in Fig. 4.1). This ensured that the water entering over these boundaries was consistent with the measured groundwater temperature at the study site.

- **Prescribed river temperature** at the river inlet. Measured river water temperature (10 min frequency) was aggregated into hourly values and assigned to the nodes at the river inlet.
- **Heat flux at the river outlet** is calculated by the model based on calculated river discharge and temperature at the boundary nodes
- **Atmospheric energy input** calculated by means of the ambient air temperature and incoming short wave and long wave solar radiation (Verseghy et al., 1991, APPENDIX 4.A). Air temperature was measured at the study site (0.2 m above ground). Incoming short wave and long wave solar radiation was measured at the nearby DWD climate station Aschersleben. The use of the atmospheric energy input allowed the simulation of river water temperature based on atmospheric and subsurface energy input (river temperature not fixed at the nodes of the surface domain).
- **Prescribed groundwater temperature** at the bottom of the domain. The mean of the measured groundwater temperatures over the simulation period (9.03 °C) was assigned as a constant value to all bottom nodes (dashed orange line in Fig. 4.1).

4.2.4 Parameter sensitivity analysis and calibration strategy

We applied a global sensitivity analysis to evaluate the effect of model parameterization on the simulation results (river-groundwater exchange flux, groundwater hydraulic heads and temperatures) and to prove the benefits of temperature in model parameterization. Based on these analyses, we identified the most relevant model parameters and output variables for model calibration (parameter prioritization).

All parameters classified as sensitive to the simulation results were calibrated using PEST (John Doherty, Watermark Numerical Computing, 2005), a model-independent parameter estimator. PEST reduces the discrepancies between model outputs and field observations to a minimum in the weighted-least-squares sense by iteratively adjusting the calibration parameters. For practicability, calibration and sensitivity analysis were limited to a 90-day period from October 2011 to January 2012. This period was chosen because it represents a considerable dynamics in river discharge and temperature. Each of the sensitivity and calibration model runs was initialized by starting with the base line pressure head and temperature distribution for May 2011, followed by half of a temperature cycle as model spin-up period for the perturbed parameter setup.

For the global sensitivity analysis, we applied Morris' elementary effects screening method (Morris, 1991) using the R software package sensitivity (R Development Core Team, 2011; Pujol, 2009). The Morris method was selected because of avoiding otherwise too high computational requirements for simulating transient, coupled water flow

and heat transport. The Morris screening method is designed to work at low computational cost and provides the average (μ) and standard deviations (σ) of local sensitivities obtained at different locations in parameter space. A high value of μ indicates a large influence of the corresponding input parameter on model output and a large value of σ indicates that the corresponding input parameter is attributed to non-linearity and/or interactions with other model parameters (Morris, 1991; Saltelli et al., 2004; Srivastava et al., 2014). The mean value of μ over all parameters considered ($\bar{\mu}$) serves as criterion to identify more influential parameters over less influential ones, namely all observed parameters with $\mu > \bar{\mu}$ are selected as most sensitive parameters and are considered in model calibration. The results of Morris' method are presented as scatter plots of μ versus σ and a linear function representing double the standard error of the mean of all elementary effects $\mu = 2 \times SEM$; with $SEM = \frac{\sigma}{\sqrt{r}}$ (Morris, 1991; Srivastava et al., 2014). Parameters lying below that line correspond to parameters indicating high sensitivity but little non-linearity and/or interaction effects. Such parameters are sensitive over the entire parameter space without much variability in the individual sensitivity. Based on initial sensitivity evaluations carried out for the transient coupled water flow and heat transport model, a setting with 60 repetitions and 5 levels was chosen for the Morris screening (requiring 780 model runs). These values correspond to settings proposed by Morris (1991) and Campolongo et al. (2007) to achieve meaningful analysis. With these settings, stable results were obtained for extended analysis.

The calibrated model was run from May 2011 to June 2013. To quantify the model quality, we used the average water balance error, the mean absolute error (MAE) and the Nash Sutcliffe efficiency (NSE) criteria. The model results were evaluated with Tecplot 360, Version 2012 R1 (TecPlot Inc.), a model-independent visualization and data analysis tool.

4.2.5 Flow path analysis via particle tracking

A particle tracking analysis was performed to evaluate hyporheic flow path lengths, hyporheic travel times and hyporheic flow path temperatures. Forward advective particle tracking (based on a second-order Runge-Kutta integration) was conducted using Tecplot 360 (TECPLOT User's Manual, 2012), following the analytical procedure described by Trauth et al. (2013). Massless particles were released from each boundary node of the wetted streambed area. Particle transport followed the steady-state pore water velocity field extracted from the HGS simulation for selected time steps. The particle integration stops when the particles leave the model domain. In the subsequent analysis, particle tracks following hyporheic flow paths were extracted to calculate the length, residence time and temperature for each individual hyporheic flow path. Average parti-

cle track (flow path) temperature was calculated along each individual hyporheic flow path in order to get a single flow path specific temperature estimate (flow path temperature). To calculate the hyporheic exchange fluxes within the study site, the hyporheic flow paths were flux weighted using the simulated river-groundwater exchange flux by the HGS model at the infiltration point of each particle.

4.2.6 Heat transport and subsurface temperature patterns

To quantify the relative importance of advective heat transport over heat conduction, we calculated the thermal Peclet number for each cell of the model domain, as the ratio between heat transported by advection and heat transported by conduction. Temporal snapshots of the subsurface temperature were extracted at representative and characteristic times and visualized. For the calculation of daily average subsurface temperatures and daily amplitudes, the simulation results were extracted every 30 minutes over the course of one day. On this basis, daily average temperatures and amplitudes were calculated and extracted along the river channel transect (Fig. 4.1).

In order to handle different temperature conditions, a normalized flow path temperature difference (T_{norm}) was defined and evaluated for all simulation time steps with a temperature difference between river and groundwater temperatures larger than 3 °C. The normalization was based on the river temperature (T_{river}) of the particular simulation time *t* and the average groundwater temperature (T_{GW}) as:

$$T(t)_{norm} = \frac{T(t)_{flow\ path} - T(t)_{river}}{T_{GW} - T(t)_{river}} \tag{4.1}$$

The value of T_{norm} is usually, but not necessarily between 0, if flow path temperature is equal to river temperature, and 1, if flow path temperature is equal to groundwater temperature. The general relation was applied to selected snapshots, highlighting the dependence of hyporheic residence times on hyporheic flow path temperatures for positive and negative temperature gradients between the river and groundwater.

4.2.7 Temperature dependent biogeochemical processes in the streambed

The fraction of consumed oxygen along hyporheic flow paths (oxygen consumption) is described by first order reaction kinetics (Schroth et al., 1998; González-Pinzón et al., 2012, Vieweg et al., 2016):

$$fraction\ of\ consumed\ oxygen = 1 - e^{(-k(t)\ x\ t_{res}(t))} \quad (4.2)$$

where k is the first order respiration rate coefficient and t_{res} is the residence time. The temperature dependent first-order respiration rate coefficient is calculated based on an empirical relation derived at the in-stream gravel bar (Vieweg et al., 2016):

$$k(t) = 0.187\ d^{-1}\ \times\ e^{0.232\ °C^{-1} \times \overline{T_{effective}(t)}} \quad (4.3)$$

where $T_{effective}(t)$ is the mean effective flow path temperature. To estimate the influence of residence time-dependent flow path temperatures on oxygen consumption, we calculated the relative error (%) between fraction of consumed oxygen using river temperature as the effective temperature ($T_{effective}(t)$), and residence time-dependent flow path temperatures ($T_{flow\ path}$, see Section 4.3.5, Equation 4.4), as the effective temperature in Equation (3), respectively.

4.3 Results

4.3.1 Hydraulic conductivity

The mean K_h of the streambed was 1.4×10^{-3} m s^{-1} ranging from 1.1×10^{-4} m s^{-1} to 9.2×10^{-3} m s^{-1}. We found significant differences for grouped mean K_h related to the location relative to the geomorphological structure, but not over time or with increasing depth below the riverbed surface (Table 4.2). The median (1.2×10^{-3} m s^{-1}) and the range (9.0×10^{-3} m s^{-1}) of hydraulic conductivity at the crest was higher than the median (0.8×10^{-3} m s^{-1} / 0.7×10^{-3} m s^{-1}) and range (0.4×10^{-3} m s^{-1} / 0.6×10^{-3} m s^{-1}) of the hydraulic conductivity at the head and center of the geomorphological structures (APPENDIX 4.B). The measured hydraulic conductivity within the aquifer slightly decreased with depth (Table 4.3).

Table 4.2: Analyses of riverbed hydraulic conductivity variance

Source	Groups (degree of freedom)	Sum of squares	Mean square	p-value
Time	2011, 2012, 2013	3.68	1.84	0.071
Depth (m)	0-0.2, >0.2 - 0.4, >0.4 - 0.8	0.97	0.24	0.841
Location (reach)	In-stream gravel bar, Point bar, River	1.86	1.86	0.101
Location (structure)	Head, Crest, Tail	6.57	3.28	**0.009**
Total	231	191.39		

Table 4.3: Measured riverbed and aquifer hydraulic conductivities

Location (depth below surface)	Average hydraulic conductivity	Model Layer
Riverbed (< 0.80 m)	1.40×10^{-3} m s^{-1}	1-14
Shallow (1.70 m)	1.06×10^{-3} m s^{-1}	12,13 [*2]
Middle (2.70 m)	6.93×10^{-4} m s^{-1}	14-15[*2]
Deep (3.70 m)	2.30×10^{-4} m s^{-1}	16 - 27[*2]
Bottom[*1] *(9.00 m)*	*2.30×10^{-8} m s^{-1}*	*28*[*2]

[*1] small hydraulic conductivity at the last model layer represents impermeable underlying sediment (value not measured)[*2] homogeneous for the entire layer

4.3.2 Parameter sensitivity analysis

River-groundwater exchange derived from the coupled water flow and heat transport simulations was substantially influenced by the properties characterizing the distribution of the hydraulic conductivity (mean, variance and anisotropy) and was also sensitive to the bulk density of the sediment, thermal conductivity and dispersion length (Fig. 4.2a). The hydraulic conductivity and dispersion length are directly related to the subsurface heat flux (advection-conduction equation), whereas the bulk density and thermal conductivity of the sediment are used to describe the temperature dependence of the hydraulic conductivity (Molson et al., 1992, APPENDIX 4.B).

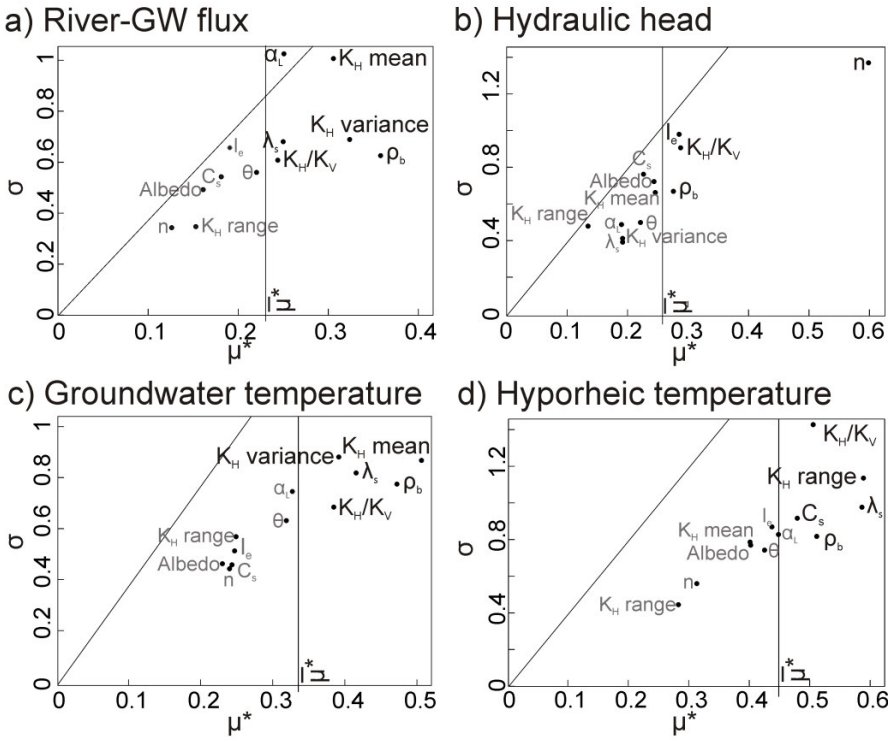

Figure 4.2: Morris plots of μ* versus σ of the elementary effect of each parameter with respect to (a) river-groundwater exchange flux, (b) hydraulic head, (c) groundwater temperatures, and (d) hyporheic temperatures. See Table 4.1 for a description of parameter symbols.

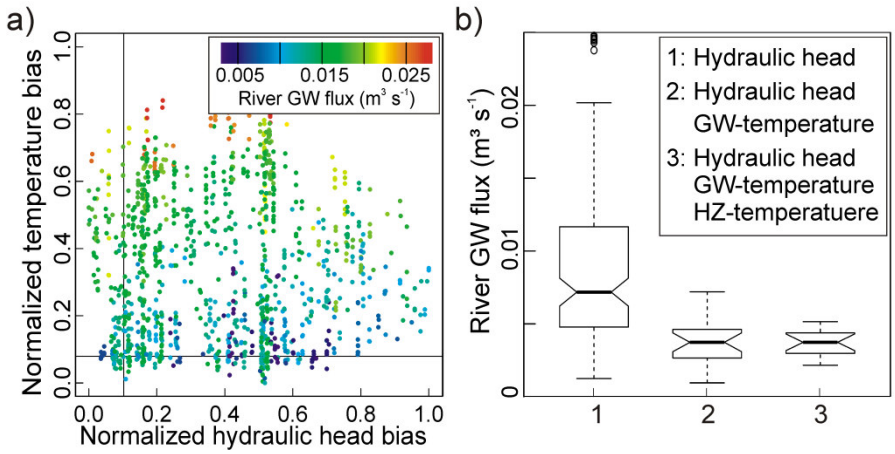

Figure 4.3: (a) Relation between hydraulic head bias and temperature bias, with river-groundwater exchange flux indicated in color, for all sensitivity simulations. (b) Distribution of simulated river-groundwater exchange flux considering the best 10 % of all sensitivity simulations regarding the hydraulic head bias, hydraulic head and groundwater temperature bias, and the hydraulic head and groundwater/hyporheic temperature bias.

River and groundwater hydraulic heads were found to be more sensitive to properties assigned to the surface domain, especially to the riverbed friction, than to the properties of the sediment (Fig. 4.2b). The riverbed friction mainly controls the water level in the river, according to the Manning Strickler formula. Changes in river level also altered the simulated hydraulic heads in the adjacent groundwater, but the hydraulic head was insensitive to the mean and variance of the hydraulic conductivity.

Besides the properties characterizing the distribution of the hydraulic conductivity (mean, variance and anisotropy), the most sensitive parameters affecting the groundwater and hyporheic temperatures were the thermal conductivity, bulk density and heat capacity (Fig. 4.2c, d). These parameters are directly related to the general equation for variably saturated subsurface heat transport (Molson et al., 1992, APPENDIX 4.A). In general, subsurface temperatures across the domain were influenced by the same parameters affecting the river-groundwater exchange flux (with some differences in the order of importance and apart from the dispersion length), highlighting the benefits of temperature in constraining fully-integrated models in order to accurately simulate river-groundwater exchange (Fig. 4.2).

Most of the parameters observed had substantial direct effects on the simulation results, with weak non-linear/interaction effects. Only the dispersion length was characterized by strong non-linear/interaction effects on the simulated river-groundwater exchange flux (Fig. 4.2).

Figure 4.3a demonstrates the relation between hydraulic head bias, temperature bias and river-groundwater exchange flux for all sensitivity simulations. The average river-groundwater exchange flux of the best 10 % of all simulations with respect to the hy-

draulic head (normalized hydraulic head BIAS < 0.1) was 7.2×10^{-3} m^3 s^{-1}, ranging between 1.3×10^{-3} m^3 s^{-1} and 6.0×10^{-2} m^3 s^{-1}. In contrast, the average exchange flux for all simulations with a normalized groundwater temperature BIAS < 0.1 was 3.9×10^{-3} m^3 s^{-1}, ranging between 6.1×10^{-4} m^3 s^{-1} and 9.9×10^{-3} m^3 s^{-1}. A substantial change in the mean and variance of the simulated exchange flux was achieved by including the temperature in addition to the hydraulic head information for model validation (Fig. 4.3b).

The model was calibrated to the river and groundwater hydraulic heads, as well as to streambed and groundwater temperatures. Values for the auto-calibrated parameters are presented in Table 4.1. The calibrated mean and variance of the K_h field slightly differ from the slug test derived values. The best simulation results were achieved by increasing the measured mean K_h by a factor of 1.6 and the variance of K_h by a factor of 1.3 compared to the observed values.

4.3.3 Model validation

The simulated hydraulic heads in the river clearly represented the observed hydraulic heads (MAE = 0.03, NSE = 0.92) and also matched their seasonal dynamics (Fig. 4.4a). MAE and NSE comparing observed and simulated hydraulic heads in the groundwater ranged from 0.02 to 0.08 and from 0.63 to 0.95, respectively (Fig. 4.5, first row). There

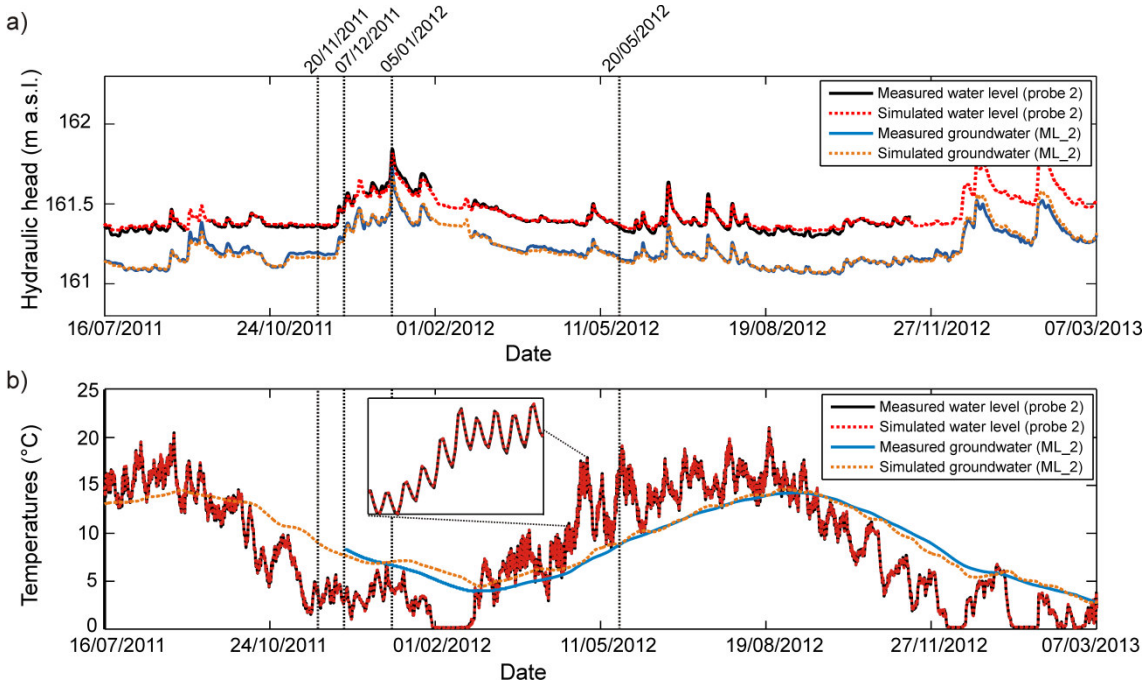

Figure 4.4: (a) Observed and simulated hydraulic heads, and (b) observed and simulated temperatures of the calibrated model. Measurement locations of the river (161.14 m a.s.l.) and ML_2 (157.9 m a.s.l.) are indicated in Fig. 4.1a.

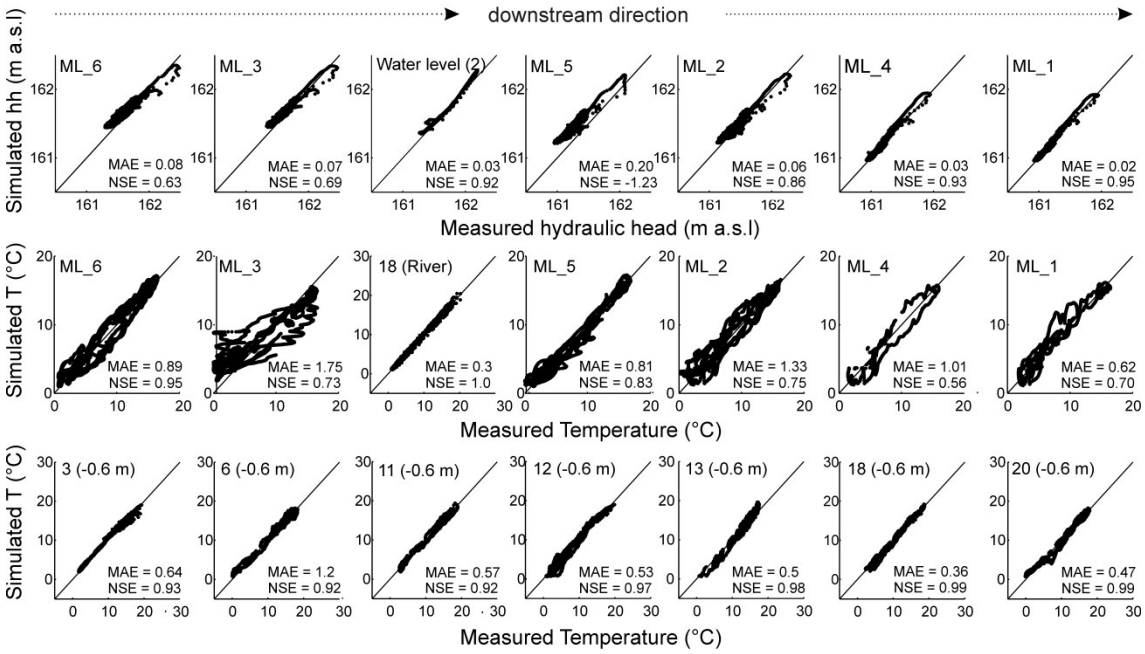

Figure 4.5: Measured vs. simulated hydraulic heads (first row), groundwater temperatures (second row) and riverbed temperatures (third row) for the calibrated model. Hydraulic head and temperature time series of the river and ML_2 are shown in Fig. 4.4. All measurement locations are indicated in Fig. 4.1a.

is one exception, observation point ML_5, where the simulated hydraulic head was systematically overestimated (MAE = 0.2). Another observation is that during high discharge events (January 2012 and December 2012), hydraulic heads in the groundwater were slightly underestimated for the rising limb of the hydrograph and slightly overestimated during peak discharges and flood recession (Fig. 4.4a, 4.5).

Simulated temperatures in the river were clearly able to closely represent the observed temperatures (MAE = 0.3, NSE = 1) and also matched well their seasonal and daily dynamics (Fig. 4.4b), proving the accurate model setup of the surface domain, where the temperature dynamics were mainly driven by river boundary conditions and atmospheric input. MAE and NSE comparing observed and simulated groundwater and riverbed temperatures ranged from 0.3 to 1.75 and from 0.56 to 1, respectively (Fig. 4.5). In general, the riverbed temperatures were reproduced accurately for all selected locations within the riverbed, the head, crest and tail of the intensively monitored geomorphological structures. The differences between observed and simulated temperatures slightly increased with increasing aquifer depth. This deviation was a mismatch in the simulated amplitude of the temperature signal. In most cases, the simulated annual temperature extremes were lower compared to the observed. That deviation was most obvious at ML_3, where the summer maximum temperatures were systematically underestimated and the winter minimum temperatures were systematically overestimated (Fig. 4.5). Overall, while using heads only leaves an ambiguity for fluxes, by including temperature data, which reflect also advective heat transport, the simulated fluxes are better constrained to the real values, though not being close everywhere.

4.3.4 Water flux across the river-groundwater interface and hyporheic exchange

In Figure 4.6, the simulated hydraulic head distribution, the resulting flow field (a-c), the river-groundwater exchange flux (d-f) and hyporheic flow path lengths and residence times (g-i) are presented. The selected snapshots are representative for low (0.25 $m^3 s^{-1}$), moderate (1.28 $m^3 s^{-1}$) and high (3.65 $m^3 s^{-1}$) river discharges and include a discharge-dependent shape of the river shoreline.

For low river discharges, hyporheic flow cells formed across the in-stream gravel bar, the point bar, and around the riffle (Fig. 4.6a). Median flow path length for low river discharges was 9.4 m and the median residence time was 37.7 h. Flow path lengths and residence times were lognormally distributed (Fig. 4.6g). Total hyporheic exchange was 2.8×10^{-3} $m^3 s^{-1}$. The volume of hyporheic exchange was two orders of magnitude smaller than the river discharge over the river length of about 250 m and 1.12 % of the river discharge penetrated through the saturated sediment. Dominant river water infiltration, with infiltration rates up to 4.5×10^{-5} m s^{-1}, occurred upstream of the geomorphological structures extending across the whole river channel at the upstream side of the riffle, whereas exfiltration mainly occurred at the downstream sides of the geomorphological structures (Fig. 4.6d). At 3.5×10^{-5} m s^{-1}, the highest exfiltration rates appeared at the deep pool downstream of the point bar and the riffle, where the effect of hyporheic exfiltration was increased by the lateral inflow of riparian groundwater.

For moderate river discharges, the direction of the hyporheic flow paths substantially changed in comparison to the low river discharges (Fig. 4.6b). Median flow path length for moderate discharges was 8.3 m and the median residence time was 7.8 h. Residence times of the hyporheic flow paths were bimodally distributed, with two comparably shaped modes peaking at 1.5 h and at 5.1 h (Fig. 4.6h). The shift from the lognormal towards the bimodal distribution reflected the changing relation between hyporheic exchange flux at the in-stream gravel bar and around the point bar. Absolute hyporheic exchange was 2.4×10^{-3} $m^3 s^{-1}$, thus slightly decreased in comparison to low river discharges (- 14 %). Hyporheic exchange comprised only a fraction of moderate river discharges (0.19 %) over the river length of about 250 m. Dominant river water infiltration occurred upstream of the in-stream gravel bar and the point bar, whereas infiltration upstream of the riffle diminished for moderate river discharges (Fig. 4.6e).

For high river discharges, the dominant riverbed structures submerged, and the hyporheic exchange almost disappeared. Total hyporheic exchange was 9.12×10^{-5} $m^3 s^{-1}$, several orders of magnitude smaller than the river discharge, but larger than for smaller river discharges. Median flow path length for high discharges was 7.3 m and the median residence time was 4.8 h. With increasing river discharge, the bulk of losing flow paths

at both riverbanks increased (Fig. 4.6c). At 1.8×10^{-5} m s^{-1}, the highest infiltration rates towards the riparian groundwater occurred at the southern riverbank. The central parts of the river channel were characterized by comparably low infiltration rates (Fig. 4.6f).

Most of the infiltrated river water outside the characteristic hyporheic flow cells left the domain via the lateral boundaries of the model domain (Fig. 6a-c), which is the result of the river reach characterized by losing conditions. The overall losing flux was the highest, 3.3×10^{-3} m^3 s^{-1}, that is 312 % more than for low river discharge, with

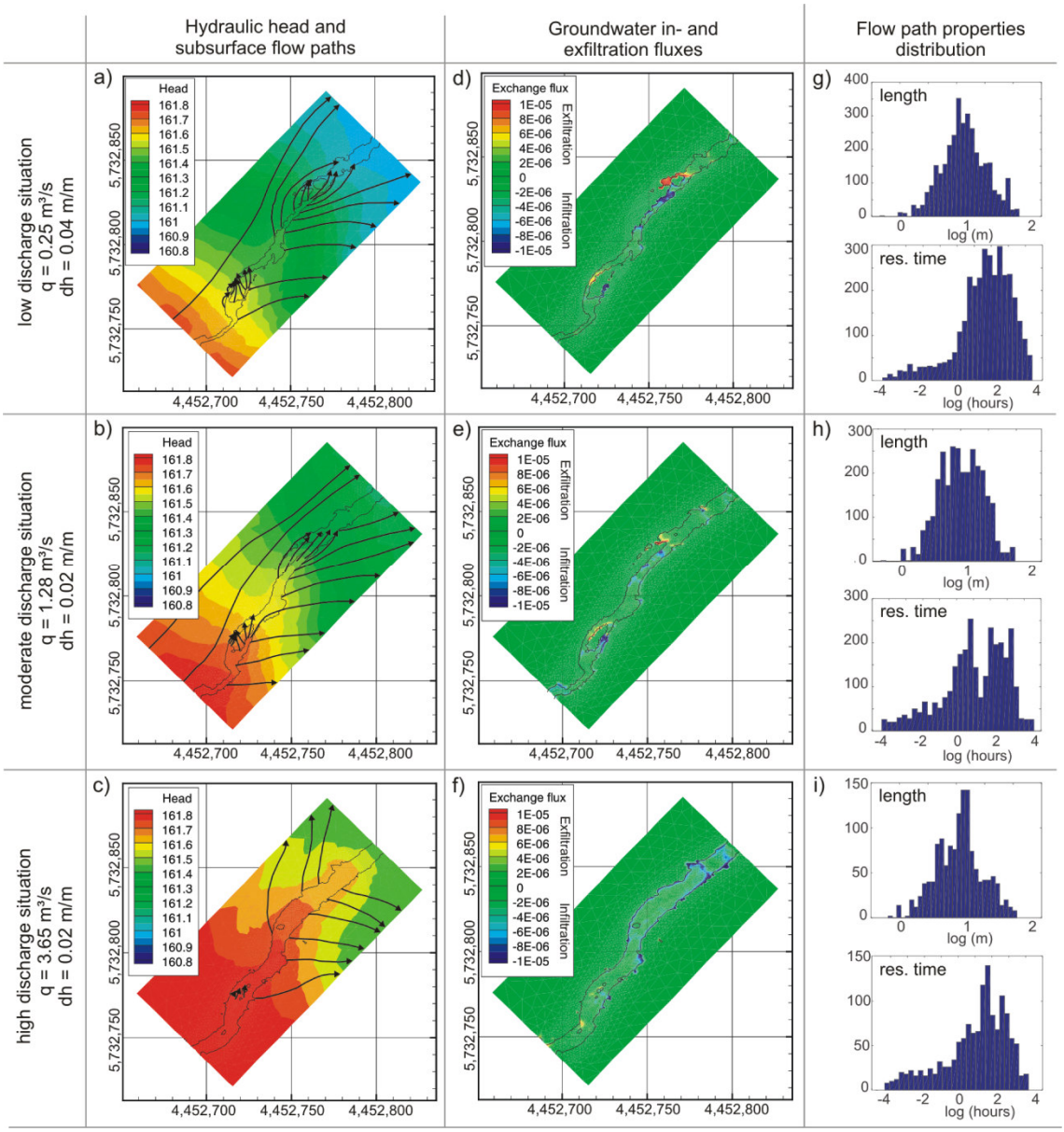

Figure 4.6: (a-c) Hydraulic heads of the streambed and groundwater streamlines for low, moderate and high river discharges under loosing conditions. (d-f) River-groundwater exchange flux (Negative values indicate surface water infiltration to groundwater); the black solid line shows the actual river shape. (g-i) Flow path length (upper) and residence time distributions for hyporheic flow path. The x-axis is scaled logarithmically.

0.8×10^{-3} m^3 s^{-1}. Since, the hyporheic exchange flux decreased and, in turn, the net water exchange remained relatively constant, ranging between 3.6×10^{-6} m^3 s^{-1} and 3.3×10^{-6} m^3 s^{-1} (- 8 %) for presented river discharges.

Simulated median hyporheic residence times at the river reach varied inversely with the river discharge. We observed an exponential relationship between river discharge and median hyporheic residence times for the entire simulation period (APPENDIX 4.B). Median residence time for all discharges smaller than 1 m^3 s^{-1} was 37.1 h and decreased to median residence times of 7.1 h for river discharges higher than 1 m^3 s^{-1}. The median residence times were uncorrelated with the strength of the vertical hydraulic gradient between river and groundwater (correlation coefficient (CC) = -0.08, p-value = 0.02). We observed no significant correlation between river discharge and total hyporheic exchange (CC = -0.02, p-value = 0.57) (APPENDIX 4.B). The average hyporheic exchange for discharges smaller than 3.5 m^3 s^{-1} was 2.4×10^{-3} m^3 s^{-1} with a variance of 4×10^{-7} m^3 s^{-1}. For discharges above 3.5 m^3 s^{-1}, the dominant riverbed structures submerged, and hyporheic exchange almost disappeared (average value = 8.6×10^{-6} m^3 s^{-1}).

4.3.5 Heat transport and subsurface temperature patterns

The advective heat transport in the shallow streambed for selected cases of low (0.25 m^3 s^{-1}), moderate (1.28 m^3 s^{-1}) and high (3.65 m^3 s^{-1}) river discharges was always much larger than the conductive flux and thus dominated the net heat exchange (APPENDIX 4.B). Heat was moving from the river into the saturated sediment along the hyporheic and losing flow paths, driving the temperature dynamics in the shallow riverbed sediments. The subsurface temperature regime is presented for low river discharges (0.25 m^3 s^{-1}), as well as spring-summer (20 May 2012) (Fig. 4.7a, b) and autumn-winter (22 November 2011) temperature conditions (Fig. 4.7c).

On May 20th, characteristic for the spring-summer period, the riverbed at hyporheic and losing flow paths experienced larger daily temperature amplitudes and higher average daily temperatures originating from infiltrating river water than the gaining locations (Fig. 4.7a, b). This yields an overall, high spatial variability of the daily amplitudes and average daily temperatures in the river bed (Fig. 4.7d, e). Below a depth of ~1 m, temperatures were almost independent of the diurnal fluctuations at the land surface, and the amplitudes diminished.

The temperatures in the river (15 °C) were higher than the groundwater temperatures (9.5 °C). The warmer areas were dominated by heat advection from the river and the absence of upwelling groundwater. The thermal impact, originating from the river (15 °C), on the subsurface temperature reached a depth of 2.7 m (T > 13 °C) at the in-

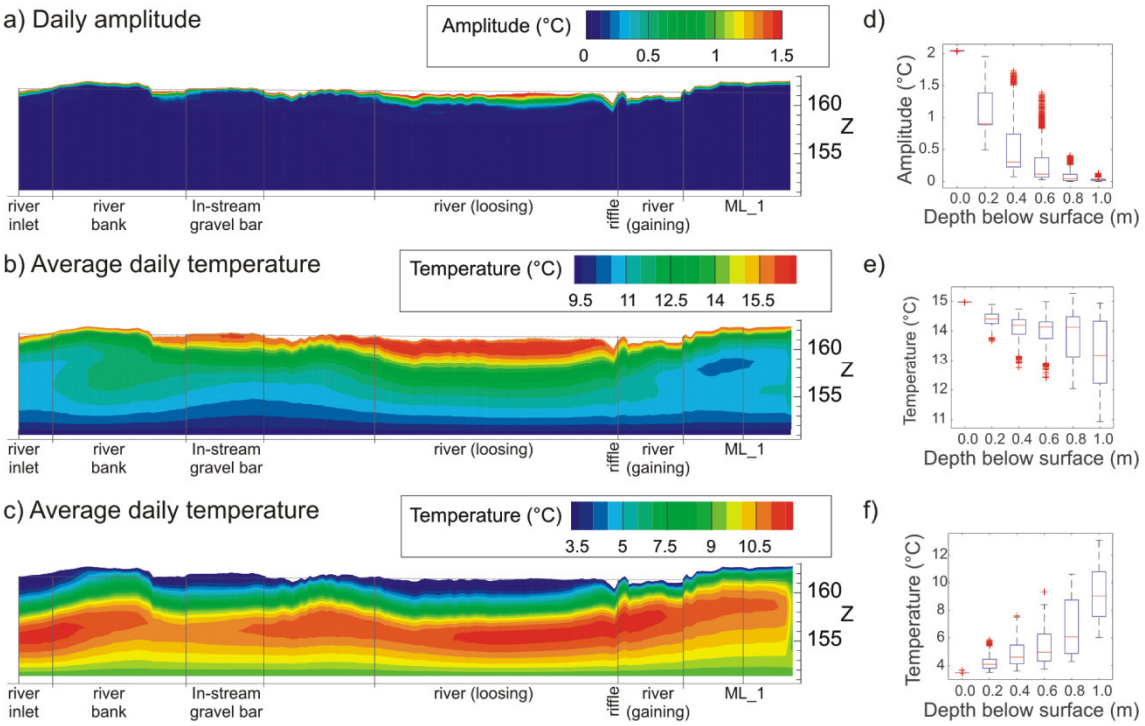

Figure 4.7: Cross-sections along transect A-B showing (a) daily temperature amplitudes for low discharges (q = 0.25 m³/s) and moderate amplitudes (A = 2 °C), (b) daily average temperatures for spring-summer (negative temperature gradient between river and groundwater), and (c) autumn-winter (positive temperature gradient between river and groundwater). (d-f) Boxplot of average daily temperature for each streambed node at 0, 0.2 m, 0.4 m 0.6 m, 0.8 m and 1 m depth below the river-groundwater interface.

stream gravel bar and 4.2 m at the infiltration location in the river channel. It reduced to 0.3 m at the discharge location at the back of the point bar/riffle where heat transport was dominated by conduction (Fig. 4.7b). With increasing depth, the sediment temperature decreased to 13.1 °C at 1 m below the riverbed and thus was almost 2 °C lower than the river temperature (Fig. 4.7e). The subsurface temperature variance increased with increasing depth from 0.05 °C at 0.2 m to 1.3 °C at 1 m below the riverbed (Fig. 4.7e).

On November 22nd , characteristic for the autumn-winter period, the river temperature was 3.5 °C only (Fig. 4.7c). Generally, the hyporheic and losing zones of the river channel experienced lower average daily temperatures than the gaining parts of the river channel. The thermal impact, originating from the river, on the subsurface temperature was overall comparable to the spring-summer condition, though opposite in direction. With increasing depth, the sediment temperature significantly increased to 9.2 °C at 1 m below the riverbed and thus was about 5.7 °C higher than the river temperature (Fig. 7f). The subsurface temperature variance increased with increasing depth, from 0.2 °C at 0.2 m to 3.2 °C at 1 m below the riverbed (Fig. 4.7f).

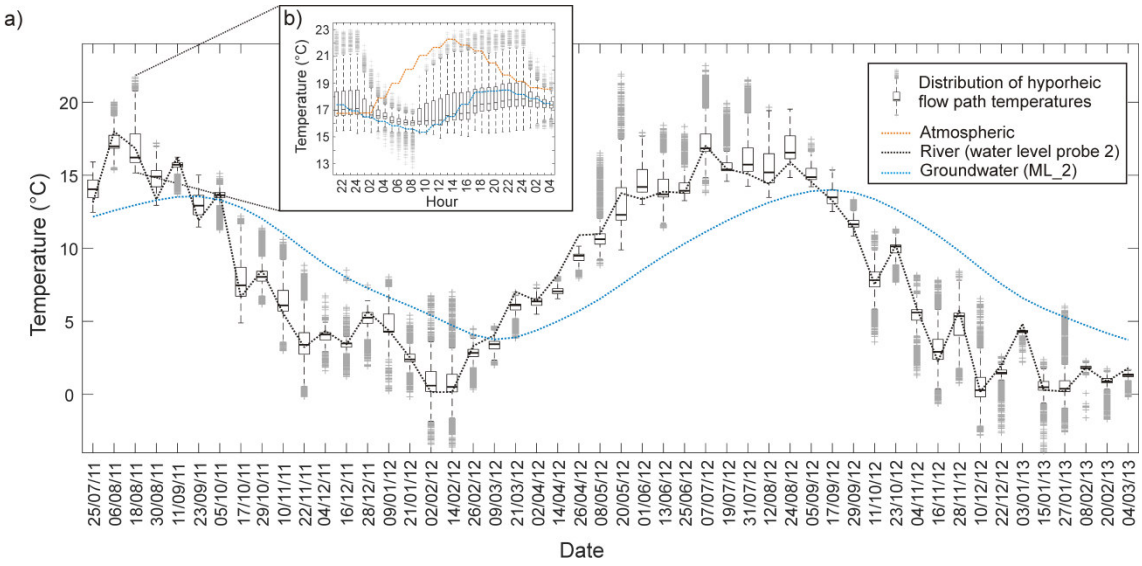

Figure 4.8: (a) Distribution of hyporheic flow path temperatures every 6 days from July 2011 until March 2013 compared to simulated average daily temperature for river and groundwater. (b) Distribution of hyporheic flow path temperatures on 18 August 2011 every hour (+ 4 hours of the previous and following day).

Driven by the seasonal and daily temperature dynamics in the river, the average hyporheic temperature varied on seasonal and daily time scales (Fig. 4.8). Generally, the average temperature of the hyporheic zone strongly depends on the river temperatures (CC = 0.99), whereas the variance in hyporheic flow path temperatures was only weakly correlated with daily temperature amplitudes in the river (CC = 0.14, p-value = 0.5). The maximum annual temperature difference was 19.2 °C; with a maximum average hyporheic temperature of 19.4 °C (1 July 2012) and a minimum average hyporheic temperature of 0.16 °C (26 February 2013).

Maximum daily difference of the day selected for the zoom-in (Fig. 4.8b) was 1.7 °C, with a maximum average hyporheic temperature of 17.8 °C (at 12:00 p.m.) and a minimum average hyporheic temperature of 16.1 °C (at 08:00 a.m.). The variance in hyporheic flow path temperatures was up to 2.8 °C (at 04:00 p.m.), with a minimum flow path temperature of 15.0 °C (1.8 °C colder than average hyporheic temperature) and maximum flow path temperature of 22.9 °C (6.1 °C warmer than current river temperature).

We analysed for a relationship between the average hyporheic flow path temperature and hyporheic residence times depending on the temperature gradient between river and groundwater (Fig. 4.9). In autumn-winter, the average temperature of slow and long flow paths tends to be higher compared to quick and short flow paths (Fig. 4.9a), especially for the very long residence times. On opposite in spring-summer the average temperature for longer flow paths is lower than for shorter ones (Fig. 4.9b). The distribution

between flow path temperatures ($T_{flow\ path}$) and residence times (t_{res}) follow a power law relationship with exponent of 0.37 ($R^2 = 0.56$, $t_{res} > 0.37$ h) (Fig. 4.9c):

$$log(T_{norm}) = -1.06 + 0.3684 \times log(t_{res}) \quad (4.4a)$$

$$T_{flow\ path} = T_{river} + 0.0864 \times {t_{res}}^{0.3684} \times (T_{GW} - T_{river}) \quad (4.4b)$$

Including hyporheic flow paths with residence times smaller than 0.37 h would decrease the accuracy (R^2) of the derived empirical model; the model is not valid for quick and short flow paths where flow path temperature is additionally affected by the atmospheric energy input.

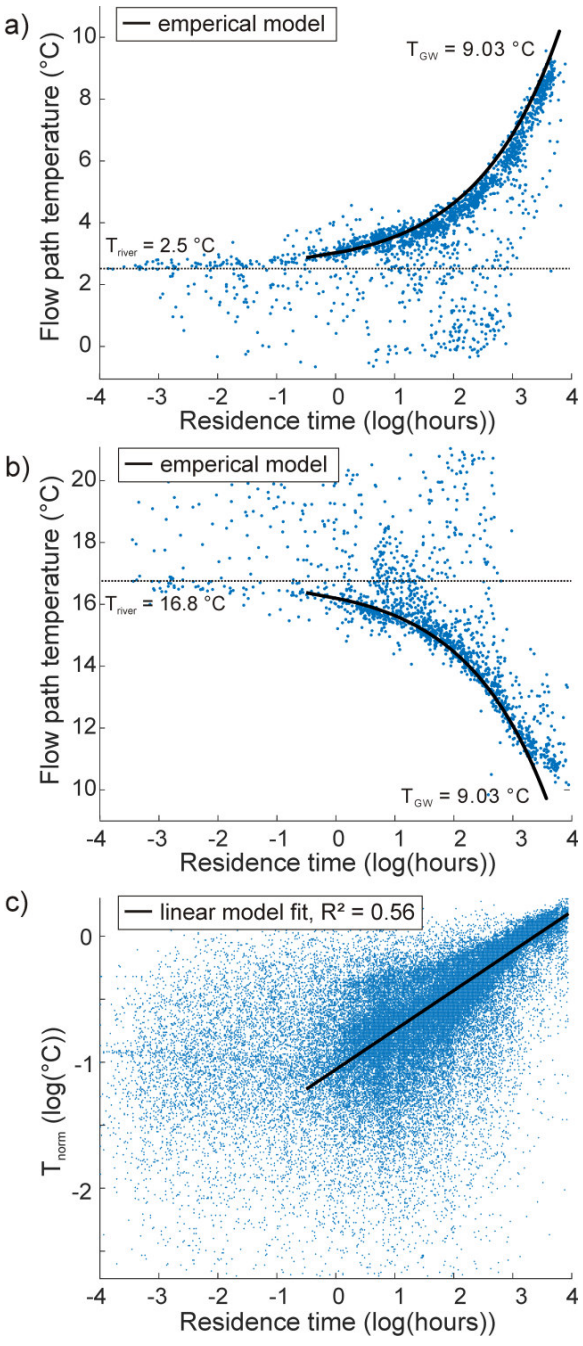

Figure 4.9: Relation between residence time of hyporheic flow paths (t_{res}) versus average flow path temperature ($T_{flow\ path}$) for (a) an autumn day (22 November 2011) and (b) a spring day (20 May 2012). The empirical model is presented in equation 4.4b. (c) Relation between residence time of hyporheic flow paths versus normalized flow path temperature (T_{norm}) for all simulation time steps, with temperature differences between river (T_{river}) and groundwater (T_{GW}) > 3 °C. The fitted linear model is presented in equation 4.4a.

4.3.6 Implications of hyporheic residence time and temperature for biogeochemical processes in the streambed

Both, hyporheic residence times and temperatures influence the turnover of dissolved substances in the hyporheic zone. This will be reflected in the oxygen concentrations along the flow paths. Taking the river temperature as proxy for the usually unknown hyporheic flow paths will imply some error. We can evaluate that error, based on the simulated flow path residence time, simulated river temperature, the empirical equation 4b and an empirical oxygen consumption rate (Fig. 4.10). The relative difference (%) between fraction of consumed oxygen evaluated based on river temperature only versus using the empirical flow path temperature ($T_{flow\ path}$, see Equation 4.4) as the effective temperature in equation (4.3) can be substantial. In general, longer residence times lead to higher absolute oxygen consumption (Zarnetske et al. 2011; Marzadri et al. 2012). Our results demonstrate that oxygen consumption was substantially increased in autumn-winter (flow paths with long residence times are potentially warmer than short ones) and decreased in spring-summer (flow paths with long residence times are potentially cooler than short ones), when the effect of hyporheic flow path temperature on solute transformation is regarded (Fig. 4.10). For example, oxygen consumption in flow paths with residence times of about 37.7 h (median residence time at the Selke river reach for low discharges) and river temperatures of 2.6 °C was found to be 29 % higher when accounting for residence time-dependent temperature relationships.

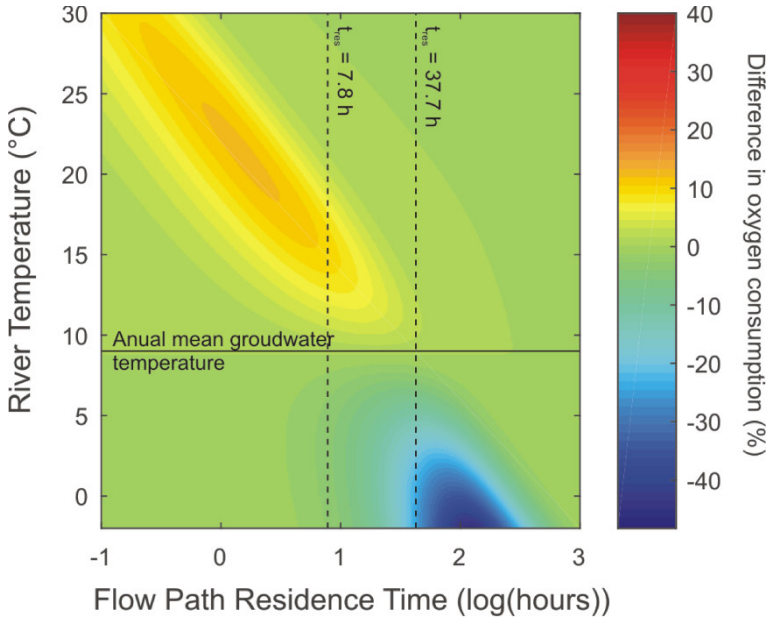

Figure 4.10: Difference between empirical oxygen consumption calculated via river temperature and via empirical flow path temperature (Equation 4.4).

4.4 Discussion

4.4.1 Hydraulic conductivity

Previous modelling studies have revealed the need for a heterogeneous representation of riverbed hydraulic conductivities to accurately simulate river-groundwater exchange, hyporheic flow path and residence times (Naranjo et al., 2012; Karan et al., 2014). Especially processes within the hyporheic zone are controlled by residence times of river water within the sediment, which strongly depends on heterogeneity in the riverbed hydraulic conductivity (Salehin et al., 2004; Sawyer and Cardenas, 2009; Tonina et al., 2016). We found that the riverbed hydraulic conductivity depends on the relative position around the geomorphological structures. The lower hydraulic conductivity at the head of the gravel and point bar could be caused by continuous river water infiltration into the riverbed, transporting organic matter and fine sediments. These materials potentially accumulate in the sediment interstices within the river water infiltration zones (clogging), decreasing the hydraulic conductivity of the riverbed (Brunke and Gonser, 1997; Packman and Mackay, 2003). The best simulation results were achieved by increasing the implemented mean K_h by a factor of 1.6 compared to the measured values, demonstrating the relevance of parameter calibration even if there is a profound experimental data base. Furthermore, although the Hvorslev falling head slug test is considered a robust method for measuring K_h in shallow riverbed sediments (Landon et al., 2001), there could be a slight basis for layered media, e.g. by a vertical flow component in the slug tests.

The observed hydraulic conductivities of the streambed sediments slightly decreased with depth (Table 4.3) which has been reported by other studies (Landon et al., 2001; Song et al., 2007). The hydraulic conductivity of an unconsolidated sediment tends to decrease with depth as a result of sediment compaction caused by increasing overburden pressures (Helm, 1976). Decreasing hydraulic conductivity within the alluvial deposits below the streambed may limit the penetration depth of river-groundwater exchange fluxes.

The anisotropy ratio of 17 for the horizontal to vertical hydraulic conductivity found in this study is rather high, but plausible and within the range of values reported by Trauth et al. (2015) for a smaller-scale numerical model representing the in-stream gravel bar. The anisotropy within the riverbed can be explained by the strong preferential orientation of ellipsoidal, flat gravels and cobble stones in the direction of flow (imbrication), which has been observed at the streambed surface and in freeze cores of the streambed sediments. Comparable anisotropy ratios have been observed for alluvial aquifers (e.g. Chen and Chen, 2003).

4.4.2 Model setup and model validation

The presented model setup goes beyond existing modelling efforts of river reaches, as the heat transport is driven by the use of atmospheric input routines allowing the simulation of river temperatures. Often, the surface heat boundary in models has been defined as fixed temperatures at the top nodes of the modelling domain (e.g. Bartsch et al., 2014; Karan et al., 2014). Such settings do not account for the potential influence of groundwater discharge on the stream temperatures, which might be reasonable for a river under losing conditions but not for gaining conditions, especially when the temperature gradient between river and groundwater is high.

The calibrated model fit the observed hydraulic heads with the exception of a single observation point, ML_5, where the simulated hydraulic head was systematically overestimated (MAE = 0.2). The hydraulic head at this location was sensitive to changes in riverbed friction and hydraulic conductivity. That indicates that the mismatch was caused by strong heterogeneities in the riverbed structure or in the hydrogeology of the south-eastern part of the river banks, which seems not to have been resolved with sufficient detail.

The highest deviations in maximum and minimum annual temperatures were found in groundwater where simulated temperature peaks were generally lower than the observed ones. The mismatch in temperature variations could be caused by an underestimation of river-groundwater exchange at the river bank (bank filtration), limiting the advective heat exchange along the losing flow paths. On the other hand, the missing temperature dynamics could also be related to the definition of the lateral temperature boundaries in the model, as the deep subsurface flow field was characterised by groundwater entering the domain via the lateral boundary. An underestimation in temperature dynamics at the lateral boundaries would therefore result in an underestimation of the groundwater temperature dynamics at the observation wells.

In the region of interest, the shallow zone of the saturated sediment where hyporheic exchange dominates, the simulated temperatures perfectly matched the observed temperature, highlighting that the modelled magnitude and direction of exchange fluxes as well as the temperature dynamics accurately represents the condition within the river reach. Thus, the coupled water flow and heat transport model for this Selke river reach provides a sound basis for quantitatively investigating variations in hyporheic exchange fluxes, hyporheic residence times, and hyporheic temperatures.

4.4.3 Implications of coupled water flow and heat transport simulation for river-groundwater exchange

For reach-scale applications, three-dimensional numerical modelling in conjunction with point measurements has been used earlier to quantify the exchange flux across the river-sediment interface (e.g. Storey et al., 2003; Wondzell et al., 2009; Munz et al., 2011). While the exchange flux is the main variable of interest (besides the state variables itself), model calibration is based on the simulated hydraulic heads, or other state variables and their discrepancies to the corresponding values from field measurements. Previous studies have shown that model calibration and validation based on observed hydraulic heads was not sufficient to constrain the model parameters sufficiently (Bravo et al., 2002; Naranjo et al., 2012). Thus, temperature data have been used to better constrain the estimation of subsurface parameters in steady-state groundwater models and e.g. support calibration of hydraulic conductivities (Doussan et al., 1994; Karan et al., 2014). The assimilation of temperature data was also reported to lead to a better characterization of the spatial distribution of leakage parameters (Kurtz et al., 2014).

Going beyond steady-state, in our model simulations that progressed to transient conditions, the hydraulic head turned out to be insensitive to parameter variations in mean, variance and range of the saturated hydraulic conductivity (Fig. 4.2). For the hydraulic gradient between groundwater and river is highly restricted by the lateral model boundary and the surface inflow and outflow boundaries in combination with the riverbed roughness determining the hydraulic head in the surface domain. Changes in hydraulic conductivity directly alter the simulated river-groundwater exchange flux but do not affect the hydraulic head patterns (Fig. 4.2).

In contrast, simulated temperatures are highly sensitive to variations in mean, variance, and range of the saturated hydraulic conductivity, highlighting that heat is an additional quantity which helps to constrain highly parameterized, fully-integrated models commonly affected by parameter non-uniqueness. Besides the improvements in model calibration (reduction in head and temperature residuals), we aimed to quantify the benefits of temperature on simulated water flux across the river-groundwater interface. A substantial change in the mean of the simulated exchange flux was achieved (- 46 %) by including the temperature in addition to the hydraulic head information in order to constrain the estimation of the subsurface parameters of transient, fully-integrated numerical models.

4.4.4 Water flux across the river-groundwater interface and hyporheic exchange

The fully-integrated modelling approach allows the calculation of water flux across the entire surface domain, hyporheic exchange flux and hyporheic residence times. Our study reveals how a typical lowland river reach and groundwater are dynamically connected.

The ratio of hyporheic exchange to river discharge decreased for the considered flow conditions. With increasing discharge (increasing water level), hydraulic head gradients across the geomorphological structures decreased and in turn also total hyporheic exchange. The head difference across the non-submerged geomorphological structures was highest for low discharges (low water level) because the low discharges forced river heads to follow riverbed morphology more closely. Thus, hyporheic exchange at the reach-scale is highly variable in space and time and strongly depends on river discharge. In contrast, the net water flux across the river-groundwater interface remained relatively constant. The portion of hyporheic versus loosing flow paths changed in dependence on river discharge. Also, hyporheic residence times of the partly submerged geomorphological structures varied inversely with the river discharge, as observed also in other studies (Shope et al., 2012; Trauth et al., 2015).

Simulated hyporheic residence times for the Selke river reach were slightly higher than residence times simulated for the isolated in-stream gravel bar itself, earlier calculated with an idealized boundary condition (Trauth et al., 2015). But the different modelling scales substantially altered simulated residence times, as larger domain sizes allow for longer hyporheic flow paths with higher residence times especially under losing conditions (infiltrating particles might re-join the river further downstream instead of leaving the modelling domain). Furthermore, hyporheic exchange at the reach-scale was also generated by deeper hyporheic flow paths with longer hyporheic flow paths through the riverbank, substantially increasing the median and variance of the residence time distribution. And finally the deviation could be explained in part by a resulting different parametrization of both models, i.e. the average hydraulic conductivity of 5.96×10^{-3} m s^{-1} used by Trauth et al. (2015) was about five times higher than the average hydraulic conductivity used in this study.

4.4.5 Heat transport and subsurface temperature patterns

Advective heat flux in the shallow streambed and in the unconfined aquifer is the major process controlling heat exchange between river and groundwater at the reach-scale. Only non-submerged geomorphological structures in our study did not really affect river

temperatures at the reach-scale by hyporheic exchange. These findings agree with small-scale (~ 0.6 m) experimental results showing that atmospheric heating rather than hyporheic advection caused thermal shifts within the surface water around weir-type instream geomorphic structure (Hester et al., 2009, Sawyer et al., 2012).

A strong variability in daily temperature patterns within riverbed sediments arises due to hyporheic exchange beneath dune-like triangular bedforms (Cardenas et al., 2007; Norman and Cardenas, 2014), riffles (Storey et al., 2003; Marzadri et al., 2013), as well as beneath weirs and large woody debris (Hester et al., 2009; Sawyer et al., 2012). Our results show how hyporheic up- and downwelling induced by non-submerged geomorphological structures drive substantial thermal heterogeneity within riverbed sediments at the reach-scale.

The average temperature in the hyporheic zone follows the temperature in the river (characterized by distinct annual and daily cycles), but along individual hyporheic flow paths, temperatures vary substantially around the average hyporheic temperature. The average hyporheic flow path temperature ranges between the atmospheric temperature and the yearly average groundwater temperature, strongly depending on the flow path residence time (flow path length) and the temperature gradient between river and groundwater. Average river temperature is a good predictor for the average hyporheic temperature. Individual hyporheic flow path temperature can be estimated by the power law relationship derived from the detailed numerical simulations (Equation 4.4) that accounts for hyporheic residence time, river and groundwater temperature.

4.4.6 Implications of hyporheic residence time and temperature for biogeochemical processes in the streambed

Microbially mediated solute transformation in the hyporheic zone, where up to 97 % of the entire stream respiration occurs (Naegeli and Uehlinger, 1997; Fellows et al., 2001), is predominantly controlled by the availability of oxygen and carbon. Biogeochemical cycles are typically strongly correlated to daily and seasonal temperature dynamics (Kaplan and Bott, 1989; Haliday et al., 2013), since the higher the temperatures, the higher the rates for microbially mediated solute transformation (Thamdrup and Fleischer, 1998; Acuna et al., 2008). Vieweg et al. (2016) found an exponential relationship between the first-order respiration rate constant and temperature in the streambed (Equation 4.2), in which the respiration rate increased by a factor of about 10 for temperature changes of 10 °C. Our simulation results highlight the strong relationship between hyporheic residence time, hyporheic flow path temperature and oxygen consumption. The time scale of oxygen consumption substantially differs when the empirical relationship between flow path residence time and flow path temperature (Equa-

tion 4.4) was used to calculate the oxygen consumption instead of an effective, flow path-independent temperature derived from the river temperature only. Both hyporheic residence times and hyporheic temperature patterns are important for quantifying the biogeochemical processes in the hyporheic zone, since the longer the residence time and the higher the temperature, the higher the potential for microbially mediated solute transformation.

4.5 Summary and conclusions

The goal of this study was to investigate the factors dominating water and heat fluxes across the river-groundwater interface and hyporheic temperature patterns along a natural lowland river reach and to aim for a better quantitative basis to account for their effect on temperature-sensitive microbial processes. We used the fully-integrated, surface-subsurface flow and heat transport model HydroGeoSphere in combination with particle tracking techniques in order to simulate these processes, based on continuous measurements of hydraulic heads and temperatures at different depths in the river bank and within the river over a two-year period from May 2011 until June 2013. Based on the field investigations and the simulation results, the following conclusions can be drawn:

1. Horizontal hydraulic conductivity depends on the location relative to the geomorphological structures, and is lowest at the head and increasing towards the center and tail.
2. The most sensitive parameters affecting the groundwater and hyporheic temperatures –in addition to the properties characterizing the distribution of the hydraulic conductivity (mean, variance and anisotropy) are the parameters related to the heat transport itself, i.e. thermal conductivity, bulk density and heat capacity.
3. Including the temperature in addition to the hydraulic head information constrains the estimation of subsurface parameters and decreases uncertainty in simulated exchange flux substantially. This leads to more accurate estimates of the flux between stream and groundwater systems.
4. Non-submerged streambed structures drive substantial thermal heterogeneity within riverbed sediments at the reach-scale.
5. The average hyporheic temperature is controlled by the river temperature, with daily and seasonal temperature differences up to 2.8 °C and 19.2 °C, respectively.
6. Individual mean hyporheic flow path temperature strongly depends on the flow path residence time and the temperature gradient between river and groundwater. In autumn-winter, the average temperature of long flow paths is potentially higher to the ones of short flow paths, whereas in spring-summer the average temperature of longer flow paths is lower than for shorter ones. Variations in hyporheic flow path

temperatures go up to 7.9 °C, significantly higher than daily averages, but still lower than average seasonal hyporheic temperature differences. The distribution between flow path temperatures and residence times follow a power law relationship with exponent of 0.32, derived by reach-scale simulations calibrated to field data.

7. Reach-scale hyporheic oxygen consumption can be adjusted for hyporheic residence times and average flow path temperature.

Our analysis highlights the hyporheic temperature variations in space and time and demonstrate how they relate to river temperature, groundwater temperature and hyporheic residence times. Understanding these links provides the basis from which to assess hyporheic temperature conditions in river reaches. Since biogeochemical processes depend on solute residence time and temperature, an understanding of flow and temperature regimes in the riverbed sediments is essential to quantify the reactive potential of hyporheic zones.

The model setup developed here is furthermore a sound basis from which to investigate water and heat fluxes across the river-groundwater interface and hyporheic temperature patterns, only relying on measurements of discharge, groundwater heads and climate conditions and could be particularly useful for extreme discharges when direct measurements at the river-groundwater interface are difficult to conduct.

APPENDIX 4.A: Surface-subsurface heat transport in HydroGeoSphere

Surface-subsurface heat transport for variably saturated conditions is incorporated in HGS together with temperature-dependent fluid properties, viscosity and density (Graf and Therrien 2005; Brookafield et al., 2009). The general equation for variably saturated subsurface heat transport is given by:

$$\frac{\partial \rho_b}{\partial t} = \nabla[q\,\rho_w c_w T - (k_b + \rho_b c_b D)T] \pm Q_T + \Omega_0 \tag{4.A1}$$

where q is the calculated darcy flux, $\rho_w c_w$ is the density and heat capacity of water, k_b is the bulk thermal conductivity, $\rho_b c_b$ is the density and heat capacity of the bulk volume, D is the thermal dispersion tensor, Q_T is the thermal source/sink term and Ω_0 the thermal surface-subsurface coupling term. In Equation (4.A1), the darcy flux (q) is calculated from Richards' equation, which is valid for fully saturated and unsaturated conditions. Changes in subsurface temperature affect fluid properties such as density or viscosity, thus also the hydraulic conductivity of the porous media. Whereas changes in fluid density remain small for the temperature range in natural surface water (0 °C – 30 °C), changes in fluid viscosity might alter the hydraulic conductivity by a factor of 2.3 between summer maximum (30 °C) and winter minimum (0 °C) temperatures, influencing the overall advective subsurface water flux and exchange flux between the surface and subsurface domains. The temperature-dependent viscosity for the temperature range from 0 °C - 40 °C is defined as (Molson et al., 1992):

$$\mu(T) = \mu_0\, exp^{[(-3.288\times10^{-2}+1.962\times10^{-4}\times T)\times T]} \tag{4.A2}$$

where $\mu_0 = 1.787 \times 10^{-3}$ kg m^{-1} s^{-1}.

The temperature dependent density for the temperature range from 0 °C - 40 °C is defined as (Molson et al., 1992):

$$\rho_w(T) = \rho_0\{1 + [-7.583 \times 10^{-6} + 4.462 \times 10^{-8} \times (T-4)] \times (T-4)^2\} \tag{4.A3}$$

where $\rho_0 = 1000$ kg m^{-3}.

Coupling of surface and subsurface domains is equivalent to the advective-dispersive transport using a first-order exchange relationship (Brookfield et al., 2009; Therrien et al. 2010).

$$\Omega_0 = \rho_w c_w T_{ups} \beta_0 + \alpha_0 \rho_w c_w (T - T_0) \quad (4.A4)$$

where T_{ups} upstream temperature, β_0 is the aqueous exchange flux between the surface and subsurface domains, α_0 is the heat transfer coefficient and $T - T_0$ is the difference in the temperature of the bulk surface and the surface domain.

The atmospheric thermal input to the surface domain is described by the ambient air temperature and incoming short-wave and long-wave solar radiation (Verseghy et al., 1991; Brookafield et al., 2009).

$$E_{atm} = K_* + L_* + Q_H + Q_E \quad (4.A5)$$

where K_* is the net shortwave radiation, L_* is the net long-wave radiation calculated in HydroGeoSphere based on the actual atmospheric temperature and the integrated emissivity of the atmosphere and the canopy using the formulation given by Fassnacht et al. (2001), Q_H is the sensible heat flux and Q_E is the latent heat flux. If heat exchange with the atmosphere is simulated, the user can either predefine any potential evaporation or simulate it based on the heat exchange with the atmosphere. The full details on the implementation of heat transport are discussed by Graf and Therrien (2005; 2007) and Brookfield et al. (2009).

APPENDIX 4.B: Coupled simulation of water and heat fluxes across the river-groundwater interface

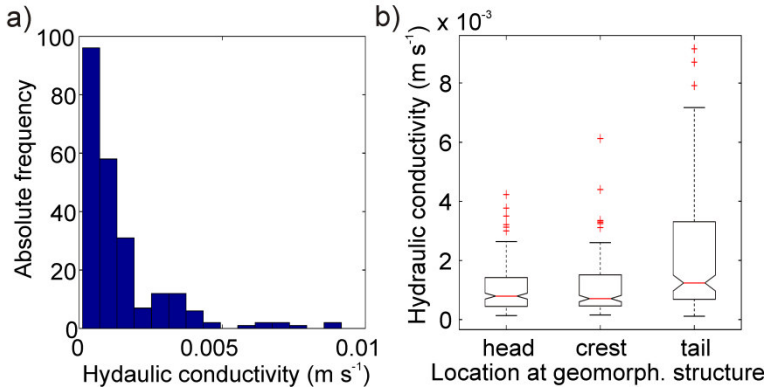

Figure 4.B1: (a) Frequency distribution of hydraulic conductivities estimated from riverbed slug tests. (b) Variation in hydraulic conductivity grouped according to the location relative in particular geomorphological structure.

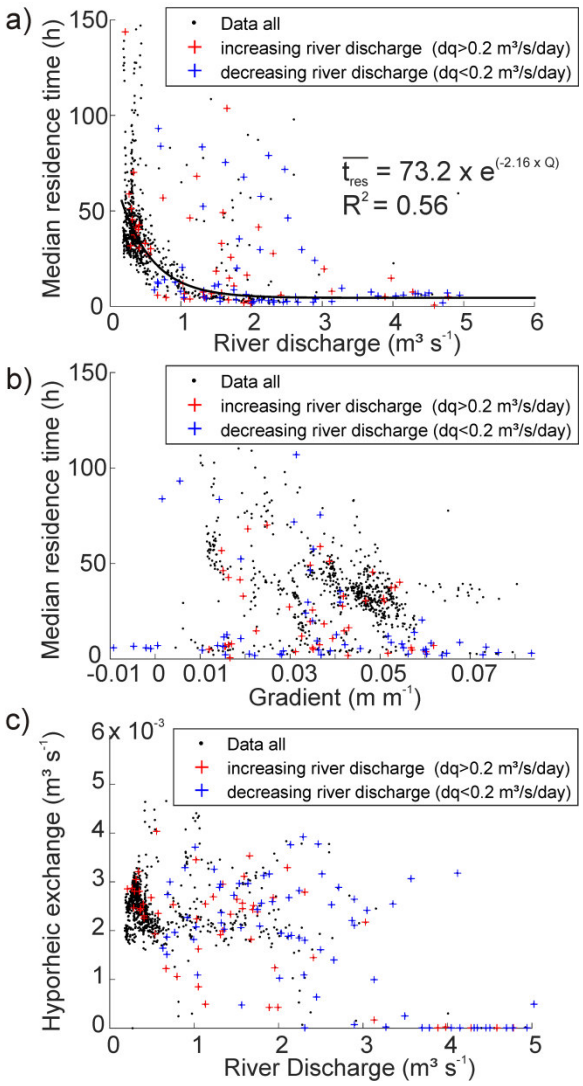

Figure 4.B2: (a) River discharge (Q) versus median residence time of hyporheic flow paths t_{res}, (b) Vertical hydraulic gradient versus median residence time of hyporheic flow paths and (c) river discharge versus hyporheic exchange for each day of the simulation.

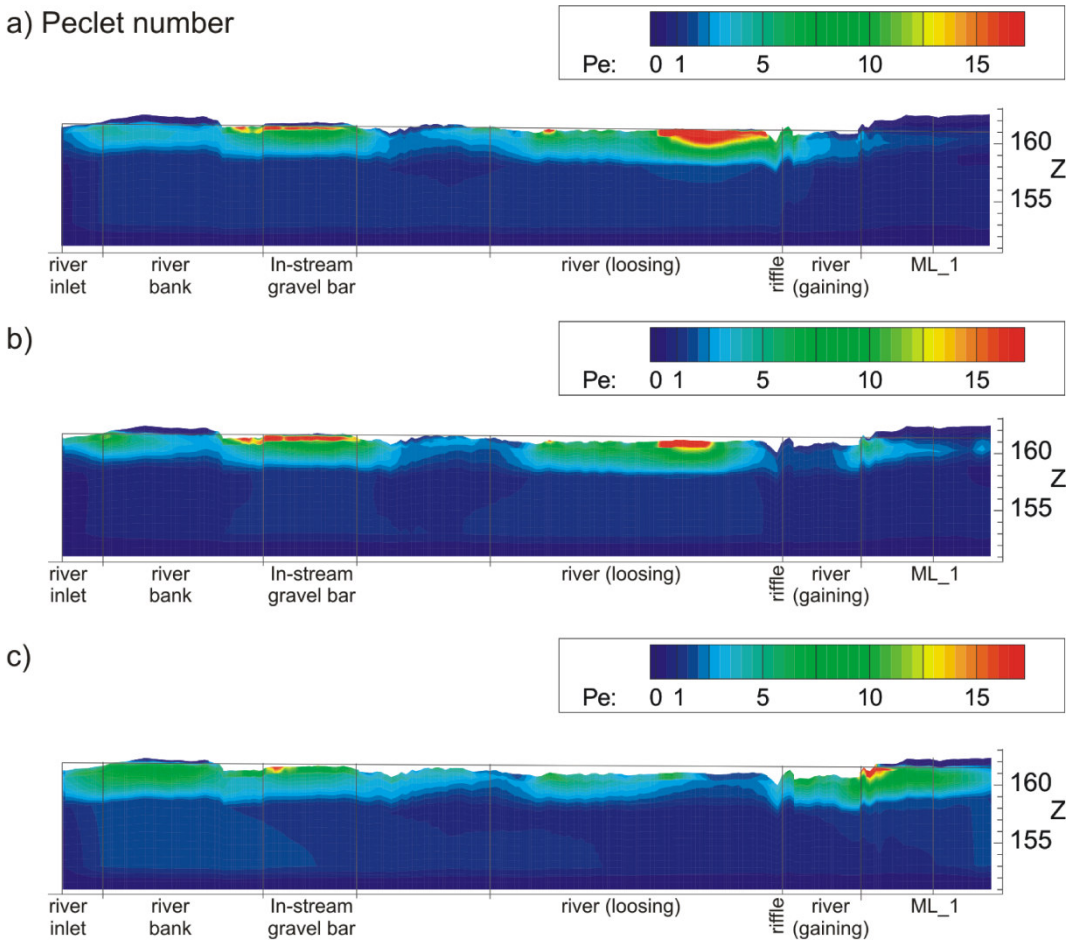

Figure 4.B3: Cross-sections along transect A-B demonstrating the relation between advective and conductive heat flux by Peclet number (Pe) for (a) low, (b) moderate, and (c) high river discharges.

5 General discussion and conclusions

5.1 Synthesis of the research results

The integrated approach of this thesis, ranging from the acquisition of field data, method development to the implementation of a reach scale water flux and heat transport model, provided numerous scientific outcomes. The main developments and findings of the work are summarized in the following sections.

5.1.1 Heat as a natural tracer to infer the geometry of the subsurface flow path and to quantify river-groundwater exchange fluxes

Characterizing the flow conditions in the streambed can be challenging because of the complex, multi-dimensional flow patterns driven by time variable vertical hydraulic gradients and groundwater discharge. The identification of horizontal flow paths is essential to identify hyporheic exchange processes at the interface between river and groundwater and, in turn, to capture the functioning of this interface as an important zone for the water quality, the ecological health and the resilience of streams and riparian ecosystems. In this thesis I developed a methodology to analyse the geometry of subsurface water flux using vertical temperature profiles. The approach relies on changes in daily temperature amplitude between subsurface temperature sensors and is based on the recognition that natural temperature variations in streams propagate into the streambed depending on exchange flow direction and magnitude (passive heat tracing). Beyond the one-dimensional vertical exchange flow, major flow patterns could be identified and systematically categorised in purely vertical and horizontal (hyporheic, parafluvial) components.

The presented method is independent of the magnitude of the exchange flux and the sediment thermal properties, and captures the normalised difference between horizontal and vertical flux. This approach goes beyond established passive heat tracing techniques, which provide detailed information on vertical exchange fluxes between rivers and groundwater, and existing active heat tracing techniques, which are able to also capture multi-dimensional exchange fluxes between river and groundwater. Active heat tracing is practicable in shallow sediments (0 – 0.1 m) and rivers with fine sediments (Lewandowski et al., 2011; Angermann et al., 2012; Mehrtens, 2016), but may not be practical in streams with coarser sediments, to infer hyporheic flow in depth below 0.1 m, or to continuously monitor hyporheic exchange processes. The identification of

horizontal flow path using natural occurring temperature variations has fewer data requirements and requires less effort in setup and data handling compared to numerical approaches normally used to evaluate multi-dimensional subsurface water flux. Taking advantage of this simplicity, the presented approach could be routinely used to check for exchange conditions before applying one-dimensional analytical methods to estimate magnitudes of subsurface water fluxes (flow velocity). Established analytical solutions applied to infer the magnitude of exchange fluxes at the interface between river and groundwater require a stationary, one-dimensional vertical flow field which is frequently violated in natural systems.

In this thesis, a new computer code (FLUX-BOT) was developed to estimate vertical water fluxes from measured temperature profiles. Flexibility in the temperature boundary conditions allows for better representation of measured temperatures and enables the direct use of all natural temperature conditions without the need of any data preprocessing (e.g. curve fitting, frequency analysis). The code uses a numerical solver of the one dimensional conduction equation. This approach automates the entire workflow to calculate vertical water fluxes from raw temperature time series and, thus, provides a handy and flexible tool to allow analysis of transient vertical exchange fluxes in saturated porous media. FLUX-BOT does not bypass common limitations of using temperature measurements to estimate seepage rates, including streambed heterogeneity and the need to estimate streambed thermal properties, and has been implemented and tested so far only for saturated conditions. But the model application is simple and straightforward to apply to routinely measured temperature profiles over time, i.e. not restricted in temperature boundary condition. The automated time-varying functionality of FLUX-BOT (24 hours windows or greater) and the automated uncertainty assessment are features not available in established one-dimensional numerical models, as for example in 1DTempPro (Voytek et al., 2013; Koch et al., 2015).

The developed methods allow fundamental research and interpretation of exchange fluxes between surface water and groundwater at the point scale. Their application on routinely measured temperature profiles will further improve the general understanding of the in-situ direction and magnitude of fluid fluxes within the shallow streambed. Such methods are an important contribution to identifying the path and direction of subsurface flow and to assessing how much water is exchanged across the river-groundwater interface. Both quantities must be recognised for their impact on the quality and quantity of water resources.

Advancements made in the development of these methods will furthermore help to assess the effects of river restoration activities like the artificial introduction of geomorphological structures to enhance hyporheic exchange. Boulton (2007) advocated the need to develop and implement such techniques to facilitate the rehabilitation and resto-

ration of surface water and groundwater interaction as part of an integrated water resource management. The restoration of geomorphological structures to enhance hyporheic exchange remains an ongoing goal for current research and is of high relevance as the linkages within many riverine systems have been reduced, impaired or lost as a result of anthropogenic activities (Brunke and Gonser, 1997; Hancock, 2002).

5.1.2 Hyporheic exchange flux, hyporheic residence times and temperatures

Gravel bars and fluvial islands are common streambed structures in a large range of natural and regulated river channels that induce hydraulic head gradients with the potential to drive hyporheic exchange flow. The evaluation of measured temperature profiles along a characteristic point bar and in-stream gravel bar at the study site highlight that river-groundwater exchange flux at the head, crest and tail of geomorphological structures significantly deviated from the one-dimensional vertical flow, having a significant horizontal advective component. These subsurface flow patterns indicated the formation of shallow hyporheic exchange across the geomorphological structures. The hyporheic exchange developed independently of the vertical hydraulic gradient (losing condition) and remained persistent over time until the geomorphological structure became completely submerged. The flow system changed from a distinct hyporheic flow cell across the point bar/instream gravel bar to a dominant losing condition with a significant vertical flow component in the riverbed. At the thalweg of the river the exchange flux between river and groundwater could be directly quantified due to its one-dimensional, vertical behaviour. The exchange flux exhibited a clear seasonal cycle with exchange velocities up to 2000 L m^{-2} d^{-1} during the summer months, when groundwater levels were at a minimum, and near zero in the winter months, when groundwater levels were highest.

The presence of horizontal advective water and associated heat flux within the shallow riverbed created unique environments with potential implications for the spatial and temporal dynamics of biogeochemical processes and related reaction kinetics, which was addressed in more detail by the integrated modelling approach. Numerical modelling greatly improved the ability to quantify exchange fluxes and heat exchange across surface water-groundwater interfaces and provided important insights into drivers and controls of spatial patterns and temporal dynamics in exchange fluxes, residence time distributions, and subsurface temperature pattern. The calibrated and validated 3D fully-integrated numerical model gave an accurate representation of the reach-scale water and heat fluxes across the river-groundwater interface with predictive capabilities.

The presented results suggest that fluvial islands are key drivers and significant components of river-groundwater interactions and hyporheic water flow and heat exchange. Water and heat exchange across the river groundwater interface substantially varied based on season and event-based conditions. The hydraulic head gradients across the non-submerged geomorphological structures were highest for low discharges (low water level) because the low discharges forced river heads to follow riverbed morphology more closely. The hydraulic head gradients across the geomorphological structures decreased with increasing discharge. Also, hyporheic residence times of the partly submerged geomorphological structures varied inversely with the river discharge.

Advective heat flux in the shallow streambed was the major process controlling heat exchange between river and groundwater at the reach-scale. Hyporheic up- and downwelling induced by non-submerged geomorphological structures caused substantial thermal heterogeneity within riverbed sediments at the reach-scale with zones of daily temperature oscillations penetrating deep into the saturated sediment and spots of daily constant temperature determined by the average groundwater temperature. The average temperature in the hyporheic zone followed the temperature in the river (characterized by distinct annual and daily cycles), but along individual hyporheic flow paths, temperatures substantially varied around the average hyporheic temperature. The average hyporheic flow path temperature ranged between the atmospheric temperature and the yearly average groundwater temperature, strongly depending on the flow path residence time (flow path length) and the temperature gradient between river and groundwater. In autumn-winter, the average temperature of long flow paths was potentially higher than the ones of short flow paths, whereas in spring-summer the average temperature of longer flow paths was lower than for shorter ones. Average river temperature was a good predictor for the average hyporheic temperature. Individual hyporheic flow path temperature ($T_{flow\,path}$) could be estimated by the power law relationship derived from the detailed numerical simulations $\left[T_{flow\,path} = T_{river} + 0.0864 \times {t_{res}}^{0.3684} \times (T_{GW} - T_{river})\right]$ that accounts for hyporheic residence time (t_{res}), river (T_{river}) and groundwater temperature (T_{GW}). Given that relation reach-scale biogeochemical cycling of nutrients and contaminants can be adjusted for hyporheic residence times and average flow path temperature. Both hyporheic residence times and hyporheic temperature patterns are important for quantifying the biogeochemical processes in the hyporheic zone, since the longer the residence time and the higher the temperature, the higher the potential for temperature sensitive solute transformation rates (Gillooly et al., 2001; Enquist et al., 2003; Yvon-Durocher et al., 2012). The simulation results show that the time scale of oxygen consumption substantially depends on the average hyporheic flow path temperature.

5.2 Implications for future research

This thesis provides novel methods and answers to important questions related to surface water-groundwater interaction processes. It further raises new aspects and stipulates directions of future research.

5.2.1 Use of heat as a tracer to quantify horizontal streambed flux for hyporheic flow fields

The rate of ongoing research highlights continuing interest in heat as a tracer and proves that it is regarded as a potentially powerful tool for the quantification of the localised vertical water flux in near surface sediments (Rau et al., 2014). Several studies have explored the effects of two- and three-dimensional non-steady flow fields on the performance of 1D analytical solutions for vertical exchange flux. Specifically, non-uniform flow fields with a strong horizontal flow component and flow lines that converge or diverge produce the largest errors in simulated streambed fluxes (Lautz, 2010; Roshan et al., 2012; Cuthbert and Mackay, 2013; Revers and Hatch, 2016).

The quantification of horizontal fluxes is of primary importance to assess hyporheic transport and residence time (Binley et al., 2013; Munz et al., 2016). Active heat-pulse tracing enables highly resolved in-situ measurements of direction and magnitude of hyporheic flow (Lewandowski et al., 2011; Angermann et al., 2012; Mehrtens, 2016). This method is practicable in shallow sediments (0 – 0.1 m) and rivers with fine sediments, but may not be practical in streams with coarser sediments or to infer hyporheic flow in depth below 0.1 m.

In this thesis a method was presented to analyse the geometry of subsurface water flux using vertical riverbed temperature profiles (Munz et al., 2016). This method was shown to be independent of the magnitude of the exchange flux. Lautz (2010) and Roshan et al. (2012) demonstrated that errors in vertical flux estimates increase with the magnitude of a horizontal flow component (i.e. overestimation for losing condition). I hypothesize that this approach allows quantification of the error made when one-dimensional solutions were applied to calculate water flux in hyporheic flow fields and, in turn, can be used in combination with established one-dimensional methods to quantify horizontal as well as vertical water flux components based on measured streambed temperatures. The combination of both methods has the potential to solve problems normally associated with the in-situ quantification of multi-dimensional hyporheic exchange for a wide range of streambed sediments.

5.2.2 Performance of heat transport models in estimation of vertical fluid flux with respect to uncertain transport parameter

In recent years there has been a rapid expansion in the use of heat as a quantitative tracer of vertical water flux based on improved temperature sensors, signal processing techniques, new analytical and numerical solutions, and computer software to apply them (Constantz, 2008; Gordon et al., 2012; Rau et al., 2014). The most common heat signal that is traced in the subsurface is diurnal temperature variations, typically represented as sine functions, which are used as upper boundary condition in analytical solutions. Common analytical methods use the amplitude or the phase information of the daily temperature signal (Hatch et al., 2006; Keery et al., 2007) or use both of them simultaneously (McCallum et al., 2012; Luce et al., 2013) to solve for vertical water flux at the interface between surface water and groundwater. Recent extensions to these analytical solutions allow the inclusion of the entire frequency spectrum into the estimation procedure (Wörman et al., 2012; Vandersteen et al., 2015; Schneidewind et al., 2016). Numerical codes iteratively solving the one-dimensional conductive-advective heat transport equation were specifically developed for simulating and inverting vertical temperature profiles with irregular temperature boundaries that cannot be approximated with a sine curve (Voytek et al., 2013; Koch et al., 2015). Most of the methods using heat as a natural tracer offer the opportunity to automate the process for evaluating long temperature time series at a daily time step (Hatch et al., 2006; Keery et al., 2007; McCallum et al., 2012; Luce et al., 2013; Munz and Schmidt, 2017).

All methods cited above rely on specific formulations of the one-dimensional heat transport equation (that takes into account both convective and conductive transport (e.g. de Marsily, 1986)) but differ in their implementation of temperature boundary condition and their exact solutions. Common to all solutions is the inclusion of thermal parameters which need to be measured or are derived from literature values. Uncertainties in thermal parameters and inaccuracy of temperature measurements can lead to large errors in the velocity estimates, in particular for low flows (Munz et al., 2011; Shanafield et. al., 2011; Roshan et al., 2012). The uncertainty in thermal parameters generally has a stronger impact on the upward flux solution due to the strong dependence of observed thermal differences with depth on the parameters that control downward heat conduction (Shanafield et. al., 2011).

The implementation of analytical and numerical solutions in relatively comprehensive codes such as VFLUX (Gordon et al., 2012) and FLUX-BOT (Munz and Schmidt, 2017) easily enable the user to undertake parameter uncertainty analyses. I hypothesize that the impact of thermal parameter uncertainty and surface temperature characteristics

(signal-to-noise ratio) on velocity results depend on the method in use. Each researcher chose a method to apply independent of the dominant environmental exchange condition and the required accuracy of estimated exchange velocity. A systematic evaluation of a wide range of one-dimensional heat transport models available needs to be conducted in order to give guidance under which circumstances (flow condition, sediment type, temperature condition) which model is preferred; i.e. provide flux estimates less sensitive to uncertain thermal parameters. Fundamentally, the researcher must choose between amplitude and phase-based fluid analytical or numerical flux models to apply to specific field condition. A detailed model intercomparison could provide recommendation which method (or method category) should be used for which data sets and environmental exchange conditions.

5.2.3 Influence of hydrodynamic forces on water and heat exchange at the scale of non-submerged streambed structures

Hyporheic exchange flux is driven by hydrostatic and hydrodynamic forces within rivers and floodplains (Elliott and Brooks, 1997; Cardenas et al., 2004; Boano et al., 2014). At the scale of non-submerged streambed structures hyporheic exchange flux is dominated by the hydrostatic component of total hydraulic head (sum of streambed height above sea level and height of overlying water column) (Woessner, 2000; Hester and Doyle, 2008; Cardenas, 2008). Hydrostatically influenced hyporheic exchange is affected by the variability in the height and slope of the stream water surface across non-submerged streambed structures (Harvey and Bencala, 1993; Wondzell and Gooseff, 2013). In flowing water there are also dynamic contributors to the total hydraulic head. The hydrodynamic component of total head is the sum of velocity head, and the non-hydrostatic pressure head that arises from surface water flow around streambed structures and the resulting momentum transfer to the bed (Elliott and Brooks, 1997). Hydrodynamic driven exchange (topography-current induced exchange) typically dominates in streambed structures that are smaller than the stream depth e.g., submerged ripples and dunes, cobbles and grain clusters, and pool riffle sequences (Elliot and Brooks, 1997; Cardenas and Wilson, 2007; Stonedahl et al., 2013). Hydrodynamic driven exchange correlates positively with mean stream velocity and negatively with increasing wavelength of the associated streambed structure (Elliott and Brooks, 1997; Boano et al., 2014) and, in turn, also effect exchange processes at larger scales of non-submerged streambed structures, especially in high order streams with high streambed slope and high stream flow velocity.

To date a variety of numerical simulation platforms have been developed to solve coupled surface water-groundwater flow. These models couple surface and subsurface pro-

cesses with the aim of representing the relevant physical processes driving exchange at the interface between stream and groundwater. Model applications to research water flux across this interface range from the scale of single morphological structures to the river reach scale (see chapter 1.4). At scales of submerged ripples up to the gravel bar numerical models are applied that rely on hydrodynamic and hydrostatic forces (Cardenas and Wilson, 2007; Trauth et al., 2015), whereas on scales from the gravel bar towards the reach-scale numerical models are applied that rely on the hydrostatic forces only (Storey et al., 2003; Shope et al., 2012; Munz et al., 2017). Especially at the scale where both approaches overlap the influence of model choice and, in turn, the influence of processes taken into account (choice of the simulation platform) should be systematically evaluated in respect to depth and magnitude of hyporheic exchange flux and hyporheic residence times.

Extent, magnitude and residence time of hyporheic exchange flux require accurate quantification as they are crucial for understanding environmental processes in the hyporheic zone. Only if these quantities are precisely known, their influence on solute transformation rates could be accurately quantified. A systematic model evaluation would provide insight into the relevant processes which need to be taken account of to accurately simulate hyporheic exchange processes at the scale of non-submerged stream bed-forms and would furthermore provide insights if model simplifications normally used at this scale accurately represent the driving forces within rivers and floodplains.

5.2.4 Influence of streambed heterogeneity on reach scale hyporheic residence time and temperature distributions in a gravel bed river

Hyporheic residence time and hyporheic thermal regime are key parameters for quantifying hyporheic processes including solute transient storage, dilution rates and solute transformation rates. The effect of streambed morphological structures (dunes and riffles, submerged pool riffle sequences) on streambed residence is well understood (Boano et al., 2014). Also the effect of heterogeneity of streambed hydraulic properties has received an increased research focus (Tonina et al., 2016; Stewardson et al., 2016). Tonina et al. (2016) quantified the importance of streambed heterogeneity on the distribution of hyporheic residence times of dune-like bedforms. However, the impact of heterogeneity of fluvial sediments on hyporheic exchange processes is controversially discussed (Salehin et al., 2004; Sawyer and Cardenas, 2009; Bardini et al., 2013). To approach this discrepancy, Trauth et al. (2016) advocate further studies which systematically analyse the effect of heterogeneities on hyporheic residence time distribution by simulating scenarios consisting of a realistic range of variants of correlation lengths, dipping angles and standard deviations of hydraulic conductivities. Whereas the effect

of streambed hydraulic conductivity on hyporheic residence times was addressed for submerged streambed structures in recent studies, the effect of streambed hydraulic conductivity on hyporheic residence time for non-submerged streambed structures and especially on hyporheic thermal regime received less attention from the community. Coupled simulation of reach-scale water and heat fluxes across the river-groundwater interface including non-submerged streambed structures as well as a heterogeneous implemented streambed hydraulic conductivity (conditional, sequential Gaussian simulation relying on mean, variance and range of the hydraulic conductivity) (Munz et al., 2017) provides a sound basis to address the afore discussed issues. I recommend addressing the effect of heterogeneity in streambed hydraulic conductivity on hyporheic residence times and especially on hyporheic temperature patterns as both are known to substantially affect solute transformation rates in streambed sediments. Knowledge about hyporheic residence time distribution allow the quantification of solutes exposed to reactive streambed environments, whereas knowledge about the hyporheic temperature distribution is important to address the temperature dependence of natural reaction rates. Such investigations would have the potential to provide further insight in how to upscale heterogeneity effects from the reach to the catchment scale.

5.3 Conclusions

The presented methods offer reliable and robust in-situ field-based approaches for identifying horizontal water fluxes and easily quantifying vertical exchange flux at the river-groundwater interface. The presence of horizontal advective water and the associated heat flux within the shallow riverbed creates unique environments with potential implications for the spatial and temporal dynamics of biogeochemical processes and related reaction kinetics which were addressed in more detail by the use of a the 3D fully-integrated numerical model. The calibrated and validated model of reach-scale water and heat fluxes across the river-groundwater interface highlight the correlation between exchange flux and subsurface temperature patterns. Understanding these links provides the basis from which to assess hyporheic temperature conditions in river reaches. Since biogeochemical processes depend on solute residence time and temperature, an understanding of flow and temperature regimes in the riverbed sediments is essential for quantifying the reactive potential of hyporheic zones. The results of this thesis contribute to an improved understanding of hyporheic exchange and heat transport processes at the interface between surface water and groundwater from the point scale to the scale of a river reach. The numerical model is a sound basis for investigating quantitatively variations of sediment properties, boundary conditions and streambed morphology and also for subsequent generalization of river-groundwater exchange on reach scale river stretches and beyond.

Bibliography

Acuna, V., Wolf, A., Uehlinger, U., Tockner, K., 2008. Temperature dependence of stream benthic respiration in an Alpine river network under global warming. Freshwater Biol, 53(10): 2076-2088.

Akaike, H., 1998. Information Theory and an Extension of the Maximum Likelihood Principle. In: Parzen, E., Tanabe, K., Kitagawa, G. (Eds.), Selected Papers of Hirotugu Akaike. Springer Series in Statistics. Springer New York, pp. 199-213.

Anderson, M.P., 2005. Heat as a ground water tracer. Ground Water, 43(6): 951-968.

Arrigoni, A.S. et al., 2008. Buffered, lagged, or cooled? Disentangling hyporheic influences on temperature cycles in stream channels. Water Resour Res, 44(9).

Baratelli, F., Flipo, N., Moatar, F., 2016. Estimation of stream-aquifer exchanges at regional scale using a distributed model: Sensitivity to in-stream water level fluctuations, riverbed elevation and roughness. J Hydrol, 542: 686-703.

Bardini, L., F. Boano, M. B. Cardenas, A. H. Sawyer, R. Revelli, and L. Ridolfi, 2013. Small-scale permeability heterogeneity has negligible effects on nutrient cycling in streambeds, Geophys. Res. Lett., 40, 1118–1122.

Barlow, P.M. and Reichard, E.G., 2010, Saltwater intrusion in coastal regions of North America, Hydrogeology Journal, 18: 247-260.

Barthel, R., Banzhaf, S., 2016. Groundwater and Surface Water Interaction at the Regional-scale - A Review with Focus on Regional Integrated Models. Water Resour Manag, 30(1): 1-32.

Bartsch, S. et al., 2014. River-aquifer exchange fluxes under monsoonal climate conditions. J Hydrol, 509: 601-614.

Battin, T.J., Besemer, K., Bengtsson, M.M., Romani, A.M., Packmann, A.I., 2016. The ecology and biogeochemistry of stream biofilms. Nat Rev Microbiol, 14(4): 251-263.

Birkinshaw, S.J., Webb, B., 2010. Flow pathways in the Slapton Wood catchment using temperature as a tracer. J Hydrol, 383(3-4): 269-279.

Boano, F., Demaria, A., Revelli, R., Ridolfi, L., 2010. Biogeochemical zonation due to intrameander hyporheic flow. Water Resour Res, 46.

Boano, F. et al., 2014. Hyporheic flow and transport processes: Mechanisms, models, and biogeochemical implications. Rev Geophys, 52(4): 603-679.

Boano, F., Poggi, D., Revelli, R., Ridolfi, L., 2009. Gravity-driven water exchange between streams and hyporheic zones. Geophys Res Lett, 36.

Boano, F., Revelli, R., Ridolfi, L., 2009. Quantifying the impact of groundwater discharge on the surface-subsurface exchange. Hydrol Process, 23(15): 2108-2116.

Boulton, A.J., Findlay, S., Marmonier, P., Stanley, E.H., Valett, H.M., 1998. The functional significance of the hyporheic zone in streams and rivers. Annu Rev Ecol Syst, 29: 59-81.

Bravo, H.R., Jiang, F., Hunt, R.J., 2002. Using groundwater temperature data to constrain parameter estimation in a groundwater flow model of a wetland system. Water Resour Res, 38(8).

Bredehoeft, J.D., Papadopulos, I.S., 1965. Rates of Vertical Groundwater Movement Estimated from Earths Thermal Profile. Water Resour Res, 1(2): 325.

Briggs, M.A., Voytek, E.B., Day-Lewis, F.D., Rosenberry, D.O., Lane, J.W., 2013. Understanding Water Column and Streambed Thermal Refugia for Endangered Mussels in the Delaware River. Environ Sci Technol, 47(20): 11423-11431.

Brookfield, A.E., Sudicky, E.A., Park, Y.J., Conant, B., 2009. Thermal transport modelling in a fully integrated surface/subsurface framework. Hydrol Process, 23(15): 2150-2164.

Brunke, M., Gonser, T., 1997. The ecological significance of exchange processes between rivers and groundwater. Freshwater Biol, 37(1): 1-33.

Burkholder, B.K., Grant, G.E., Haggerty, R., Khangaonkar, T., Wampler, P.J., 2008. Influence of hyporheic flow and geomorphology on temperature of a large, gravel-bed river, Clackamas River, Oregon, USA. Hydrol Process, 22(7): 941-953.

Caissie, D., Kurylyk, B.L., St-Hilaire, A., El-Jabi, N., MacQuarrie, K.T.B., 2014. Streambed temperature dynamics and corresponding heat fluxes in small streams experiencing seasonal ice cover. J Hydrol, 519: 1441-1452.

Campolongo, F., Cariboni, J., Saltelli, A., 2007. An effective screening design for sensitivity analysis of large models. Environ Modell Softw, 22(10): 1509-1518.

Cardenas, M.B., Wilson, J.L., 2007. Dunes, turbulent eddies, and interfacial exchange with permeable sediments. Water Resour Res, 43(8).

Cardenas, M.B., Wilson, J.L., 2007. Effects of current-bed form induced fluid flow on the thermal regime of sediments. Water Resour Res, 43(8).

Cardenas, M.B., Wilson, J.L., 2007. Exchange across a sediment-water interface with ambient groundwater discharge. J Hydrol, 346(3-4): 69-80.

Chen, X.H., Chen, X., 2003. Effects of aquifer anisotropy on the migration of infiltrated stream water to a pumping well. J Hydrol Eng, 8(5): 287-293.

Conant, B., 2004. Delineating and quantifying ground water discharge zones using streambed temperatures. Ground Water, 42(2): 243-257.

Constantz, J., 2008. Heat as a tracer to determine streambed water exchanges. Water Resour Res, 44.

Cranswick, R.H., Cook, P.G., Shanafield, M., Lamontagne, S., 2014. The vertical variability of hyporheic fluxes inferred from riverbed temperature data. Water Resour Res, 50(5): 3994-4010.

Cuthbert, M.O., Mackay, R., 2013. Impacts of nonuniform flow on estimates of vertical streambed flux. Water Resour Res, 49(1): 19-28.

Dahm, C.N., Grimm, N.B., Marmonier, P., Valett, H.M., Vervier, P., 1998. Nutrient dynamics at the interface between surface waters and groundwaters. Freshwater Biol, 40(3): 427-451.

De Marsily, G., 1986, Quantitative Hydrogeology: Groundwater Hydrology for Engineers, Academic Pr Inc

De Vries, D.A., 1966. Thermal properties of soils, in van Wijk, W.R., ed., Physics of plant environment. North-Holland Publishing Co., Amsterdam, 210–235 pp.

D'Errico, J., 2006. Bound constrained optimization using fminsearch (http://www.mathworks.com/matlabcentral/fileexchange/8277-fminsearchbnd--fminsearchcon), MATLAB Central File Exchange.

Diersch, H.-J.G., 2005. FEFLOW— Finite Element Subsurface Flow & Transport Simulation System — Reference Manual, Berlin, Germany.

Doherty, J., 2005. PEST: Model-indipendent Parameter Estimation. User Manual, Selected Papers of Hirotugu Akaike. fifth ed. Watermark Numerical Computing, Brisbaine, Australia.

Doussan, C. et al., 1994. Coupled Use of Thermal and Hydraulic-Head Data to Characterize River Groundwater Exchanges. J Hydrol, 153(1-4): 215-229.

Duff, J. H., and F. J. Triska (2000), Nitrogen biogeochemistry and surface-subsurface exchange in streams, in Streams and Groundwaters, edited by J. B. Jones and P. J. Mulholland, pp. 197–220, Academic Press, San Diego, Calif.

Duque, C., Calvache, M.L., Engesgaard, P., 2010. Investigating river-aquifer relations using water temperature in an anthropized environment (Motril-Salobrena aquifer). J Hydrol, 381(1-2): 121-133.

Ebel, B.A., Mirus, B.B., Heppner, C.S., VanderKwaak, J.E., Loague, K., 2009. First-order exchange coefficient coupling for simulating surface water-groundwater interactions: parameter sensitivity and consistency with a physics-based approach. Hydrol Process, 23(13): 1949-1959.

Elliott, A.H., Brooks, N.H., 1997. Transfer of nonsorbing solutes to a streambed with bed forms: Laboratory experiments. Water Resour Res, 33(1): 137-151.

Enquist, B. J., E. P. Economo, T. E. Huxman, A. P. Allen, D. D. Ignace, and J. F. Gillooly. 2003. Scaling metabolism from organisms toecosystems, Nature, 423(6940), 639–642.

Fanelli, R.M., Lautz, L.K., 2008. Patterns of water, heat, and solute flux through streambeds around small dams. Ground Water, 46(5): 671-687.

Fellows, C.S., Valett, H.M., Dahm, C.N., 2001. Whole-stream metabolism in two montane streams: Contribution of the hyporheic zone. Limnol Oceanogr, 46(3): 523-531.

Findlay, S., 1995. Importance of Surface-Subsurface Exchange in Stream Ecosystems - the Hyporheic Zone. Limnol Oceanogr, 40(1): 159-164.

Flipo, N. et al., 2014. Continental hydrosystem modelling: the concept of nested stream-aquifer interfaces. Hydrol Earth Syst Sc, 18(8): 3121-3149.

Fox, A., Boano, F., Arnon, S., 2014. Impact of losing and gaining streamflow conditions on hyporheic exchange fluxes induced by dune- shaped bed forms. Water Resour Res, 50(3): 1895-1907.

Gillooly, J. F., J. H. Brown, G. B. West, V. M. Savage, and E. L. Charnov, 2001. Effects of size and temperature on metabolic rate, Science, 293(5538), 2248–2251

Gomez-Velez, J.D., Harvey, J.W., 2014. A hydrogeomorphic river network model predicts where and why hyporheic exchange is important in large basins. Geophys Res Lett, 41(18): 6403-6412.

Gordon, R.P., Lautz, L.K., Briggs, M.A., McKenzie, J.M., 2012. Automated calculation of vertical pore-water flux from field temperature time series using the VFLUX method and computer program. J Hydrol, 420: 142-158.

Goto, S., Yamano, M., Kinoshita, M., 2005. Thermal response of sediment with vertical fluid flow to periodic temperature variation at the surface. J Geophys Res-Sol Ea, 110(B1).

Graf, T., Therrien, R., 2005. Variable-density groundwater flow and solute transport in porous media containing nonuniform discrete fractures. Adv Water Resour, 28(12): 1351-1367.

Graf, T., Therrien, R., 2007. Coupled thermohaline groundwater flow and single-species reactive solute transport in fractured porous media. Adv Water Resour, 30(4): 742-771.

Grimm, N.B., Fisher, S.G., 1984. Exchange between Interstitial and Surface-Water - Implications for Stream Metabolism and Nutrient Cycling. Hydrobiologia, 111(3): 219-228.

Halliday, S.J. et al., 2013. Upland streamwater nitrate dynamics across decadal to sub-daily timescales: a case study of Plynlimon, Wales. Biogeosciences, 10(12): 8013-8038.

Hannah, D.M., Malcolm, I.A., Bradley, C., 2009. Seasonal hyporheic temperature dynamics over riffle bedforms. Hydrol Process, 23(15): 2178-2194.

Hansen, T.M., Mosegaard, K., 2008. VISIM: Sequential simulation for linear inverse problems. Comput Geosci-Uk, 34(1): 53-76.

Harvey, J., Gooseff, M., 2015. River corridor science: Hydrologic exchange and ecological consequences from bedforms to basins. Water Resour Res, 51(9): 6893-6922.

Harvey, J.W., Bencala, K.E., 1993. The Effect of Streambed Topography on Surface-Subsurface Water Exchange in Mountain Catchments. Water Resour Res, 29(1): 89-98.

Hatch, C.E., Fisher, A.T., Revenaugh, J.S., Constantz, J., Ruehl, C., 2006. Quantifying surface water-groundwater interactions using time series analysis of streambed thermal records: Method development. Water Resour Res, 42(10).

Healy, R.W., Ronan, A.D., 1996. Documentation of computer program VS2Dh for simulation of energy transport in variably saturated porous media; modification of the US Geological Survey's computer program VS2DT. 96-4230.

Helm, D.C., 1976. One-Dimensional Simulation of Aquifer System Compaction near Pixley, California .2. Stress-Dependent Parameters. Water Resour Res, 12(3): 375-391.

Henzler, A.F., Greskowiak, J., Massmann, G., 2016. Seasonality of temperatures and redox zonations during bank filtration – A modeling approach. J Hydrol, 535: 282-292.

Hester, E.T., Doyle, M.W., Poole, G.C., 2009. The influence of in-stream structures on summer water temperatures via induced hyporheic exchange. Limnol Oceanogr, 54(1): 355-367.

Hinkelmann, R., 2005. Efficient numerical methods and information-processing techniques for modeling hydro and environmental systems. Lecture notes in applied and computational mechanics. Springer, Berlin ; New York, x, 305 p. pp.

Hornberger, G.M., Spear, R.C., 1981. An Approach to the Preliminary Analysis of Environmental Systems. Journal of Environmental Management, 12: 7-18.

Hvorslev, M.J., 1951. Time lag and soil permeability in groundwater observations.

Irvine, D.J., Cranswick, R.H., Simmons, C.T., Shanafield, M.A., Lautz, L.K., 2015. The effect of streambed heterogeneity on groundwater-surface water exchange fluxes inferred from temperature time series. Water Resour Res, 51(1): 198-212.

Irvine, D.J., Lautz, L.K., Briggs, M.A., Gordon, R.P., McKenzie, J.M., 2015. Experimental evaluation of the applicability of phase, amplitude, and combined methods to determine water flux and thermal diffusivity from temperature time series using VFLUX 2. J Hydrol, 531: 728-737.

Jensen, J.K., Engesgaard, P., 2011. Nonuniform Groundwater Discharge across a Streambed: Heat as a Tracer. Vadose Zone J, 10(1): 98-109.

Kalbus, E., Reinstorf, F., Schirmer, M., 2006. Measuring methods for groundwater - surface water interactions: a review. Hydrol Earth Syst Sc, 10(6): 873-887.

Kaplan, L.A., Bott, T.L., 1989. Diel Fluctuations in Bacterial-Activity on Streambed Substrata during Vernal Algal Blooms - Effects of Temperature, Water Chemistry, and Habitat. Limnol Oceanogr, 34(4): 718-733.

Karan, S., Engesgaard, P., Rasmussen, J., 2014. Dynamic streambed fluxes during rainfall- runoff events. Water Resour Res, 50(3): 2293-2311.

Kaser, D.H., Binley, A., Heathwaite, A.L., Krause, S., 2009. Spatio-temporal variations of hyporheic flow in a riffle-step-pool sequence. Hydrol Process, 23(15): 2138-2149.

Keery, J., Binley, A., Crook, N., Smith, J.W.N., 2007. Temporal and spatial variability of groundwater-surface water fluxes: Development and application of an analytical method using temperature time series. J Hydrol, 336(1-2): 1-16.

Kiel, B.A., Cardenas, M.B., 2014. Lateral hyporheic exchange throughout the Mississippi River network. Nat Geosci, 7(6): 413-417.

Koch, F.W. et al., 2015. 1DTempPro V2: new features for inferring groundwater/surface-water exchange. Groundwater Monitoring & Remediation.

Kolditz, O. et al., 2012. OpenGeoSys: an open-source initiative for numerical simulation of thermo-hydro-mechanical/chemical (THM/C) processes in porous media. Environ Earth Sci, 67(2): 589-599.

Krause, S., Hannah, D.M., Blume, T., 2011. Interstitial pore-water temperature dynamics across a pool-riffle-pool sequence. Ecohydrology, 4(4): 549-563.

Krause, S. et al., 2011. Inter-disciplinary perspectives on processes in the hyporheic zone. Ecohydrology, 4(4): 481-499.

Krause, S., Tecklenburg, C., Munz, M., Naden, E., 2013. Streambed nitrogen cycling beyond the hyporheic zone: Flow controls on horizontal patterns and depth distribution of nitrate and dissolved oxygen in the upwelling groundwater of a lowland river. J Geophys Res-Biogeo, 118(1): 54-67.

Kulongoski, J.T., Izbicki, J.A., 2008. Simulation of fluid, heat transport to estimate desert stream infiltration. Ground Water, 46(3): 462-474.

Kurtz, W., Hendricks Franssen, H.J., Kaiser, H.P., Vereecken, H., 2014. Joint assimilation of piezometric heads and groundwater temperatures for improved modeling of river-aquifer interactions. Water Resour Res, 50(2): 1665-1688.

Kurylyk, B.L., Moore, R.D., MacQuarrie, K.T.B., 2016. Scientific briefing: quantifying streambed heat advection associated with groundwater-surface water interactions. Hydrol Process, 30(6): 987-992.

Lagarias, J.C., Reeds, J.A., Wright, M.H., Wright, P.E., 1998. Convergence properties of the Nelder-Mead simplex method in low dimensions. Siam J Optimiz, 9(1): 112-147.

Landon, M.K., Rus, D.L., Harvey, F.E., 2001. Comparison of instream methods for measuring hydraulic conductivity in sandy streambeds. Ground Water, 39(6): 870-885.

Langevin, C.D., Thorne, Daniel T.J., Dausman, A.M., Sukop, M.C., Guo, W., 2008. SEAWAT Version 4: A computer program for simulation of multi-species solute and heat transport. USGS Florida Integrated Science Center.

Lapham, W.W., 1989. Use of temperature profiles beneath streams to determine rates of vertical ground-water flow and vertical hydraulic conductivity. 2337.

Lautz, L.K., 2010. Impacts of nonideal field conditions on vertical water velocity estimates from streambed temperature time series. Water Resour Res, 46.

Lautz, L.K., 2012. Observing temporal patterns of vertical flux through streambed sediments using time-series analysis of temperature records. J Hydrol, 464: 199-215.

Lautz, L.K., Kranes, N.T., Siegel, D.I., 2010. Heat tracing of heterogeneous hyporheic exchange adjacent to in-stream geomorphic features. Hydrol Process, 24(21): 3074-3086.

Lewis, F., Butler, A., Gilbert, L., 2011. A unified approach to model selection using the likelihood ratio test. Methods Ecol Evol, 2(2): 155-162.

Liggett, J.E., Werner, A.D., Simmons, C.T., 2012. Influence of the first-order exchange coefficient on simulation of coupled surface-subsurface flow. J Hydrol, 414: 503-515.

Luce, C.H., Tonina, D., Gariglio, F., Applebee, R., 2013. Solutions for the diurnally forced advection-diffusion equation to estimate bulk fluid velocity and diffusivity in streambeds from temperature time series. Water Resour Res, 49(1): 488-506.

Magliozzi, C., Grabowski, R., Packman, A.I., Krause, S., 2017. Scaling down hyporheic exchange flows: from catchments to reaches. Hydrol. Earth Syst. Sci. Discuss., 2017: 1-53.

Malcolm, I.A., Hannah, D.M., Donaghy, M.J., Soulsby, C., Youngson, A.F., 2004. The influence of riparian woodland on the spatial and temporal variability of stream water temperatures in an upland salmon stream. Hydrol Earth Syst Sc, 8(3): 449-459.

Marzadri, A., Tonina, D., Bellin, A., 2012. Morphodynamic controls on redox conditions and on nitrogen dynamics within the hyporheic zone: Application to gravel bed rivers with alternate-bar morphology. J Geophys Res-Biogeo, 117.

Marzadri, A., Tonina, D., Bellin, A., 2013. Effects of stream morphodynamics on hyporheic zone thermal regime. Water Resour Res, 49(4): 2287-2302.

Mayer, K.U., Frind, E.O., Blowes, D.W., 2002. Multicomponent reactive transport modeling in variably saturated porous media using a generalized formulation for kinetically controlled reactions. Water Resour Res, 38(9).

McCallum, A.M., Andersen, M.S., Rau, G.C., Acworth, R.I., 2012. A 1-D analytical method for estimating surface water-groundwater interactions and effective thermal diffusivity using temperature time series. Water Resour Res, 48.

McLaren, R.G., 2008. GRID BUILDER: A Pre-processor for 2-D, Triangular Element, Finite-Element Programs. Groundwater Simul. Group.

Mehrtens, 2016, Turnover processes along flow paths in the hyporheic zone of a low-land river in norhtern Germany, Master's Thesis, University of Potsdam.

Molson, J.W., Frind, E.O., Palmer, C.D., 1992. Thermal-Energy Storage in an Unconfined Aquifer: 2. Model Development, Validation, and Application. Water Resour Res, 28(10): 2857-2867.

Morris, M.D., 1991. Factorial Sampling Plans for Preliminary Computational Experiments. Technometrics, 33(2): 161-174.

Mouhri, A. et al., 2013. Designing a multi-scale sampling system of stream-aquifer interfaces in a sedimentary basin. J Hydrol, 504: 194-206.

Mulholland, P.J. et al., 2008. Stream denitrification across biomes and its response to anthropogenic nitrate loading. Nature, 452(7184): 202-U46.

Munz, M., Krause, S., Tecklenburg, C., Binley, A., 2011. Reducing monitoring gaps at the aquifer-river interface by modelling groundwater-surface water exchange flow patterns. Hydrol Process, 25(23): 3547-3562.

Munz, M., Oswald, S.E., Schmidt, C., 2011. Sand box experiments to evaluate the influence of subsurface temperature probe design on temperature based water flux calculation. Hydrol Earth Syst Sc, 15(11): 3495-3510.

Munz, M., Oswald, S.E., Schmidt, C., 2016. Analysis of riverbed temperatures to determine the geometry of subsurface water flow around in-stream geomorphological structures. J Hydrol, 539: 74-87.

Munz M and Schmidt, C., 2017. Estimation of vertical water fluxes from temperature time series by the inverse numerical computer program FLUX-BOT, Hydrological Processes, 31:2713–2724.

Munz, M., Oswald, S.E., Schmidt, C., 2017. Coupled long-term simulation of reach-scale water and heat fluxes across the river-groundwater interface for retrieving hyporheic residence times and temperature dynamics, Water Resources Research, 53, https://doi.org/10.1002/2017WR020667.

Mutiti, S., Levy, J., 2010. Using temperature modeling to investigate the temporal variability of riverbed hydraulic conductivity during storm events. J Hydrol, 388(3-4): 321-334.

Naegeli, M.W., Uehlinger, U., 1997. Contribution of the hyporheic zone to ecosystem metabolism in a prealpine gravel-bed river. J N Am Benthol Soc, 16(4): 794-804.

Naranjo, R.C., Niswonger, R.G., Stone, M., Davis, C., Mckay, A., 2012. The use of multiobjective calibration and regional sensitivity analysis in simulating hyporheic exchange. Water Resour Res, 48.

Naranjo, R.C., Pohll, G., Niswonger, R.G., Stone, M., Mckay, A., 2013. Using heat as a tracer to estimate spatially distributed mean residence times in the hyporheic zone of a riffle-pool sequence. Water Resour Res, 49(6): 3697-3711.

Norman, F.A., Cardenas, M.B., 2014. Heat transport in hyporheic zones due to bedforms: An experimental study. Water Resour Res, 50(4): 3568-3582.

Nützmann, G., Levers, C., Lewandowski, J., 2014. Coupled groundwater flow and heat transport simulation for estimating transient aquifer-stream exchange at the lowland River Spree (Germany). Hydrol Process, 28(13): 4078-4090.

Packman, A.I., MacKay, J.S., 2003. Interplay of stream-subsurface exchange, clay particle deposition, and streambed evolution. Water Resour Res, 39(4).

Poole, G.C., Stanford, J.A., Running, S.W., Frissell, C.A., 2006. Multiscale geomorphic drivers of groundwater flow paths: subsurface hydrologic dynamics and hyporheic habitat diversity. J N Am Benthol Soc, 25(2): 288-303.

Pryet, A., Labarthe, B., Saleh, F., Akopian, M., Flipo, N., 2015. Reporting of Stream-Aquifer Flow Distribution at the Regional Scale with a Distributed Process-Based Model. Water Resour Manag, 29(1): 139-159.

Pujol, G., Iooss, B., Janon, A., 2016. R Package 'sensitivity'.

Rau, G.C., Andersen, M.S., Acworth, R.I., 2012. Experimental investigation of the thermal time-series method for surface water-groundwater interactions. Water Resour Res, 48.

Rau, G.C., Andersen, M.S., McCallum, A.M., Acworth, R.I., 2010. Analytical methods that use natural heat as a tracer to quantify surface water-groundwater exchange, evaluated using field temperature records. Hydrogeol J, 18(5): 1093-1110.

Rau, G.C., Andersen, M.S., McCallum, A.M., Roshan, H., Acworth, R.I., 2014. Heat as a tracer to quantify water flow in near-surface sediments. Earth-Sci Rev, 129: 40-58.

Reilly, T.E., Goodman, A.S., 1987, Analysis of saltwater upconing beneath a pumping well, Journal of Hydrology, Volume 89, Issue 3, 1987, Pages 169-204

Reimann, C., P. Filzmoser, R.G. Garrett, R. Dutter, 2008. Statistical data analysis explained. Applied Environmental Statistics with R, John Wiley & Sons, Chichester.

Roshan, H., Rau, G.C., Andersen, M.S., Acworth, I.R., 2012. Use of heat as tracer to quantify vertical streambed flow in a two-dimensional flow field. Water Resour Res, 48.

Salehin, M., Packman, A.I., Paradis, M., 2004. Hyporheic exchange with heterogeneous streambeds: Laboratory experiments and modeling. Water Resour Res, 40(11).

Saltelli, A. et al., 2008. Global Sensitivity Analysis: The Primer. WILEY.

Sawyer, A.H., Cardenas, M.B., 2009. Hyporheic flow and residence time distributions in heterogeneous cross-bedded sediment. Water Resour Res, 45.

Sawyer, A.H., Cardenas, M.B., Buttles, J., 2012. Hyporheic temperature dynamics and heat exchange near channel-spanning logs. Water Resour Res, 48.

Schmidt, C., Bayer-Raich, M., Schirmer, M., 2006. Characterization of spatial heterogeneity of groundwater-stream water interactions using multiple depth streambed temperature measurements at the reach scale. Hydrol Earth Syst Sc, 10(6): 849-859.

Schmidt, C., Musolff, A., Trauth, N., Vieweg, M., Fleckenstein, J.H., 2012. Transient analysis of fluctuations of electrical conductivity as tracer in the stream bed. Hydrol Earth Syst Sc, 16(10): 3689-3697.

Schneidewind, U. et al., 2016. LPMLE3: A novel 1-D approach to study water flow in streambeds using heat as a tracer. Water Resour Res, 52(8): 6596-6610.

Shanafield, M., Pohll, G., Susfalk, R., 2010. Use of heat-based vertical fluxes to approximate total flux in simple channels. Water Resour Res, 46.

Shope, C.L. et al., 2012. Influence of a large fluvial island, streambed, and stream bank on surface water-groundwater fluxes and water table dynamics. Water Resour Res, 48.

Šimůnek, J., van Genuchten, M.T., M., Š., 2006. The HYDRUS Software Package for Simulating Two- and Three-Dimensional Movement of Water, Heat, and Multiple Solutes in Variably-Saturated Media. PC Progress, Technical Manual, Version 1.0.

Song, J.X., Chen, X.H., Cheng, C., Summerside, S., Wen, F.J., 2007. Effects of hyporheic processes on streambed vertical hydraulic conductivity in three rivers of Nebraska. Geophys Res Lett, 34(7).

Srivastava, V., Graham, W., Munoz-Carpena, R., Maxwell, R.M., 2014. Insights on geologic and vegetative controls over hydrologic behavior of a large complex basin - Global Sensitivity Analysis of an integrated parallel hydrologic model. J Hydrol, 519: 2238-2257.

Stallman, R.W., 1963. Computation of groundwater velocity from temperature data, Washington, DC.

Stallman, R.W., 1965. Steady 1-Dimensional Fluid Flow in a Semi-Infinite Porous Medium with Sinusoidal Surface Temperature. J Geophys Res, 70(12): 2821-&.

Stanford, J.A., Ward, J.V., 1988. The Hyporheic Habitat of River Ecosystems. Nature, 335(6185): 64-66.

Stewardson, M.J., T. Datry, N. Lamouroux, H. Pella, N. Thommeret, L. Valette, S.B. Grant, 2016. Variation in reach-scale hydraulic conductivity of streambeds, Geomorphology, Volume 259, Pages 70-80,

Stonedahl, S.H., Harvey, J.W., Detty, J., Aubeneau, A., Packman, A.I., 2012. Physical controls and predictability of stream hyporheic flow evaluated with a multiscale model. Water Resour Res, 48.

Stonedahl, S.H., Harvey, J.W., Packman, A.I., 2013. Interactions between hyporheic flow produced by stream meanders, bars, and dunes. Water Resour Res, 49(9): 5450-5461.

Stonedahl, S.H., Harvey, J.W., Worman, A., Salehin, M., Packman, A.I., 2010. A multiscale model for integrating hyporheic exchange from ripples to meanders. Water Resour Res, 46.

Stonestrom, D.A., Blasch, K.W., 2003. Determining temperature and thermal properties for heat-based studies of surface-water ground-water interactions. U. S. Geological Survey(Circular 1260): 73–80.

Storey, R.G., Howard, K.W.F., Williams, D.D., 2003. Factors controlling riffle-scale hyporheic exchange flows and their seasonal changes in a gaining stream: A three-dimensional groundwater flow model. Water Resour Res, 39(2).

Stubbington, R., Wood, P.J., Boulton, A.J., 2009. Low flow controls on benthic and hyporheic macroinvertebrate assemblages during supra-seasonal drought. Hydrol Process, 23(15): 2252-2263.

Su, G.W., Jasperse, J., Seymour, D., Constantz, J., 2004. Estimation of hydraulic conductivity in an alluvial system using temperatures. Ground Water, 42(6): 890-901.

Suzuki, S., 1960. Percolation Measurements Based on Heat Flow through Soil with Special Reference to Paddy Fields. J Geophys Res, 65(9): 2883-2885.

Swanson, T.E., Cardenas, M.B., 2010. Diel heat transport within the hyporheic zone of a pool-riffle-pool sequence of a losing stream and evaluation of models for fluid flux estimation using heat. Limnol Oceanogr, 55(4): 1741-1754.

Swanson, T.E., Cardenas, M.B., 2011. Ex-Stream: A MATLAB program for calculating fluid flux through sediment-water interfaces based on steady and transient temperature profiles. Comput Geosci-Uk, 37(10): 1664-1669.

Team, R.D.C., 2011. R: A language and environment for statistical computing. Vienna, Austria. ISBN 3-900051-07-0, URL http://www.R-project.org/.

Thamdrup, B., Fleischer, S., 1998. Temperature dependence of oxygen respiration, nitrogen mineralization, and nitrification in Arctic sediments. Aquat Microb Ecol, 15(2): 191-199.

Therrien, R., McLaren, R.G., Sudicky, E.A., S.M., P., 2010. HydroGeoSphere, a Three-dimensional Numerical Model Describing Fully-Integrated Subsurface and Surface Flow and Solute Transport. Groundwater Simul. Group.

Thibodeaux, L.J., Boyle, J.D., 1987. Bedform-Generated Convective-Transport in Bottom Sediment. Nature, 325(6102): 341-343.

Tonina, D., Buffington, J.M., 2007. Hyporheic exchange in gravel bed rivers with pool-riffle morphology: Laboratory experiments and three-dimensional modeling. Water Resour Res, 43(1).

Tonina, D., and J. Buffington (2009), Hyporheic exchange in mountain rivers. I: Mechanics and environmental effects, Geogr. Compass., 3, doi:10.1111/j.1749-8198.2009.00226.x.

Tonina, D., de Barros, F.P.J., Marzadri, A., Bellin, A., 2016. Does streambed heterogeneity matter for hyporheic residence time distribution in sand-bedded streams? Adv Water Resour, 96: 120-126.

Trauth, N., Schmidt, C., Vieweg, M., Oswald, S. E. and Fleckenstein, J. H., 2015. Hydraulic controls of in-stream gravel bar hyporheic exchange and reactions. Water Resour Res(51(4)): 2243-2263.

Trauth, N., Schmidt, C., Maier, U., Vieweg, M., Fleckenstein, J.H., 2013. Coupled 3-D stream flow and hyporheic flow model under varying stream and ambient groundwater flow conditions in a pool-riffle system. Water Resour Res, 49(9): 5834-5850.

Triska, F.J., Kennedy, V.C., Avanzino, R.J., Zellweger, G.W., Bencala, K.E., 1989. Retention and Transport of Nutrients in a 3rd-Order Stream in Northwestern California - Hyporheic Processes. Ecology, 70(6): 1893-1905.

Van Griensven, A. et al., 2006. A global sensitivity analysis tool for the parameters of multi-variable catchment models. J Hydrol, 324(1-4): 10-23.

Vandersteen, G. et al., 2015. Determining groundwater-surface water exchange from temperature-time series: Combining a local polynomial method with a maximum likelihood estimator. Water Resour Res, 51(2): 922-939.

Verseghy, D.L., 1991. Class-a Canadian Land Surface Scheme for Gcms .1. Soil Model. Int J Climatol, 11(2): 111-133.

Vieweg, M. et al., 2016. Estimating time-variable aerobic respiration in the streambed by combining electrical conductivity and dissolved oxygen time series. J Geophys Res-Biogeo, 121(8): 2199-2215.

Vogt, T. et al., 2010. Fluctuations of electrical conductivity as a natural tracer for bank filtration in a losing stream. Adv Water Resour, 33(11): 1296-1308.

Voss, C.I., 1984. A finite-element simulation model for saturated–unsaturated, fluiddensity-dependent ground-water flow with energy transport or chemically-reactive single-species solute transport.

Voytek, E.B. et al., 2013. 1DTempPro: Analyzing Temperature Profiles for Groundwater/Surface-water Exchange. Groundwater, 52(2): 298-302.

Wagener, T., Kollat, J., 2007. Numerical and visual evaluation of hydrological and environmental models using the Monte Carlo analysis toolbox. Environ Modell Softw, 22(7): 1021-1033.

Ward, A.S., 2016. The evolution and state of interdisciplinary hyporheic research. Wires-Water, 3(1): 83-103.

Winter, T. C., J. W. Harvey, O. L. Franke, and W. M. Alley (1998), Ground water and surface water—A single resources, U.S. Geol. Surv. Circular 1139.

Webb, B.W., Hannah, D.M., Moore, R.D., Brown, L.E., Nobilis, F., 2008. Recent advances in stream and river temperature research. Hydrol Process, 22(7): 902-918.

Woessner, W.W., 2000. Stream and fluvial plain ground water interactions: Rescaling hydrogeologic thought. Ground Water, 38(3): 423-429.

Wollschlager, U. et al., 2017. The Bode hydrological observatory: a platform for integrated, interdisciplinary hydro-ecological research within the TERENO Harz/Central German Lowland Observatory. Environ Earth Sci, 76(1).

Wondzell, S.M., Gooseff, M.N., 2013. Geomorphic controls on hyporheic exchange across scales: watersheds to particles. In: Shroder, J. (Editor in Chief), Wohl, E. (Ed.)(Treatise on Geomorphology. Academic Press, San Diego, CA, vol. 9, Fluvial Geomorphology): pp. 203–218.

Wondzell, S.M., LaNier, J., Haggerty, R., 2009. Evaluation of alternative groundwater flow models for simulating hyporheic exchange in a small mountain stream. J Hydrol, 364(1-2): 142-151.

Wood, P.J., Boulton, A.J., Little, S., Stubbington, R., 2010. Is the hyporheic zone a refugium for aquatic macroinvertebrates during severe low flow conditions? Fund Appl Limnol, 176(4): 377-390.

Wörman, A. et al., 2012. Spectral scaling of heat fluxes in streambed sediments. Geophys Res Lett, 39.

Yvon-Durocher, G., et al., 2012. Reconciling the temperature dependence of respiration across timescales and ecosystem types, Nature, 487(7408), 472–476

Zarnetske, J.P., Haggerty, R., Wondzell, S.M., Baker, M.A., 2011. Dynamics of nitrate production and removal as a function of residence time in the hyporheic zone. J Geophys Res-Biogeo, 116.

Zarnetske, J.P., Haggerty, R., Wondzell, S.M., Bokil, V.A., Gonzalez-Pinzon, R., 2012. Coupled transport and reaction kinetics control the nitrate source-sink function of hyporheic zones. Water Resour Res, 48.

Zheng, L.Z., Cardenas, M.B., Wang, L.C., 2016. Temperature effects on nitrogen cycling and nitrate removal-production efficiency in bed form-induced hyporheic zones. J Geophys Res-Biogeo, 121(4): 1086-1103.

Selbstständigkeitserklärung

Hiermit erkläre ich, die vorliegende Dissertation selbstständig und ohne unzulässige fremde Hilfe angefertigt zu haben. Ich habe keine anderen als die angeführten Quellen und Hilfsmittel benutzt und sämtliche Textstellen, die wörtlich oder sinngemäß aus fremden Arbeiten entnommen wurden als solche kenntlich gemacht.

Die Arbeit wurde in gleicher oder ähnlicher Form bisher nicht an einer Universität eingereicht.

Potsdam, den 11.04.2017 _____

Danksagung

Ich danke allen Personen, die mich bei der Erstellung dieser Doktorarbeit unterstützt haben. Ohne ihre Hilfe wäre diese Arbeit nicht zu einem erfolgreichen Abschluss gekommen. Besonders hervorheben möchte ich:

- Christian Schmidt für die Betreuung der Arbeit, seine hilfreichen Ideen, Diskussionen und die gemeinsame Matlab Codierung von FLUX-BOT. Er hat wichtige Anregungen und Hinweise gegeben die zur Entwicklung der temperaturbasierten Methoden geführt haben.
- Sascha Oswald für seine Unterstützung bei der erfolgreichen Bewerbung für ein Stipendium im GEOSIM Graduiertenkolleg und die anschließende Weiterbeschäftigung. Er gab mir Gelegenheit und die Freiheit meinen eigenen Forschungsschwerpunkten nachzugehen.
- Sascha Oswald für die Betreuung der Arbeit, seine Ideen und die gemeinsamen Diskussionen insbesondere zu der numerischen Modellierung, sowie seine Unterstützung bei der Erstellung und Korrektur dieser Dissertation.
- Den Kollegen und Kolleginnen im Institut für Geoökologie an der Universität Potsdam für die angenehme Arbeitsatmosphäre und ihre Unterstützung bei der Bewältigung sämtlicher anfallenden Probleme; hier im besonderen Gabriele für seine Beratung in Fragen der Sensitivitäts- und Unsicherheitsanalysen sowie Andi und Daniel für ihre Hilfe bei technischen Problemen.
- Nico, Michael und Toralf für ihre Unterstützung bei den experimentellen Arbeiten an der Selke.
- Angela, Christina und Marie für das Korrekturlesen der Manuskripte und des „Rahmens“.
- Jana und Felix für fachliche und private Diskussionen.
- Meinen Eltern für ihre beständige und andauernde Unterstützung.
- Christina für die Ausdauer, Ruhe und Geduld, mit der sie mir stets zur Seite stand und mich immer wieder aufgemuntert hat - ihr gebührt mein besonderer Dank.